Curriculum Vitae

Lora Stojanovic

lstojanovic@som.umaryland.edu

Doctor of Philosophy, 2023

Education:

1999 - 2009 **B.A., Serbian literature,** Faculty of Philosophy, Serbia

2010 - 2014 **AS., Biology,** Community College of Baltimore County, Maryland

2016 - 2018 **MS., Cellular and Molecular Biomedical Science,** University of Maryland School of Medicine, Baltimore, MD

2018 – 2023 **Ph.D. in Human genetics,** University of Maryland School of Medicine, Baltimore, MD

Conferences presentations:

Biondi, C., **Stojanovic, L.,** Baylin, S. B., Lapidus, R. G., Mahmood, J., Rassool, F. V. Enhancing the Therapeutic Effects of Low Doses of Ionizing Radiation in Non-Small Cell Lung Cancers Using a Combination of PARP Inhibitors and DNA Demethylating Agents. Abstract for poster presentation 2016. Baltimore Areas Repair Symposium (BARS). University of Maryland, Baltimore,MD.

Kogan, AA, McLaughlin, LJ, Topper, M, Muvarak, N, **Stojanovic, L**, Creed, MT, Bentzen, S, Civin, CI, Baer, MR, Kingsbury, TJ, Baylin, S, Rassool, FV. DNA demethylating agents generate a Brcaness effect in multiple sporadic tumor types: prediction for sensitivity to PARP inhibitors in AML. Abstract for poster presentation 2017. American Society of Hematology. Atlanta, GA.

McLaughlin, L**., Stojanovic, L,** Rena Lapidus, Eun Yong Choi, Ying Zou, Elizabeth Waters, Stephen B. Baylin, Feyruz V. Rassool. Impaired homologous recombination by DNA methytransferase inhibitors induces synthetic lethality with PARP inhibitors in BRCA proficient Ovarian and Triple Negative Breast Cancers. Presented at the Baltimore Areas Repair Symposium (BARS) at the University of Maryland. 2018 (oral).

McLaughlin, LJ, **Stojanovic, L,** Kogan, AA, Lapidus, R, Choi, EY, Zou, Y, Baylin, SB, & Rassool, FV. Impaired homologous recombination by DNA methyltransferase inhibitors induces synthetic lethality in BRCA-proficient ovarian and triple negative breast cancers. Abstract for poster presentation 2018. Cancer Biology Research Retreat. University of Maryland, Baltimore, MD.

Kogan, AA, McLaughlin, LJ, Topper, MJ, Muvarak, N, **Stojanovic, L**, Creed, MT, Bentzen. S, Civin, C, Baer, MR, Kingsbury, T, Baylin, SB, Abbotts, RM, Rassool, FV. DNA Demethylating Agents Generate a BRCAness Effect: Prediction for sensitivity to PARP inhibitors in AML. Abstract for poster presentation 2018. Baltimore Area Repair Symposium. Baltimore, MD

Stojanovic, L, McLaughlin, L, Zou, Y, Baylin S.B., Rassool, F.V. DNA Methyltransferase Inhibitors in Combination with PARP inhibitors Generate Synthetic Lethality in BRCA-proficient Ovarian Cancer. Abstract for poster presentation 2019. Graduate Research Conference (GRC). University of Maryland, Baltimore, MD.

Stojanovic, L, McLaughlin, L, Zou, Y, Baylin S.B., Rassool, F.V. DNA Methyltransferase Inhibitors in Combination with PARP inhibitors Generate Synthetic Lethality in BRCA-proficient Ovarian Cancer. Abstract for poster presentation 2019. Cancer Biology Research Retreat. University of Maryland, Baltimore, MD.

McLaughlin, L., Kogan, A., **Stojanovic, L.,** Baylin, S.B., Topper, M.J., Rassool, F.V. Linking the pro-inflammatory and type I interferon response to DNA repair in cancer. Abstract for poster presentation 2019. Cancer Biology Research Retreat. University of Maryland, Baltimore, MD. (first place award winning)

Stojanovic, L, McLaughlin, L, Kogan, A, Rutherford, J, Topper, M, Baylin, S. B, Rassool, F.V. Inflammation signaling is inversely linked to DNA repair signaling in OC and BC. Abstract for poster presentation 2020. Graduate Research Conference (GRC). University of Maryland, Baltimore, MD.

Stojanovic, L, McLaughlin, L, Kogan, A, Rutherford, J, Topper, M, Baylin, S. B, Rassool, F.V. Inflammation signaling is inversely linked to DNA repair signaling and can enhance PARPI efficacy in BRCA proficient OC and BC. Abstract for poster presentation 2020. Baltimore Area Repair Symposium (BARS). University of Maryland, Baltimore, MD.

McLaughlin, LJ, **Stojanovic, L**, Kogan AA, Baylin, SB, Topper, MJ, & Rassool, FV. Pharmacologic induction of innate immune signaling via STING directly drives homologous recombination deficiency. Abstract for oral presentation 2020. Baltimore Area Research Symposium (BARS). University of Maryland, Baltimore, MD

Stojanovic, L., Abbotts, R., Tripathi, K., Topper, M.J., Liu, S., Wan, J., Nephew, K.P., Baylin, S.B., and Rassool F.V. ZNFX1 is a Master Regulator of Epigenetic Reprograming in Mitochondrial Inflammasome Signaling and Pathogen Mimicry in Ovarian Cancer. Abstract for poster presentation 2023. American Association for Cancer Research (AACR) Ovarian cancer special conference, Boston, Massachusetts.

Stojanovic, L., Abbotts, R., Tripathi, K., Topper, M.J., Liu, S., Wan, J., Nephew, K.P., Baylin, S.B., and Rassool F.V. ZNFX1 is a Master Regulator of Epigenetic Reprograming in Mitochondrial Inflammasome Signaling and Pathogen Mimicry in Ovarian Cancer. Abstract for oral presentation 2023. American Association for Cancer Research (AACR) Ovarian cancer special conference, Boston, Massachusetts.

Stojanovic, L., Abbotts, R., Tripathi, K., Topper, M.J., Liu, S., Wan, J., Nephew, K.P., Baylin, S.B., and Rassool F.V. ZNFX1 is a Master Regulator of Epigenetic Reprograming in Mitochondrial Inflammasome Signaling and Pathogen Mimicry in Ovarian Cancer. Abstract for poster presentation 2023. Cancer Research Day, University of Maryland, Baltimore.

Publications:

Kogan AA, Topper MJ, Dellomo AJ, **Stojanovic L**, McLaughlin LJ, Creed TM, Eberly CL, Kingsbury TJ, Baer MR, Kessler MD, Baylin SB, Rassool FV. Activating STING1-dependent immune signaling in TP53 mutant and wild-type acute myeloid leukemia. Proc Natl Acad Sci U S A. 2022 Jul 5;119(27): e2123227119. doi: 10.1073/pnas.2123227119. Epub 2022 Jun 27. PMID: 35759659; PMCID: PMC9271208.

McLaughlin, L.J., **Stojanovic, L**., Kogan, A.A., Rutherford, J.L., Choi, E.Y., Yen, R.W.C., Xia, L., Zou, Y., Lapidus, R.G., Baylin, S.B., Topper, M.J., Rassool, F.V. "Pharmacologic Induction of Innate Immune Signaling Directly Drives Homologous Recombination Deficiency", Proceedings of the National Academy of Sciences USa, first published May 26, 2020.

Abbotts, R., Topper, M.J., Biondi, C., Fontaine, D., Goswami, R., **Stojanovic, L**., Choi, E.Y., McLaughlin, L., Kogan, A.A., Xia, L., Lapidus, R., Mahmood, J., Baylin, S.B., and Rassool, F.V. DNA methyltransferase inhibitors induce a BRCAness phenotype that sensitizes NSCLC to PARP inhibitor and ionizing radiation. Proc Natl Acad Sci USA first published October 7, 2019. https://doi.org/10.1073/pnas.1903765116.

Biondi, C., Fontaine, F., **Stojanovic, L,** Nagaria, P. Lapidus, R., Choi, E., Mahmood, J., Baylin, S.B., and Rassool, F.V. (2017). Abstract 1422: Enhancing the therapeutic effects of PARP inhibitors in combination DNA methyl transferase inhibitors, using low doses of ionizing radiation in non-small cell lung cancers. Cancer Research. 77. 1422-1422. 10.1158/1538-7445.AM2017-1422.

Abstract

Title of Dissertation: The Role of Pathogenic Mimicry Response Leading to Mitochondrial Dysfunction in Ovarian Cancer

Lora Stojanovic, Doctor of Philosophy, 2023

Dissertation Directed by: Feyruz V. Rassool, PhD, Professor, Radiation Oncology

Approximately 10-15% of epithelial ovarian cancer (EOC) patients that have BRCA mutations and homologous recombination deficiency (HRD) are successfully treated with FDA-approved poly (ADP-ribose) polymerase (PARP) inhibitors resulting in synthetic lethality and antitumor responses. While some patients with BRCA-wildtype EOC have shown a response to single agent PARP inhibitor (PARPi) therapy, the majority do not respond. This suggests the need for the development of novel combination therapies for EOC. DNA methyltransferase inhibitors (DNMTis) activate transcriptionally silenced genes and repeat sequences, including endogenous retroviruses (ERVs), that increase dsRNA in the cytosol, leading to interferon (IFN) signaling and antitumor immune responses, in a mechanism known as viral mimicry. Combining PARPi with DNA methyltransferase inhibitors (DNMTis) have been shown to not only induce synergistic cytotoxicity in multiple cancers, including EOC with wildtype BRCA, but also increase both cytosolic dsDNA dsRNA, leading to STING-mediated interferon (IFN) and inflammasome (NFKB-TNFα) signaling, resulting in generation of HRD. Recent research shows that mitochondria (mt) are a gateway to IFN/inflammasome signaling and that release of mtDNA into the cytosol can activate innate immune signaling pathways, including STING. Importantly, recent reports suggest that the little studied ds RNA/DNA sensor ZNFX1, through interaction with mt proteins, is an important regulator of the IFN

response in viral infection. Here, I show that in EOC, DNMTis and PARPi treatment increases expression of ZNFX1 and colocalization with mitochondrial antiviral protein MAVs in the mt outer membrane. This combination drug treatment also induces mt reactive oxygen species (ROS) and fragmented mtDNA release into the cytosol, resulting in STING-dependent inflammasome signaling. ZNFX1 knockout attenuates these dynamics, thus defining ZNFX1 as essential for interferon /inflammasome signaling induced by mtDNA damage. Overall, we suggest that ZNFX1 represents a novel master regulator of mt-mediated STING-dependent IFN and inflammasome signaling in OC and other solid malignancies.

The Role of Pathogen Mimicry Response Leading to Mitochondrial Dysfunction in Ovarian Cancer

by
Lora Stojanovic

Dissertation submitted to the Faculty of the Graduate School of the
University of Maryland, Baltimore in partial fulfilment
of the requirements for the degree of
Doctor of Philosophy
2023

Dedication

To my dear parents Radoslav and Gorica Saković for unconditional love and support.

Acknowledgements

From the bottom of my heart, I want to thank Dr. Rassool for being an extraordinary mentor. It is such an honor to say I am your student. Thank you for believing in me, valuing me both as a scientist and as a person, guiding me all these past years, and overall, for being the master regulator of my life. Thank you for being there for me to problem solve science and life. I hope my future work will make you proud of me, and I wish you much success and great new students.

I want to thank Dr. Nephew, Dr. Lapidus, Dr. Webb, and Dr. Fiskum for agreeing to be my committee members and helping me on this journey by giving me advice and suggestions. I especially want to thank Dr. Nephew who has been a great second mentor throughout this project. I am very grateful for every meeting and discussion on soon to be not little known ZNFX1.

I want to thank Dr. Abbotts, Dr. Tripathi, Dr. Topper, Dr. Wan, and Dr. Liu for their extraordinary help while working on this project. I especially want to thank Dr. Abbotts for all the help she provided in both professional and private settings- thank you for being there when I needed you the most.

Additionally, I want to thank all past lab members from whom I learned much. It was great having to work with Dr. Muvarak, Dr. McLaughlin, Dr. Kogan, and Dr. Dellomo.

Thank you to all my friends and neighbors who helped me stay positive and optimistic in these past years by showing me how to see a glass half full. I especially want to thank Zozefina Nahas for being an unselfish and true friend throughout many years, giving me additional strength when I needed it the most.

I want to thank my beautiful family and my sister Ana for emotional support and unconditional love. My life would be meaningless without you.

Finally, I want to thank Dr. Pavle Stojanovic for teaching me a valuable life lesson, helping me learn more about myself, and making me a stronger woman.

Table of Contents

List of Tables

List of Figures

List of abbreviations

ACSM5	Acyl-CoA synthetase medium-chain family member 5
AML	Acute Myeloid Leukemia
AZA	Azacitidine
ATM	Ataxia telangiectasia mutated
ATR	Ataxia telangiectasia and Rad3-related
APC	Antigen Presenting Cells
BAK	BCL2 Antagonist/Killer 1
BAX	Bcl-2-associated X protein
BC	Breast Cancer
BER	Base Excision Repair
BET	Bromodomain and extraterminal
BRAF	v-raf murine sarcoma viral oncogene homolog B1
BRCA 1/2	Breast cancer gene 1 or 2
BRCR	Breast Cancer Cluster Region
BSA	Bovine Serum Albumin
cDNA	Complementary DNA

CDKN2A	Cyclin-dependent kinase inhibitor 2A
COVID-19	Coronavirus disease 2019
CSIOVDB	Cancer Science Institute Singapore
CRISPR	Cluster regularly Interspaced short palindromic repeats
DDB1	UV-damaged DNA-binding protein 1
DSS1	Deleted in split hand/split foot protein 1
DMEM	Dulbecco's modified eagle medium
DNA	Deoxyribonucleic acid
cGAS	Cyclic GMP-AMP synthase
CTLA-4	Cytotoxic T lymphocyte antigen 4
CMML	Chronic myelomonocytic leukemia
CMPK2	Cytidine/Uridine Monophosphate Kinase 2
DAC	Decitabine
DAMPs	Damage-Associated Molecular Patterns
DIDC	Poly dI:dC
DNMT	DNA methyltransferase
DNMTi	DNA methyltransferase inhibitor

DSB	Double-Stranded break
dsDNA	Double-Stranded DNA
dsRNA	Double-Stranded RNA
EOC	Epithelial Ovarian Cancer
ERV	Endogenous retroviruses
EZH2	Enhancer of zeste homolog 2
FANC	Fanconi anaemia complementation group
FBS	Fetal bovine serum
FDA	Food and Drug Administration
GDAC	Guadecitabine
ICI	Immune check point inhibitor
IFN	Interferon
IFI27	Interferon alpha inducible protein 27
IKK	IκB kinase
IRF3	Interferon Regulatory Factor 3
ISG	Interferon Stimulated Genes
IUSCCC	Indiana University Simon Comprehensive Center

H2AX	H2A histone family member X
HGSC	High-grade serous cancer
HER 2	Epidermal growth factor receptor 2
HR	Homologous Recombination
HRD	Homologous Recombination Deficiency
HRP	Homologous Recombination Proficiency
KRAS	Kirsten rat sarcoma
MAVS	Mitochondrial antiviral signaling protein
MDA5	Anti-melanoma differentiation-associated gene 5
MDS	Myelodysplastic syndrome
MEK 1/2	Mitogen-activated protein kinase kinases 1 and 2
MSMD	Mendelian Susceptibility to Mycobacterial Disease
Mt	Mitochondria
mtDNA	mitochondrial DNA
mTOR	Mammalian target of rapamycin
NBS1	Nijmegen breakage syndrome protein 1
Nf-kB	Nuclear factor kappa-light-chain-enhancer of activated B Cells

NHEJ	Nonhomologous end-joining
NK	Natural Killer cells
NLRP3	Nod-Like Receptor Protein 3
NOD/SCID	Nonobese diabetic/severe combined immunodeficiency
NSCLC	Non-Small Cell Lung Cancer
LGSC	Low-Grade Serous Cancer
LIGIV	Ligase IV
LYRM4	LYR Motif Containing 4
OC	Ovarian Cancer
OCCR	Ovarian Cancer Cluster Region
OXPHOS	Oxidative phosporylation
PARP	Poly (ADP-ribose) polymerase
PARPi	Poly (ADP-ribose) polymerase inhibitors
PCR	Polymerase Chain Reaction
PD-1	Programmed cell death receptor 1
PD-L1	Programmed cell death ligand 1
PFS	Progression free survival

PI3CA	Phosphatidylinositol 3-kinase
PIC	Polyinosinic-polycytidylic acid
PETRA	PErsonalized Treatment by Real-time assessment
PMR	Pathogenic mimicry response
PTEN	Phosphatase and tensin homolog deleted on chromosome 10
PRODH/2	Proline dehydrogenase H and 2
PRP	Pattern-recognition receptors
qPCR	Quantitative Real Time PCR
RASSFLA	Ras association domain family member 1
RLRs	RIG-I-like receptors
RNA	Ribonucleic acid
RNA-seq	Ribonucleic acid Sequencing
ROS	Reactive Oxygen Species
SEM	Standard Error of the Mean
STING	Stimulator of interferon signaling
SSB	Single-Stranded Break
TAL	Talazoparib

TBK1	TANK-binding kinase 1
TCGA	The Cancer Genome Atlas
TCR	Transcription coupled DNA repair
TFAM	Mitochondrial transcription factor A
TIL	Tumor Infiltrating Lymphocytes
TK	Tyrosine Kinase
TLR3	Toll-like receptor 3
TNBC	Triple Negative Breast Cancer
TNFα	Tumor Necrosis Factor α
TP53	Tumor Protein P53
TSG	Tumor Suppressor Gene
UCP3	Uncoupling Protein 3
WT	Wild Type
XAB2	Xeroderma pigmentosum group A (XPA)-binding protein 2
XRCC2/3	X-ray repair cross complementing 2 and 3
ZBP1	Z-DNA-binding protein 1
ZNFX1	Zinc Finger NFX1-Type Containing 1

Chapter 1: Introduction

1.1 Ovarian cancer classification and treatment options

Ovarian cancer (OC) is one of the most commonly diagnosed gynecological cancers that is ranked as the fifth cause of all cancer deaths among women. The American Cancer Society estimates that by the end of the year 2023, about 13,270 deaths in women diagnosed with OC will occur, which makes this cancer the leading cause of gynecological cancer deaths (1). One of the explanations for the high mortality rate of this cancer is that mild symptoms, or even complete lack of symptoms in early stages of this disease, often delays diagnosis until after the cancer has already metastasized. In addition, the poor survival statistics could also be explained by absence of a good screening method for OC (2). Although the survival rate varies depending on the specific OC type, or the stage when the initial diagnosis is made, on average the 5-year survival rate is less than 50% (3). In general, OC can be divided into three types, cord-stromal, germ and epithelial cancer, which all arise from a different cell of origin that have different characteristics. The most common type of OC arises from epithelial tissue outside of the ovary, and it is known as epithelial ovarian cancer (EOC). Furthermore, EOC can be divided into four unique phenotypic and molecular subtypes: serous, endometroid, clear cell, and mucinous ovarian carcinoma (4). Notably, serous ovarian cancer is the most prevalent among EOC, and can be divided into highly aggressive high-grade serous (HGSC), and less aggressive low-grade serous cancer (LGSC). Nonetheless, the first line of therapy after surgery (debulking, removal of tumor, hysterectomy, removal of uterus/cervix, removal of ovaries, lymph nodes and/or omentum) for all of these ovarian cancers subtypes is still chemotherapy. For example, high-grade serous OC has the highest initial response to platinum and taxane-based chemotherapy, usually paclitaxel-carboplatin, that is given both as adjuvant and neoadjuvant therapy (followed by debulking) (4, 5). About 80% of all patients have a complete response to initial platinum-taxane chemotherapy that can last for about 3 years (6). However, platinum resistance inevitably occurs, leading to patients' death (7). Therefore, given that chemotherapy approaches lead to disease recurrence, it is crucial that novel therapy approaches are developed for ovarian cancer.

A recent important discovery is that EOC subtypes have different mutations and molecular aberrations that can determine the therapy approach and potentially lead to a personalized treatment approach. (**Fig.1.1**). This has led to studies targeting specific EOC subtypes and associated molecular lesions (8). Mutation in tumor protein P53 (TP53) identified in 97% of all HGSOC can be accompanied by a breast cancer gene 1 or 2 (BRCA1/2) mutation, which makes this cancer suitable to be treated with poly (ADP-ribose) polymerase inhibitors (PARPi) and immune checkpoint inhibitors (therapy mechanisms are discussed below and in chapter 2). Low grade serous EOC, on the other hand, have Kirsten rat sarcoma (KRAS) and v-raf murine sarcoma viral oncogene homolog B1 (BRAF) mutations and can be treated with mitogen-activated protein kinase kinases 1 and 2 (MEK 1/2) inhibitors (see below). In addition, KRAS mutations are also found in mucinous carcinoma; however, this mutation is often accompanied with human epidermal growth factor receptor 2 (HER2) amplification, which makes this cancer treatable with a monoclonal antibody that binds to the protein HER2, trastuzumab. Phosphatase and tensin homolog deleted on chromosome 10 (PTEN) mutations are exclusively found in endometroid carcinoma, while phosphatidylinositol 3-kinase (PI3CA) is found in clear cell carcinoma, and they can be treated with mammalian target of rapamycin (mTOR) inhibitors and tyrosine kinase (TK) inhibitors, respectively.

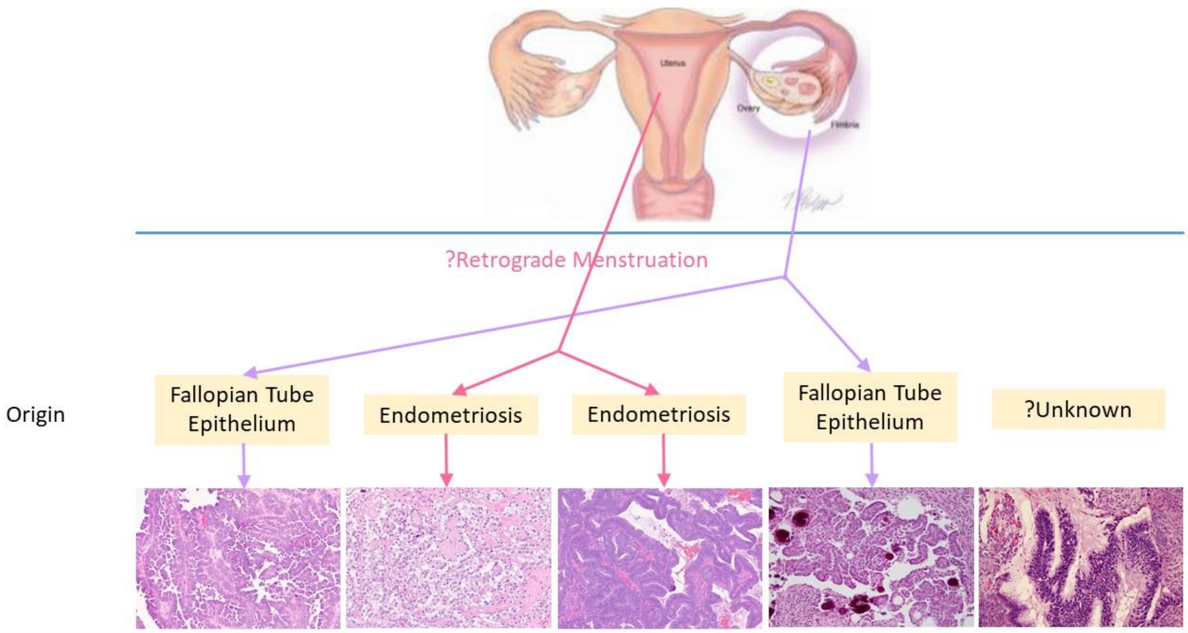

	High-Grade Serous Carcinoma	Clear Cell Carcinoma	Endometrioid Carcinoma	Low-Grade Serous Carcinoma	Mucinous Carcinoma
% of all Ovarian Carcinomas	~70%	~10%	~10%	<5%	<5%
Precursor Lesions	Serous tubal intraepithelial carcinoma (STIC)	Clear Cell Borderline Tumor	Endometrioid Borderline Tumor	Serous Borderline Tumor	Mucinous Borderline Tumor
Inherited Syndromes	BRCA1/2, Hereditary Breast and Ovarian Cancer (HBOC)	Lynch Syndrome	Lynch Syndrome	?	?
Common Mutations and Molecular Aberrations	TP53 BRCA1/2 and HRD Chromosomal instability Aneuploidy (100%)	ARID1A PIK3CA CTNNB1 PPP2R1A MSI	PTEN CTNNB1 ARID1A PPPR2R1A MSI	KRAS BRAF	KRAS HER2 amplification
Potential Molecular Targeted Therapies	PARP inhibitors, immune checkpoint inhibitors	Tyrosine kinase inhibitors	mTOR inhibitors	MEK1/2 inhibitors	Trastuzumab

Figure 1.1 Ovarian cancer subtypes, their mutations and available therapy.

Epithelial ovarian cancer subtypes arise from a different epithelial region and are presented with different molecular aberrations that can determine the particular targeted treatment for a cancer patient. Figure from Provincial Health Services Authority BC Cancer 2023.

1.2 PARP inhibitor therapy in EOC

As mentioned above, PARPis are a very exciting spectrum of drugs for treatment of EOC with BRCA1/2 mutations (9). Overall, the therapy works through interfering with how PARP functions in allowing cancer cells to survive ongoing DNA damage and induces "synthetic lethality", a lethal phenomenon in which the occurrence of a single genetic event is tolerable for cell survival, whereas the co-occurrence of multiple genetic events results in cell death (9) (discussed in detail in Chapter 2). PARP proteins contain 17 members (PARP1- 17) that are involved in numerous cellular processes, such as chromatin remodeling, DNA repair, gene regulation and apoptosis (10). However, of these, PARP1 is the most studied and its involvement in DNA repair pathway for single-stranded break (SSB) called base excision repair (BER) is currently well established (11). The role of PARP1 in BER is essential and accompanies several actions such as sensing DNA SSB, binding to the damaged site, starting the process of producing branched chains called PAR in the process of poly- (ADP-ribosyl)ation (PARylation) and attracting other SSB repair proteins to the DNA damage site for repair. Once repaired, PAR, is degraded and the DNA repair proteins are released from the repaired DNA site (12).

Several PARPis have been developed and approved by FDA as a single agent targeted therapy for OC with BRCA mutations (13) (14) (**Table 1**.). Olaparib was first approved for BRCA mutated cancers, and later approved as maintenance therapy regardless of BRCA status based on the results of the phase III SOLO-2 trial (15). Rucaparib was the second PARPi to be approved by the FDA and even though it has similar indication as olaparib, the ARIEL3 trial showed that patient treated with rucaparib have significant progression free survival, which led to approval of rucaparib for maintenance therapy followed platinum-based therapy (16). In addition, based on the NOVA trial, another PARPi niraparib was approved for maintenance therapy for patient with recurrent EOC (17). Lastly, talazoparib was approved in 2018 for the treatment of germline BRCA1/2 mutated HER2-negative locally advanced or metastatic breast cancers after phase III EMBRACA trial (18). Expansion of approval of talazoparib for OC is an ongoing process (19), and talazoparib in combination with enzalutamide recently received FDA approval for HRR gene-mutated metastatic castration-resistant prostate cancer. Currently, a new PARP1 selective inhibitor AZD5305 is in Personalized Treatment by Real-time assessment (PETRA) clinical study as a next generation PARPi in phase I/IIa to evaluate its safety, pharmacokinetics and pharmacodynamics for ovarian cancer, triple negative breast cancer (TNBC), prostate and pancreatic cancer (20). However, while robust responses are seen with PARPi therapy, this treatment is not durable. Moreover, the majority of EOC do not have BRCA1/2 mutations and do not respond fully to PARPis (21). Therefore, novel combination therapies are required to potentially extend responses for BRCA1/2 mutant EOC and to expand PARPi therapies to treat BRCA-proficient ovarian cancers.

PARP inhibitor	Approved year	Indication and Usage	Recommended dose	Associated clinical trial
Olaparib	2017 by FDA	platinum sensitive, recurrent ovarian cancer for maintenance treatment	300 mg (two 150 mg tablets) taken orally twice daily	SOLO-2 and Study 19
	2018 by FDA	BRCA1/2- mutated advanced ovarian cancer for first-line maintenance treatment	300 mg (two 150 mg tablets) taken orally twice daily	SOLO-1
	2020 by FDA	platinum sensitive and homologous recombinant deficient positive advanced ovarian cancer for combination with bevacizumab for first-line maintenance treatment	300 mg taken orally twice daily	PAOLA-1
Niraparib	2017 by FDA	platinum sensitive and recurrent ovarian cancer for maintenance treatment	based on body weight or platelet count	ENGOT-OV16/NOVA Trial
	2019 by FDA	HRD-positive ovarian cancer for maintenance treatment	300 mg taken once daily	NCT02354586
Rucaparib	2016 by FDA	BRCA1/2-mutated after receiving at least two lines of prior chemotherapy	not mention	Study 10 and ARIEL2
	2018 by FDA	platinum sensitive, recurrent ovarian cancer for maintenance treatment	600 mg (two 300 mg tablets) taken orally twice daily	ARIEL3

Table 1. PARPis recommended by 2022 NCCN clinical practice guidelines. Table from Wu *et al.*, 2023.

1.3 DNMT inhibitor therapy in EOC

Another potential therapy for EOC is DNA methyltransferase~~s~~ (DNMTs) inhibitors (DNMTis). DNMTis are approved by the FDA for treatment of myelodysplastic syndromes (MDS) (22) (23) and are used for treatment of AML as well (24) (25). DNMTs are enzymes that transfer methyl group from S-adenosyl-L-methionine to the fifth position of cytosine residues in DNA via the process called methylation (26). One of the most important roles of DMNTs is their ability to regulate gene expression through epigenetics (27). Epigenetics includes processes of altering gene activity without changing the DNA sequence, thus leading to modifications that can be transmitted to daughter cells (28).

There is increasing evidence for involvement of epigenetic mechanisms in the pathogenesis of many cancers, including EOC. Research shows that the methylation of cytosine in promoter regions of CpG island-containing genes is linked to silencing of tumor suppressor genes (TSGs) such as, cyclin-dependent kinase inhibitor 2A (*CDKN2A*, or p*16INK4*), Ras association domain family member 1 (*RASSFIA*,) and *BRCA1*, which leads to tumor initiation, progression and drug resistance (29). DNA methyltransferase inhibitors (DNMTis) prevent aberrant hypermethylation and silencing of tumor suppressor genes leading to their transcriptional reexpression. Indeed, the benefit of DNMTis as a monotherapy or in combination with other agents have been investigated in EOC among other solid tumors. There are two generations of DNMTi (**Fig.1.2**): non-nucleoside inhibitors (curcumin and procaine) that are forming non-covalent, thus, reversable inhibition of DNMT1; and nucleoside inhibitors (azacytidine and decitabine) that are analogues of cytosine and covalently incorporate into DNA/RNA to trap and degrade DNMT1 in proliferating cells (30). Since 2010, five clinical trials in EOC patients investigated combination of DNMTi with carboplatin (29). In 2010, a phase I trial at Indiana University Simon Comprehensive Center (IUSCCC) showed that low-doses decitabine in combination with carboplatin was well tolerated in patients with recurrent, platinum-resistant EOC and received clinical benefit (31). In addition, the results of the study showed that demethylation of genes linked to EOC correlates with clinical responses to some degree (31). In addition, the same group performed phase I and II studies with guadecitabine and carboplatin in platinum resistant, recurrent OC in 2018 and 2020 respectively (32) (33). The results of the phase I study showed that the combination therapy was well tolerated and effective in platinum resistant OC patients, suggesting that guadecitabine was able to reverse aberrant DNA methylation and resensitize OC to platinum (32). Their randomized phase II study further showed that guadecitabine and carboplatin treatment, although, improved 6-months progression free survival (PFS), did not show a difference in PFS compared to standard chemotherapy (33). The fourth trial was performed at M.D. Anderson Cancer Center also investigating the possibility of using DNMTis to reverse platinum resistance in EOC patients (34). This Ib-IIa study, conducted in 2011, shows a 21% partial response rate to therapy in 33 platinum resistant EOC patients when combining carboplatin with azacitidine (34). The fifth trial was conducted by a United Kingdom (UK) Cancer Research Group in 2014 as a randomized, phase II trial investigating the combination of decitabine and carboplatin and comparing it to carboplatin monotherapy in recurrent EOC cancers. (35). In contrast to the studies cited above, the results of this trial showed that decitabine reduced the efficacy of carboplatin in partially platinum sensitive EOC patients. Unfortunately, the lack of treatment efficacy in EOC patients resulted in closing the study. There are several reasons for the outcome of this study: shorter duration of exposure to treatment than required, patient selection that was either not responsive to DNMTis or too responsive, in which case hypomethylation occurred on immune-modifying genes that led to hypersensitivity to the drug, or reversion of BRCA1 expression that decreased the sensitivity to carboplatin (35). Overall, the conclusion of this study was that selecting a different DNMTi may be more beneficial to EOC patients (35). Recently, a new DNMTi ASTX727 has been developed that is an oral formulation combining decitabine and cedazuridine (cytidine deaminase inhibitor), ASTX727 is currently in a phase II study in patients who cannot tolerate chemotherapy (36). In addition, GSK-3484862 (GlaxoSmithKline; GSK) is a new class of reversable, less toxic DNMT1 selective inhibitors under development (37). Overall, DNMTis are very potent drugs that directly target hypermethylated sites; however, recent research shows that DNMTis can also influence downstream targets leading to transcriptional reprograming

(38). This knowledge is important for investigating new approaches using epigenetic therapy in combination with other therapies for treating EOC as well as other cancers.

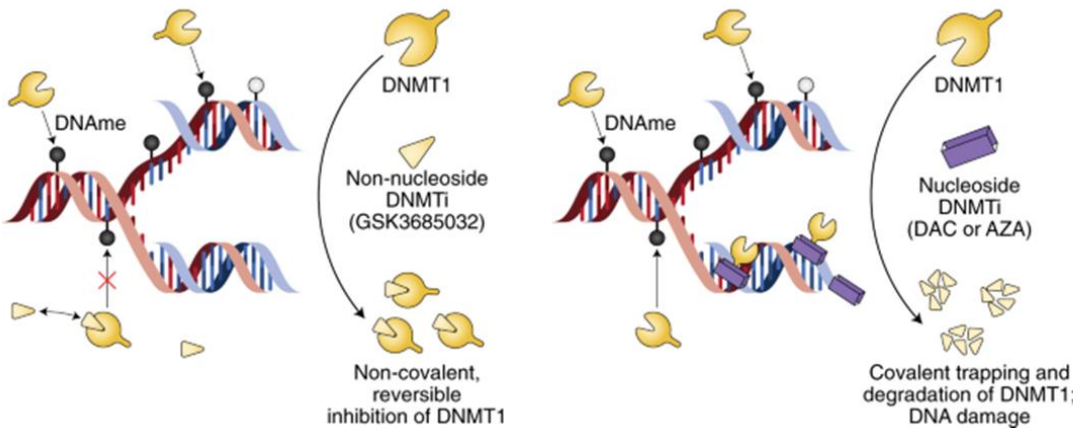

Figure 1.2 DNMTi mechanism of action.

Non-nucleoside inhibitor (left) non-covalently binds DNMT1 and prevents it from binding to cytosine at CpG in the process that is known as reversable inhibition. Curcumin and procaine are representative inhibitors. Nucleoside inhibitors (right) covalently trap DNMT1 leading to its degradation through the process that is irreversible. Azacitadine and decitabine are representative inhibitors. Figure from Mehdipour *et al*.,2021.

1.4 Immune therapy in EOC

Immune checkpoint inhibitors (ICIs) are novel agents which have immunostimulatory effects by antagonizing programmed cell death receptor 1 (PD-1; present on the surface of immune cells), its ligand PD-L1 (on tumor cells) or cytotoxic T lymphocyte antigen 4 (CTLA-4). ICIs have become an established treatment option in many malignancies like advanced lung cancer and malignant melanoma but for EOC there is no specific immunotherapeutic agent approved yet. Nevertheless, initial preclinical studies suggest that immune checkpoints may be potential targets for activating anti-tumor immunity in OC. Hamanishi *et al.* reported high PD-L1 expression in 68% of tissue samples from 70 EOC patients (39) whereas Maine *et al.* revealed that monocytes derived from peripheral blood and ascites of OC patients had significantly higher PD-L1 expression compared to benign or borderline OC tumors (40) Moreover, HGSOC showed higher PD-L1 positivity and more CD8+ tumor infiltrating lymphocytes (TILs) than less common histologies (41) (42). However, efficacy data from clinical trials with anti PD-1/PD-L1 or anti-CTLA suggested that EOC does not respond to these agents as monotherapies (43) (44). Therefore, better characterization of the tumor microenvironment and validated biomarkers are required to select EOC patients who may benefit from ICI monotherapy, and novel combination strategies with ICIs are needed to see durable responses for EOC.

Another promising therapy strategy against cancer cells that is gaining traction in the research field is activating innate mechanisms used to combat invading pathogens, including viruses, that recognize cytosolic double-stranded (ds) DNA and RNA (45). Many cancer drugs can mimic this anti-viral activation of the innate immune system, including DNMTis and PARPis (46, 47). DNMTis can transcriptionally activate hypermethylated and silenced endogenous retroviruses (ERVs) that have integrated into the human genome during evolution. The human genome contains about 8% different families of ERVs. Most of ERVs are not capable of encoding viral particles, most specifically *env-like* regions, thus, making them identifiable only at the nucleic acid level. However, there are ERV families that have ability to be expressed at the RNA level and consequently translated to proteins (48). It is well known that once transcribed, ERVs are present in the cytosol in the form of dsRNA, which then can activate innate immune responses (45) (49). The endogenous stimuli, such as cytosolic RNA or DNA, activate both innate and adaptive immune responses through two known pathways. After sensing dsRNA by anti-melanoma differentiation-associated gene 5 (MDA5) or toll-like receptor 3 (TLR3) in the cytosol, the signal is relayed to mitochondrial antiviral signaling protein (MAVS) that will induce TANK-binding kinase 1 (TBK1) activation that will lead to type I or III interferon (IFN) signaling (**Fig. 1.3**) (45). On the other hand, dsDNA is sensed in the cytosol by cyclic GMP-AMP synthase (cGAS) that catalyzes the synthesis of cyclic dinucleotide cGAMP, which binds to the stimulator of interferon signaling (STING) that will recruit TBK1 and interferon regulatory factor 3 (IRF3) and activate IFN signaling (50). High dsRNA level are a requirement for the viral mimicry approach, and OC is one of them since many ERVS are expressed in this cancer. This suggests that synergistic treatment combinations with epigenetic therapies could be an attractive therapy strategy in OC.

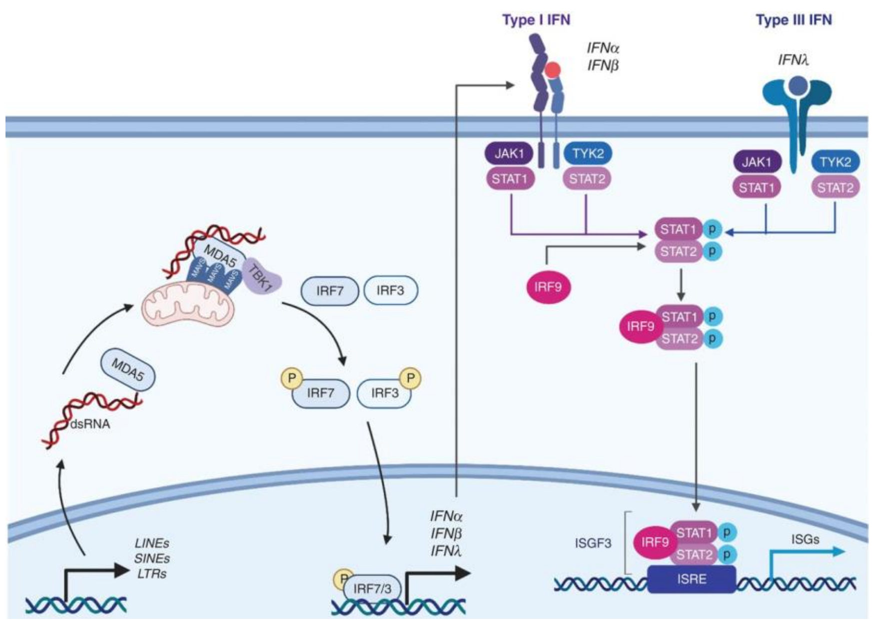

Figure 1.3 Viral mimicry activate antiviral response through ERVs.

(Left) Transcribed ERVs generate dsRNA that activate MDA5 and Toll-like receptor 3 (TLR3) cytosolic RNA sensors, leading to MAVS translocation to the mitochondria and activation of TBK1. After TBK1 phosphorylation of IFN regulatory factors 3 and/or 7 (IRF3/7), phosphorylated IRF3/7 translocate to the nucleus and activate IFN genes transcription. (Right) Type 1 interferon bind IFN receptors and activate Janus kinases (JAK) pathway that leads to ISG transcription and further immunogenicity and enhance adaptive immune response. Figure from Chen *et al.*, 2021

Chapter 2 Comprehensive critical literature review

2.1 BRCA mutations and mechanisms of PARPi action

2.1.1BRCA mutations in EOC

As discussed in Chapter 1, HGSOC is one of the most common subtypes of ovarian cancer diagnosed among women (4). Besides *TP53* mutations, breast cancer 1/2 (*BRCA1/2*) genes are the next most common mutations in this disease, often accompanying *TP53* mutations. Mutation in *BRCA1/2* genes are usually inherited, occurring in 66% and 34% respectively of OC cases with the risk for developing malignancy ranging from 39%-44% and 11%-17% respectively (51). One of the crucial factors that determine cancer development is the location of mutation in both BRCA1/2. Gayeter et al, conducted a study of 60 families with a history of breast and ovarian cancer, observing a correlation between location of the mutation in BRCA1/2 genes functional impact of the mutation on the BRCA protein and cancer incidence. They found that mutations in 3' end correlated with a low risk of developing EOC (52). Sekine *et al*. demonstrated that founder mutations in OC families were located in the ovarian cancer cluster (OCCR) in both *BRCA1/2,* a region of BRCA genes correlated with increased risk for developing OC (**Fig.2.1.1**) (53).

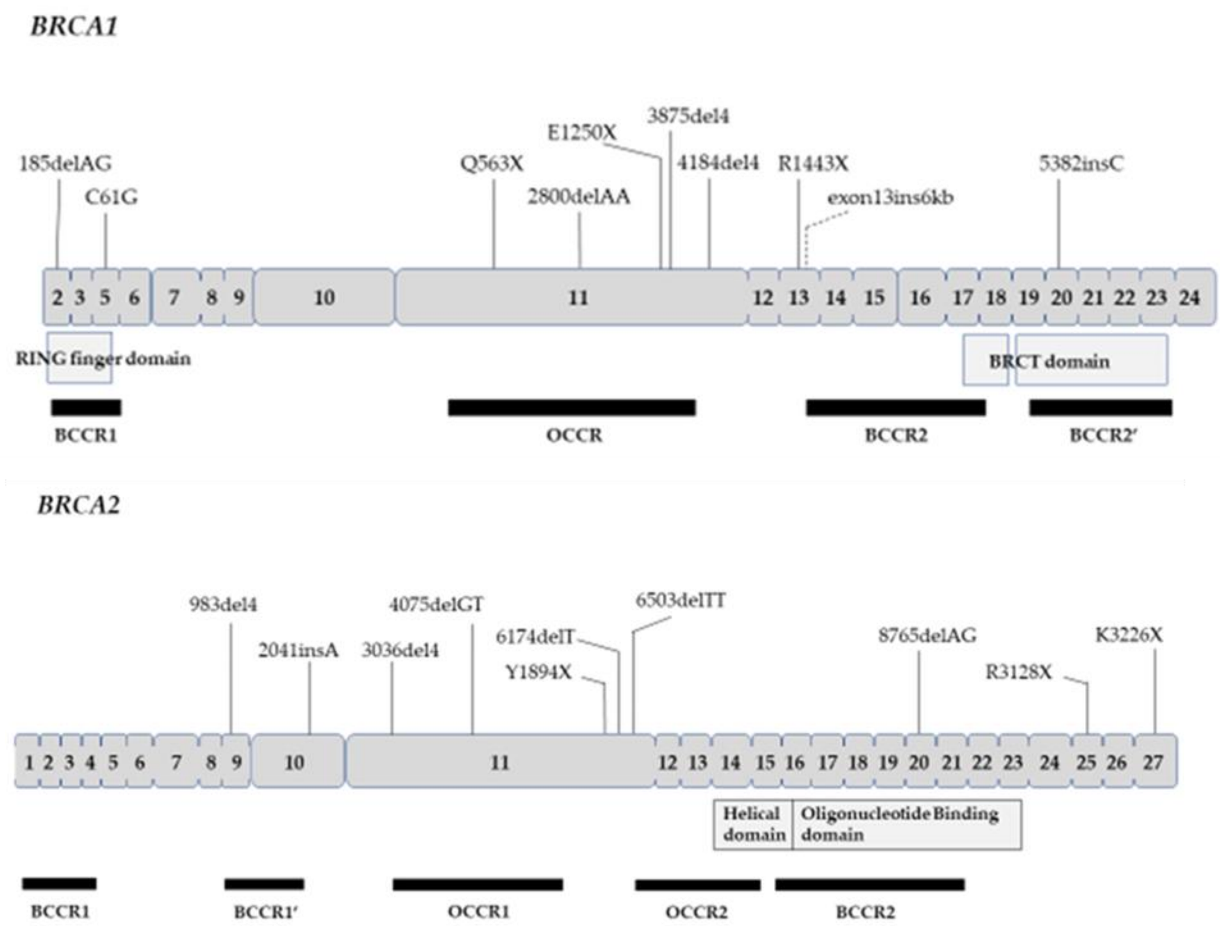

Figure 2.1.1 BRCA1/2 common founder mutations by location.

Breast cancer cluster region (BRCR) and ovarian cancer cluster region (OCCR) showing different variants commonly found in particular cancer in BRCA1 (top) and BRCA 2 gene exons shown as numbered boxes (bottom). Functional domains affected by a mutation are represented in the textbox. Figure from Sekine *et al*., 2021

However, this study does not explain the variable cancer incidence among families with identical locations of the mutations. In addition, even if one BRCA 1/2 mutant allele is inherited, the normal, wild type copy inherited from the other parent will ensure normal function of the protein and should act as a tumor suppressor gene (TSG) (54). Thus, cancer will occur only when the normal copy is impacted by a second mutation, inactivating both copies of the gene in a mechanism known as Knudsen's "Two-Hit Hypothesis" (55).

Approximately 10% of EOC patients have mutations in the BRCA1/2 gene, in particular in HGSOC, and benefit from PARPi therapy (56). Integration of PARPi into the EOC treatment paradigm is an important advance in the treatment of EOC. As discussed in the previous chapter, several PARPis are now FDA approved and in clinical use for EOC (57), such as oliparib, niraparib, rucaparib.

2.1.2 PARPi mechanisms

The basic mechanism of action of PARPis is catalytic inhibition of PARP by blocking its PARylation activity and consequently leading to DNA double-stranded break (DSB) and homologous recombination (HR) repair activation, a vital DNA repair process that uses the undamaged sister chromatid to carry out high-fidelity repair of predominantly replication-associated DSBs. HR is a major mechanism for protecting the integrity of the genome in proliferating cells, because other DSB repair pathways are error-prone and generate chromosome deletions and translocations. Therefore, EOC cancers with BRCA mutations cannot repair replication-associated DSBs by HR, leading to increased chromosomal aberration that can lead to more aggressive disease and resistance to therapy (58).

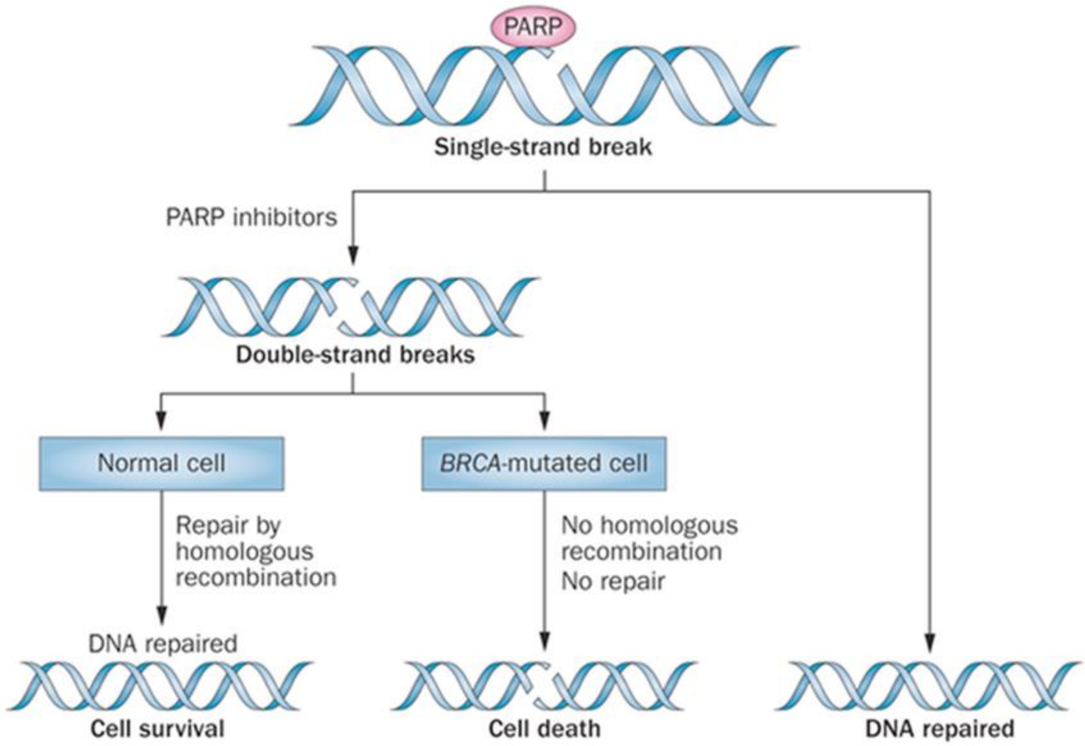

Figure 2.1.2 Synthetic lethality model

PARP is involved in repair of the single stranded DNA break (SSBs). If inhibited by PARPi, SSB will not be repaired, which will lead to double stranded break (DSBs) during the replication. A DSB that is usually repaired by HR in normal cells will not be repaired in BRCA mutated cancer cells, which will lead to cell death. Figure from Sonnenblick *et al.*, 2014.

Importantly, in cells with BRCA1/2 mutations, PARPi treatment results in cell death through a mechanism known as synthetic lethality (**Fig.2.1.2**) (9). In this context, PARPis block single-strand break (SSB) repair, leading to increased DSBs during DNA replication that cannot be repaired by HR, leading to synthetic lethal cell death (59). Moreover, development of second generation PARPis, for example, talazoparib, identified an additional mechanism through which these drugs exert their cellular toxicity. These PARPis trap PARP1/2 in DNA (**Fig.2.1.3**) (60) (61), and of the PARPi, talazoparib is the most potent PARP trapper (62). In this regard, Murai *et al*. demonstrated that PARPis trap the PARP enzymes at damaged DNA sites, and that this interaction is the major cytotoxicity effect compared to inhibition of single-strand breaks caused by PARP inactivation (61) (63).

While the majority of EOC do not have BRCA mutations and are predicted not to respond to PARPis (21), there is evidence that PARPi could be beneficial to patients without BRCA 1/2 mutations. However, the mechanisms through which these responses occur in BRCA-proficient cancers is not clear. A study by Mirza *et al.*, that shows that progression-free survival was significantly longer in patients who received PARPi niraparib regardless of BRCA status, and in 2017, niraparib was approved by FDA as maintenance therapy of recurrent platinum sensitive fallopian tube, or primary peritoneal cancer regardless of BRCA status (56) (64).

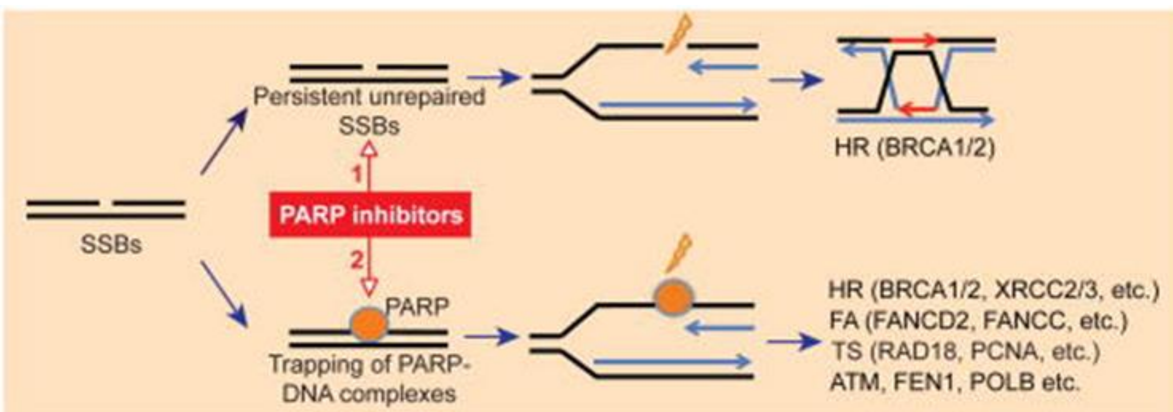

Figure 2.1.3 Dual mechanisms of PARPi

PARPi can lead to persistent unrepaired SSBs through catalytic inhibition (top) and trapping of PARP-DNA complexes (bottom). Both lead to activation of HR and subsequent repair in BRCA proficient cancer. Trapped PARP has increased cytotoxic effect in HR and HR related pathways. Figure from Murai *et al.*, 2012.

2.1.3 BRCAness

One of the possible explanations for observed PARPi efficacy in BRCA-proficient cancers is the presence of mutations in HR-related and other DNA repair genes other than BRCA1/2 that can lead to HRD. This phenomenon is called BRCAness. The term BRCAness refers to the phenotypic traits of a tumor that shows similar characteristics of HRD independent from BRCA mutations (**Fig.2.1.4**) (65).

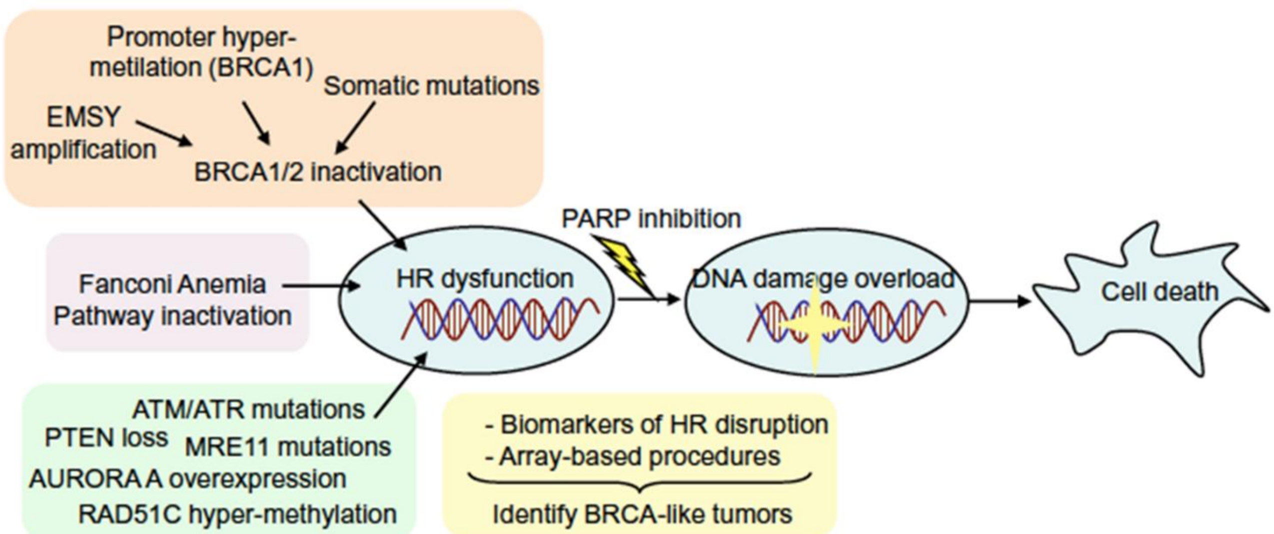

Figure 2.1.4 BRCAness-Utilization of PARPi beyond *BRCA1/2* mutation.

The cartoon shows different genetically or epigenetically altered genes and pathways that lead to HR dysfunction and sensitivity to PARPi in the same manner as BRCA mutant cancers. (yellow) Genetic testing or array-based procedures can be used to identify BRCA-like targets. Figure from Lupo and Trusolino, 2014.

Recent studies show that alteration in genes involved in HR or HR-related pathways, other than BRCA 1/2, such as ataxia telangiectasia mutated (ATM), ataxia telangiectasia and Rad3-related (ATR), CHEK1, CHEK2, deleted in split hand/split foot protein 1(DSS1), RAD51, Nijmegen breakage syndrome protein 1 (NBS1) and the Fanconi anaemia complementation group (FANC) family of genes can lead to HRD or BRCAness and increase sensitivity to PARPi (66). In addition to mutations in these genes, Murai *et al.* also reported that X-ray repair cross complementing 2 and 3 (XRCC2/3), RAD54, H2A histone family member X (H2AX), Ku70 (HRCC6), Ligase IV (LIG IV) deficiency lead to increased sensitivity to PARPi (61). Nonetheless, PARPi activity appears to involve other mechanisms in addition to the well-known role in HRD and PARP trapping. This includes downregulation of other DNA repair pathways factors such as transcription coupled DNA repair (TCR) proteins, UV-damaged DNA-binding protein 1 (DDB1) and Xeroderma pigmentosum group A (XPA)-binding protein 2 (XAB2) that currently do not have known involvement in HR repair, but could also increase sensitivity to PARPi treatment (67).

Importantly, as PARPi treatment is currently offered to a small proportion of EOC patients that are BRCA1/2 mutation or BRCAness positive, the majority of patients will not be responsive to this treatment strategy. Therefore, the current quest among many scientists is to expand the use of PARPi for BRCA-WT or HR-proficient (HRP) EOC and other cancers by inducing BRCAness in non-BRCA mutated patients. Recent studies have demonstrated pharmacologic induction of BRCAness in multiple cancers including EOC (68). In particular, pharmacological targeting of epigenetic pathways has been shown to Induce of BRCAness (**Fig.2.1.5**). Thus, combining PARPi with drugs that can potentially induce BRCAness have been in the forefront of PARPis preclinical research.

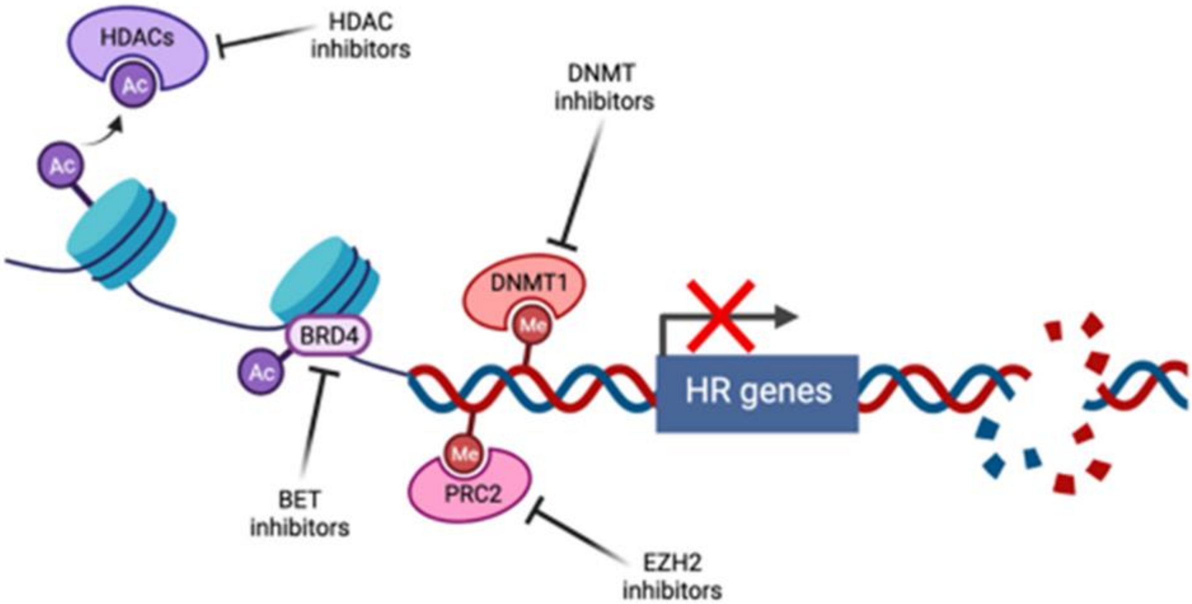

Figure.2.1.5 Targeting epigenetic pathways lead to BRCAness.

Histone deacetylation (HDAC) activity is blocked due to the histone deacetylase inhibitors (HDACi), leading to transcriptional repression. Bromodomain and extraterminal (BET) inhibitors prevent BRD4 to acetylate promoters, including the homologous recombination (HR) genes RAD51 and BRCA1. DNA methyltransferase (DNMT) and enhancer of zeste homolog 2 (EZH2) inhibitors alter DNA double strand break repair gene expression. HR genes expression is prevented due to described events and lead to induction of the BRCAness. Figure from Abbotts *et al.,* 2022.

2.1.4 Combining PARPis with epigenetic therapy

Effects of combining PARPis with epigenetic drugs has been the focus of research in the Rassool laboratory (60) (69) (70) and others for the last several years (71-73). Numerous studies have been performed with PARPi in combination with epigenetic drugs, DNA methyltransferase inhibitors (DNMTi), such as azacitadine (AZA) or decitabine (DAC). In a study conducted by Muvarak *et al*., DNMTis were shown to covalently bind DNA and increase trapping of PARP1, which leads to increased DNA damage and cytotoxicity in BRCA-proficient or HRP cancers (**Fig. 2.1.6**) (60).

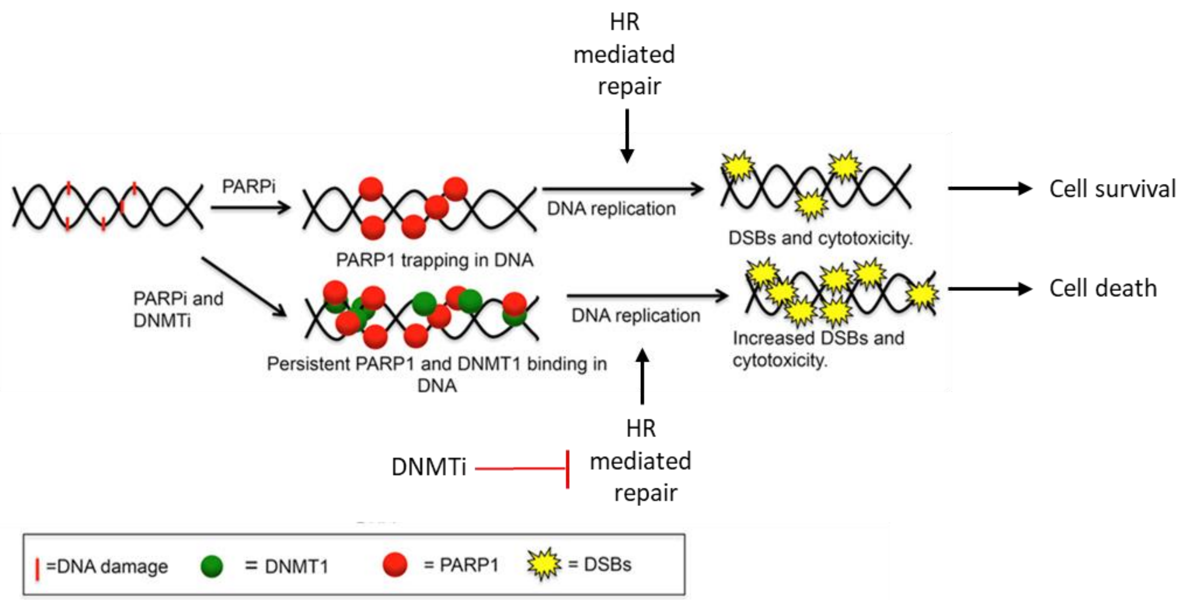

Figure 2.1.6 Model showing epigenetic therapy in combination with PARPi.

PARPi alone trap PARP1 on DNA. DNMTis alone covalently bind DNMTs into DNA and increase PARP1 binding into chromatin. This results in increased DNA damage and cytotoxicity in BRCA wild-type cancer cells. DNMTi inhibits HR mediated repair and leads to increased DNA damage and cytotoxicity. Modified from Muverak *et al*. (2016), Abbotts *et al*. (2019), and McLaughlin *et al* (2020).

In another study, conducted by Pulliam *et al.*, DNMTi guadecitabine was shown to enhance PARPi efficacy in breast and ovarian cancer. This study showed, both *in vitro* and *in vivo*, that combination of DNMTi and PARPi is effective regardless of the BRCA status. In addition, they suggest that increased accumulation of reactive oxygen species (ROS) promote PARP activation, and in a cAMP/PKA-dependent manner sensitize cancer cells to PARPi (73).

2.1.5 Combining PARPis with immune checkpoint inhibitors

Over the past decade, the success in treating variety of cancers, such as melanoma, non-small lung cancer, bladder cancer, head and neck carcinoma and Hodgkin lymphoma, rapidly increased with utilization of monoclonal antibodies that block immune checkpoints

(74) (75). As mentioned in Chapter 1, the immune system encompasses innate and adaptive immunity. For example, dendric cells, macrophages, neutrophiles, natural killer cells (NK), eosinophiles, basophiles and mast cells are part of innate immune system, that further activate adaptive immunity that consists of B lymphocytes, T lymphocytes and cytotoxic T lymphocytes to destroy cancer (76). The literature shows that NK and T lymphocytic cells play the most critical role in identifying and killing cancer through a process called cancer immunosurveillance. The concept of cancer immunosurveillance represent immunological mechanism in which cells with somatic mutations or other defects are eliminated from the system (77). In part, this concept explains why cancer does not occur more often at a younger age, considering that different reasons, such as improper DNA repair, or random somatic mutations continuously occur during the entire lifespan. Instead, cancer cells are detected by NK cell receptors that recognizes MHC class I molecule on a cancer cell or by CD8+ T lymphocytes that recognize tumor antigen and kill cancer (78). However, cancer cells often escape immunosurveillance by causing an obstruction to the immune cells ability to detect and destroy a tumor and finding a solution how to prevent this from happening in a highly active areas of research.

In recent years, it was discovered that proteins found on the surface of T cells, called Programmed death-1 PD1/PDL1 and cytotoxic T lymphocyte antigen-4 CTLA-4, play an important role in enabling some cancer cells to escape immunosurveillance. These checkpoint proteins have an ability to inhibit or stimulate T cells from attacking cancer cells (79). For example, PD1/PDL1 have inhibitory effect on T cell activation, and tumors can exploit this mechanism to escape T cell immunosurveillance by expressing PD1 on their surface and diminish the signal for T cell activation (80). An *in vivo* study conducted by Latchman *et al*. shows that PDL1 on T cells and antigen presenting cells (APC) inhibit T cells response and lead to T cell tolerance (81). This group compared CD4+ and CD8+ T cell response between generated PDL1 deficient mice and wild type mice, and observed that the response was significantly increased in the PDL1 deficient mice. In addition, *in vitro*, they observed that CD4+ T cells produced more cytokines than wild type, which demonstrates involvement of PDL1 in inhibiting APCs and T cells. This and other studies that reported importance of immune checkpoints proteins in T cell function led to FDA approval of the immune check point inhibitors therapy (ICI) ipilimumab in 2011, and the number of available and approved ICI is expanding (82). Immune check point inhibitors therapy addresses the problem of cancer escaping immunosurveillance, since these inhibitors restore anti-tumor immune response by blocking checkpoint proteins from sending a signal to inhibit T cells (82).

Unfortunately, ICIs are not effective as a single agent therapy in EOC, which suggests a possibility of combining it with other drugs in order to increase efficacy and decrease resistance. A recent study performed by *Jiao et al.* demonstrated that PARPis in combination with ICI enhanced ICI efficacy (**Fig.2.1.7**). This study found that PARPis upregulated PDL1 in both breast cancer cell lines and mouse models and led to increased efficacy of anti-PDL1 when combined with PARPis (83).

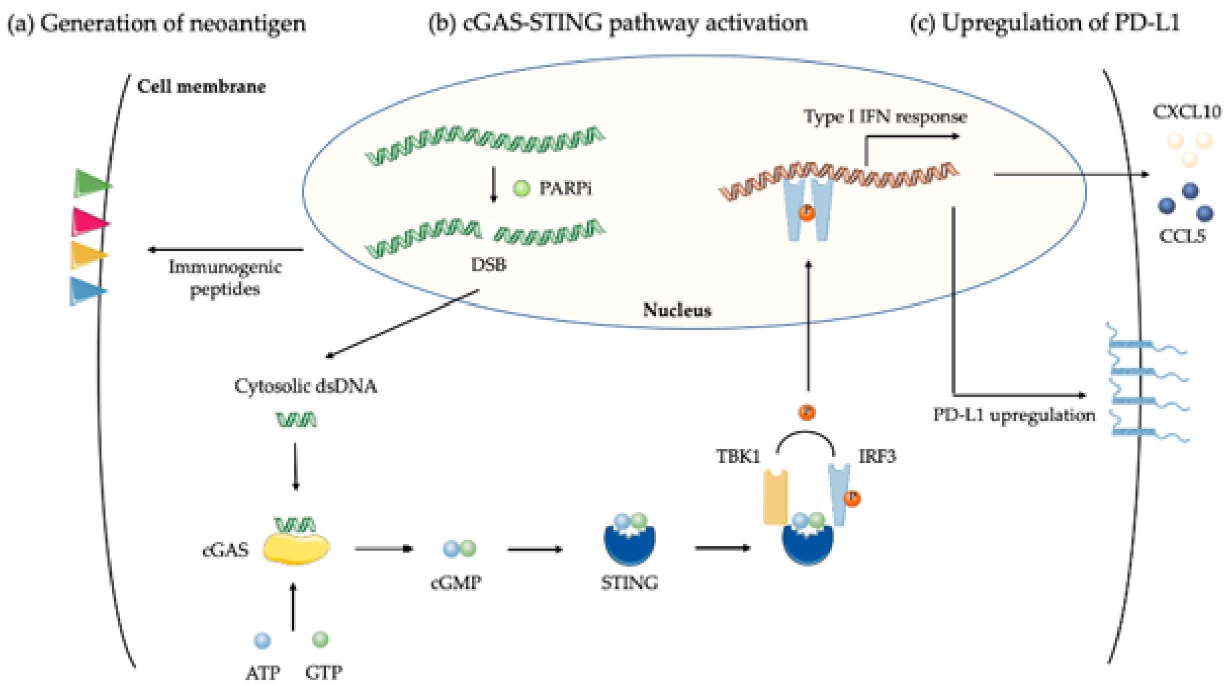

Figure 2.1.7 PARPis enhance ICI therapy in cancer treatment.

The schematic model of how PARPis enhances and promotes re-sensitization to ICI therapy. PARPi causes double-strand breaks that leads to increasing neoantigen load on tumor cell surface and accumulation of cytosolic dsDNA that will lead to stimulator or interferon genes (STING) pathway activation, in which type I interferon (IFN) response will be generated. This Type I IFN response will lead to both recruitment of T cells and upregulation of PDL1expression on the surface of the cell that will prime cell for ICI binding. Figure from Peyraud and Italiano, 2020.

In addition to promoting PDL1 expression on cells, PARPis also regulate the tumor microenvironment through other cellular mechanisms, such as increasing genomic instability and immune pathway activation (84). As mentioned above, the primary mechanism of PARPis in BRCA-deficient cells leads to cancer death through synthetic lethality, due to increased genomic instability in cancer cell. However, this is just one of the mechanisms of PARPi. Recent research shows that due to unrepaired dsDNA, misrepair and aneuploidy, DNA fragments may accumulate in the cytosol in the form of dsDNA or micronuclei that can activate immune signaling through neoantigen formation or through cGAS-STING pathway (85). STING activation is a key pathway for innate immune activation. As discussed earlier in chapter 1, STING activation is initiated by binding of cytosolic dsDNA to cyclic GMP–AMP synthase (cGAS) that will catalyze synthesis of cyclic GMP–AMP (cGAMP) that will further bind to STING. STING will than activate IκB kinase (IKK) and TBK1, which are crucial for STING phosphorylation and consequently, IRF3 recruitment. Due to phosphorylation, IRF3 will dimerize and enter the nucleus and activate expression of inflammatory genes (85).

To test the hypothesis that PARPis cause dsDNA accumulation in the cytosol and STING activation, Pantelidou *et al*. compared KB1P-G3 and KB1P-G3 BRCA-deficient cell line derived by immunocompetent genetically engineered mouse model of TNBC. They measured cytosolic DNA, evaluated phosphorylation of TBK1 and IRF3 and found that PARPi treatment in BRCA-deficient cell lines caused accumulation of dsDNA and further activated the STING pathway (86). Similar results were obtained in another study performed by Staniszewska *et al*. which showed *in vitro* activation of the cGAS-STING pathway after the treatment with dsDNA or cGAMP. They also observed similar results in patients treated with PARPi in the phase 1/2, basket trial of ICI durvalumab in combination with olaparib in solid tumors (MEDIOLA clinical trial; (87) (88)). This is a very important finding that shows translation and validation of preclinical findings in the clinic. RNA sequencing data from MEDIOLA patient biopsies before and after treatment showed that four weeks treatment with 300mg of olaparib caused upregulation of both the STING and IFN 1 pathways (88).

In summary PARPis have great potential beyond its application in BRCA-deficient cancers. Candidate combinatorial agents can enhance particular mechanisms of action in cancer cells and can guide development of optimal therapy strategies for OC and other cancers.

Chapter 2.2. DNMTI therapy and reprograming the epigenome in EOC

Ever since 1942, when Conrad Waddington first defined epigenetics as a development process between genotype and phenotype, and presented his model on epigenetic landscape, it has received increased attention in the biology field (89) (90). With new discoveries, the definition of epigenetics changed over time, and currently it is described as “the study of mitotically and meiotically heritable changes in gene function that cannot be explained by changes in DNA sequences” (90). Indeed, modern science has much evidence that epigenetic changes regulate gene expression and dictate various biological outcomes, including cancer. These epigenetic changes are possible through processes of DNA methylation, histone modification, microRNA (miRNA) interference, and nucleosome positioning (91, 92), however the most studied and best described epigenetic process among them is DNA methylation.

2.2.1 DNMTi mechanisms

As mentioned in Chapter 1.3, DNMTis have been developed that can reverse DNA methylation and transcriptionally activate epigenetically silenced genes (93). The first generation of DNMTis, nucleoside inhibitors azacytidine (AZA), decitabine (DAC) and the second generation DNMTi guadecitabine (GDAC) are cytidine analogs in which the carbon atom is replaced with nitrogen atom at 5th position in the pyrimidine ring. After the uptake of the drug, AZA is converted to azacytidine triphosphate that incorporates into RNA, and 5-aza-2′-deoxycytidine triphosphate that incorporates in the DNA during the replication. DAC and GDAC, in the active triphosphate form, on the other hand, are exclusively incorporated in the DNA (94). GDAC also has improved stability, as the drug is more resistant to deamination (95). New DNMTis that non-covalently trap DNMT1 and prevent it from binding cytidine on the DNA have also been developed (30). Currently, only AZA and DAC are FDA approved for acute myeloid leukemia (AML), high-risk myelodysplastic syndrome (MDS) or chronic myelomonocytic leukemia (CMML). Various studies show that DNMTis, as a single therapy agent used for AML and MDS, restore TSG function, and significantly increase response rates and survival compared to supportive care (96). However, high doses of DNMTi can cause renal toxicity, and central nervous system (CNS) toxicity, such as coma, myalgias, and altered mental state (97). This has led scientists to decrease DNMTi doses that could possibly expand DNMTi therapy application. Lower doses of DNMTis have led to more effective treatments in MDS and AML (98). Efforts are also underway to determine correct dosing paradigm for treatment of solid tumors (99).

2.2.2 Low doses of DNMTis reprogram the epigenome

Investigations, of the effects of low doses of DNMTis in cancer have also led to elucidation of new mechanisms of DNMTis that can lead to reprograming of the cancer transcriptome (38) (69). A study conducted by Tsai *et al*, showed that low doses of DNMTis in both liquid and solid tumors produce an anti-tumor memory response, and as such could cause changes in gene expression that can affect many processes in cancer pathways (**Fig. 2.2.1**) (38). The Baylin group treated breast cancer cell lines with three different nanomolar doses of DAC for just three days and injected them into untreated nonobese diabetic/severe combined immunodeficiency (NOD/SCID) mice. Results showed that low doses of DAC reduced tumor burden in serial transplantation experiments (**Fig. 2.2.2**). Surprisingly, they found that the lowest dose of DAC was directly proportional with the largest reduction in size of the tumor. In addition, they observed the ability of DNMTis to target the DNA methylation process, altering gene expression and ultimately change or reprogram multiple cancer pathways in the Hannahan and Weinberg cancer wheel (100). Revealing this new ability of low non-toxic nanomolar doses of DNMTis to alter gene expression suggests that this drug could potentially be a candidate for combination therapy with other agents, including DNA repair inhibitors, such as PARPis, or perhaps, ICIs.

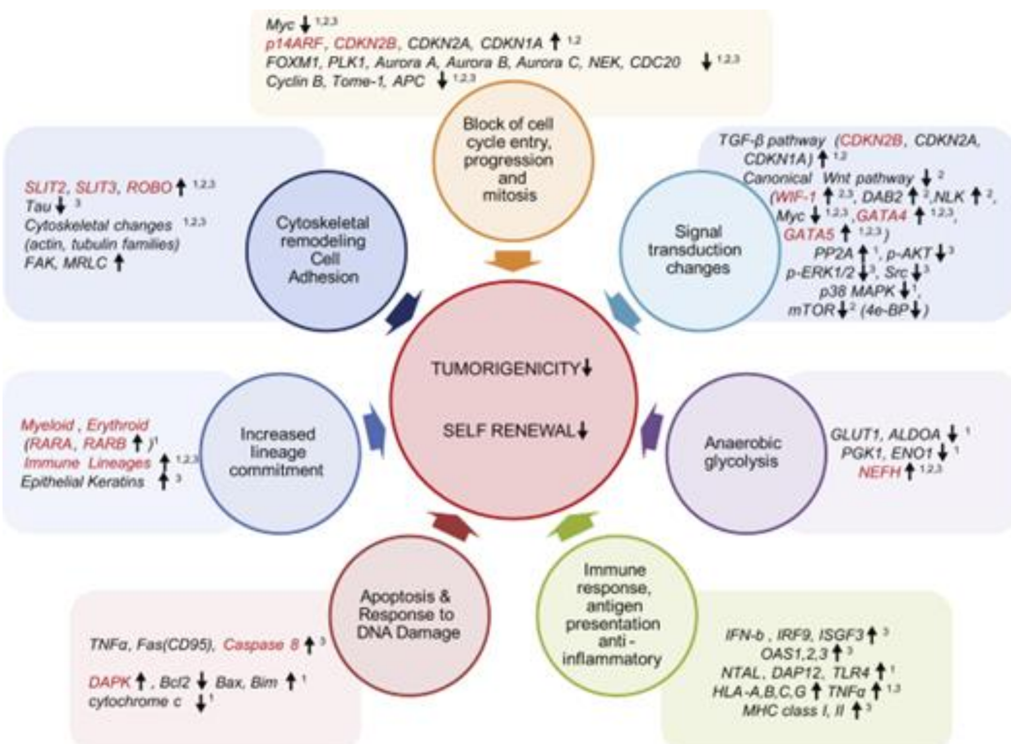

Figure 2.2.1 Low doses of DNMT1 lead to changes in gene expression involved in different pathways.

Schematic representation of different pathways modulated by DNMTi in cells. (black) Genes which change in expression are not related to promoter methylation. (red) Genes with promoter hypermethylation and increased expression. Cell lines are indicated in superscripts. Altered pathways shown on the graph lead to decreased tumorigenicity and self-renewal. Figure from Tsai *et al*, 2012.

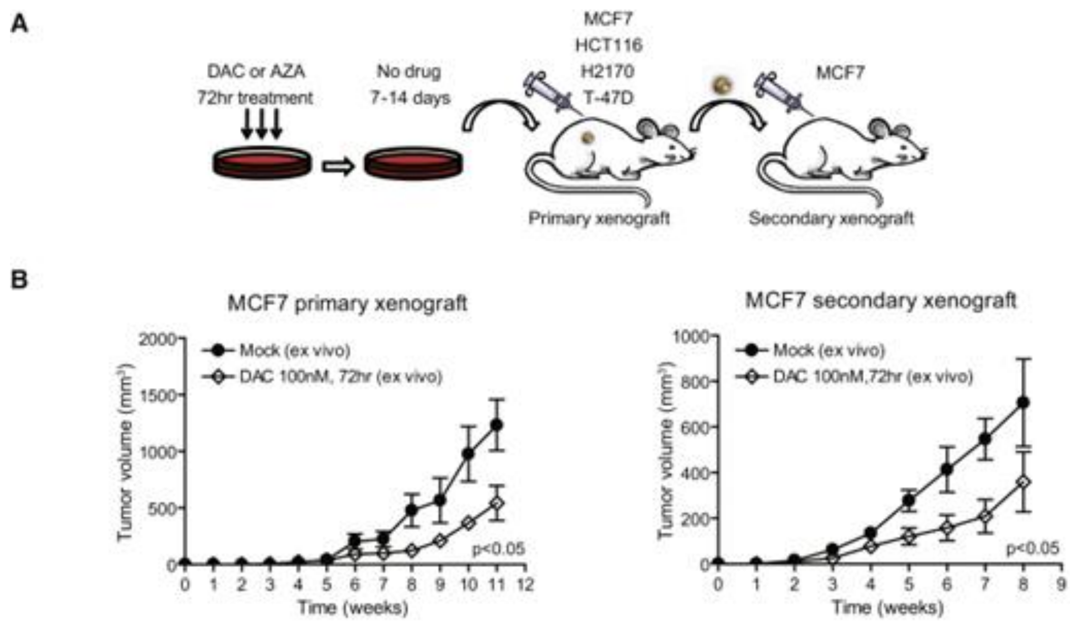

Figure 2.2.2 Low doses of DNMTi treatments induce an anti-tumor memory response.

(A) Schematic presentation showing breast cancer cell lines treated with low doses of DNMTi being injected into NOD/SCID mice for generation and further serial transplantation of xenografts (B) Breast cancer cell lines xenografts pretreated with DAC. Primary (left) and secondary (right) xenograft. Figure from Tsai *et al*., 2012.

The Baylin group subsequently demonstrated that low-dose DNMTis can activate transcription of epigenetically silenced ERVs, leading to increased cytosolic dsRNA that activates IFN signaling (45). The groundbreaking study conducted by Chiappinelli *et al.* reveals yet another mechanism of action of DNMTis (45). This group named this phenomenon "viral mimicry" (**Fig.2.2.3**). As mentioned earlier, the term viral mimicry is used to explain the similarity between a viral pathogen and cancer cell antiviral response due to endogenous stimuli. In this study, Chiappinelli *et al*. showed that DNMTi upregulates immune signaling in OC by upregulating ERV genes transcription and further activating IFNβ and interferon stimulated genes (ISG). They treated OC cell lines A2780 and TykNu for 7 days but observed upregulation of the Type I interferon pathway after just 4 days of the treatment with AZA. In addition, they observed that following AZA treatment

ERVs were upregulated 2.5-fold in OC cell lines. Hand-in-hand with this observation, they discovered that cytosolic sensors for both RNA and DNA were upregulated, which led them to conclude that DNMTis activate ERVs through hypomethylation and further immune signaling activation.

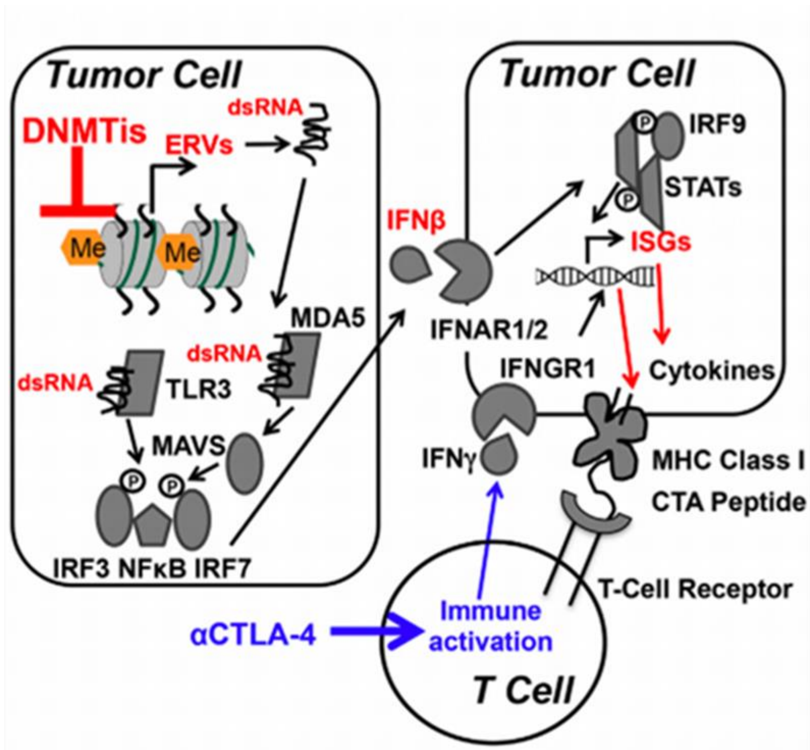

Figure 2.2.3 DNMTi demethylate ERVs and activates immune signaling.

Once DNMTi demethylate ERVs, ERVs will be transcribed and present in the cytosol. DsRNA sensors, MDA5 and TLR3 will recognize dsRNA and activate MAVS that will further signal for IFN activation. Figure from Chiappinelli *et al*, 2016.

PARPis have also been reported to act as viral mimics, increasing DNA damage and cytosolic dsDNA (101) (63). Importantly, the study of Tsai *et al*. also led ~~to~~ the Rassool lab to address the possibility that low-dose DNMTis could also reprogram DNA repair pathways, potentially leading to a BRCAness effect in BRCA-proficient or WT cancer cells. In 2019, Abbotts *et al.,* demonstrated that low-dose DNMTis in BRCA-proficient, non-small cell lung cancer (NSCLC) lead to decreases in expression of DNA repair genes involved in multiple DNA repair pathways, including HR and HR-related pathways, that in turn lead to HRD and sensitization to PARPis. Of note, another DNA repair pathway that was decreased was nonhomologous end-joining (NHEJ) that further led to increased sensitivity to radiation therapy (70). Following on this study to focus on potentially inducing BRCAness with low-dose DNMTis in BRCA-proficient TNBC and OC, McLaughlin *et al.*, made two important discoveries. First, they showed that DNMTis downregulate multiple DNA repair genes, including HR-related Fanconi anemia gene FANCD2, and thus leads to impaired HR and increased cytotoxicity of PARPi talazoparib in BRCA-proficient OC and TNBC. Second, in the same paper Mclaughlin *et al.* reported that combining low-dose DNMTi AZA with PARPi talazoparib also increases cytosolic dsDNA that activates the IFN/inflammasome-dependent STING signaling pathway (69). They named the effect of this drug combination, pathogenic mimicry response (PMR). This IFNαβ and TNFα/NF-κB signaling in turn downregulates FA/HR DNA repair-associated genes, inducing a BRCAness effect (**Fig.2.2.4**).

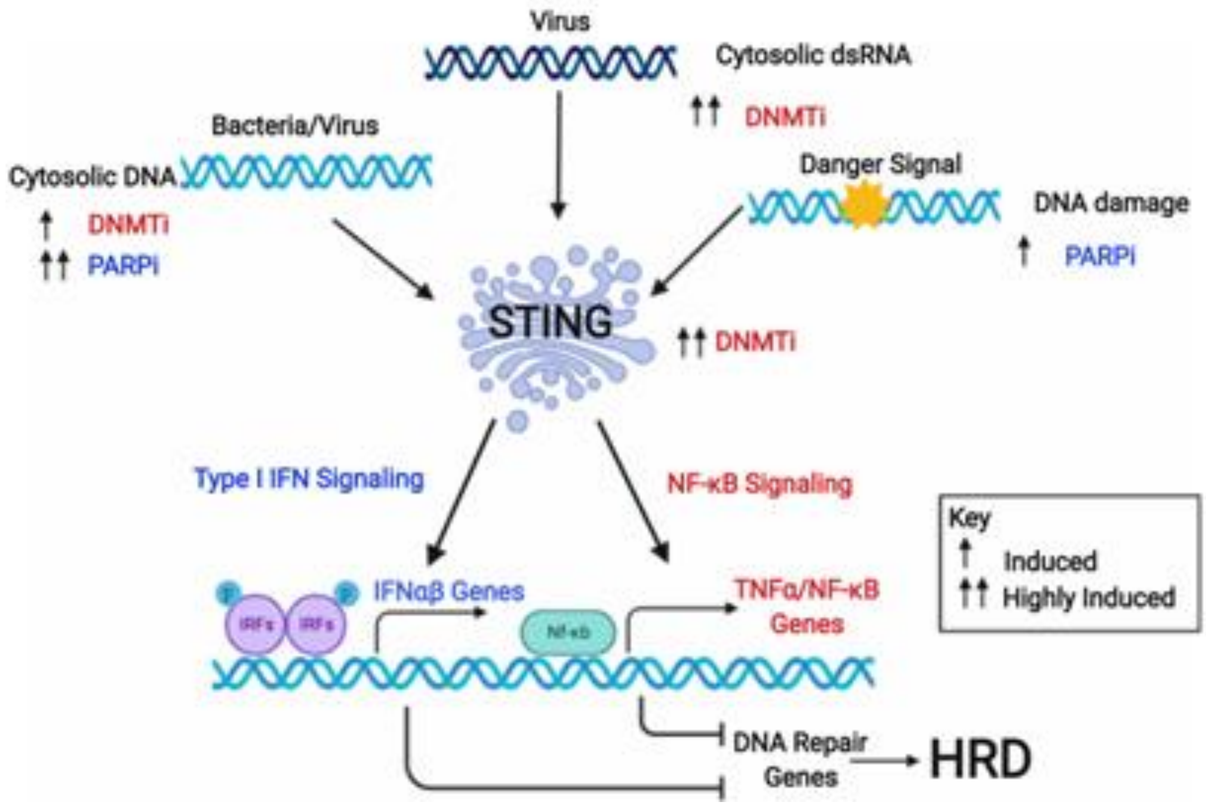

Figure 2.2.4 Schematic model of inflammatory response leading to HRD in TNBC and OC.

DNMTi in combination with PARPi increase cytosolic dsDNA that activate STING signaling pathway. This activated response is followed by transcriptional increase in IFNαβ and TNFα/NF-κB signaling that downregulate FA/HR DNA repair-associated genes in a STING pathway. The BRCAness is achieved through viral mimicry that increase sensitivity to PARPi in the BRCA proficient TNBC and OC. Figure from McLaughlin *et al*., 2020.

2.2.3 Combining DNMTi with immune checkpoint inhibitors

As mentioned above, the ability to affect gene expression of different cancer pathways, more specifically, immune pathway, suggested that DNMTis are great candidates for combination therapy with ICI. As described before, ICI therapy has demonstrated excellent responses in many cancer patients, however, the problem addressing its resistance and limited efficacy in some cancers, including OC, is an ongoing process. A study performed by Chen *et al*. showed that combination therapy of guadecitabine and pembrolizumab (anti-PD-1 antibody) induced antitumor immunity in OC (102). In this non-randomized, open-label, phase II clinical trial guadecitabine was given 4 consecutive days prior to administering pembrolizumab in recurrent platinum resistant OC patients. The results show that DNA hypomethylation was detected in both peripheral blood mononuclear cells (PBMC) and tumors, and further led to upregulation of cytokines transcripts IFNG, *CXCL9* and *IL21*, which suggests that DNA hypomethylation reactivated pathways involved in immunity. Importantly, they detected upregulation of PD-L1 on tumor cells which prime cells for more effective ICI therapy (102) In addition, Luo et al. discovered that combination therapy with anti-PDL1 ICI and DNMTis in breast cancer increase the cytotoxic CD8+ T cell response (103) They found that in addition to DNMTi treatment upregulating the major histocompatibility complex class I (MHCI) expression that leads to antigen presentation enhancement, it also increases chemokines expression and recruitment of CD8+ cells. In addition, the same study observed activation of NFκB signaling and suggested that this result may be due to increased ERV dsRNA expression, which was originally demonstrated by Chiappinelli *et al*. (45).

Nonetheless, this was a landmark study expanding the viral mimicry mechanisms for agents other than DNMTi. In 2021, two clinical studies approached this mechanism from a different angle. Wilkins *et al.* showed that viral mimicry can be achieved in response to neoadjuvant radiotherapy in rectal cancers (46). They analyzed gene expression profiling in 53 pre- and post-radiotherapy rectal cancer patients in order to explain better outcomes due to neoadjuvant radiotherapy. The result of this study shows that a total of 40 immune genes were significantly upregulated after the therapy, which suggests a reprogramed tumor microenvironment as well as viral mimicry. In another clinical study performed by Liu *et al.*, viral mimicry was achieved through nanotechnology, in which RNA is incorporated in a special nano capsule that activate viral RNA sensors and upregulate type I interferon and immune cell production (47).

However, many unanswered questions remain with regard to viral mimicry induced by DNMTis. For example, since ERV activation triggered signaling through MAVS and retinoic acid-inducible gene I (RIGI), does this suggest a more prominent role for the mitochondria in IFN signaling? If so, what are the changes in mitochondrial signaling that lead to the DNMTi-induced immune response? Understanding mechanisms of anti-viral signaling may lead to better understanding of viral mimicry that will result in better therapeutic strategies involving these anticancer viral mimics.

Chapter 2.3 Antiviral signaling, Mitochondria and ZNFX1

As introduced, in previous chapters, anti-cancer agents, such as PARPi and DNMTi treatment alone and in combination mimic anti-viral signaling that has evolved in cells to combat pathogenic infections (45) (69). This antiviral response involves activation of

IFN/inflammasome signaling leading to innate immune responses against the pathogen. The next section will discuss anti-viral signaling pathways and the key role the mitochondria play as a gateway to IFN/inflammasome signaling.

Cellular antiviral defense mechanisms are a critical component of the host response to intracellular pathogen infection, wherein recognition of pathogen-associated molecular patterns (PAMPs) or damage-associated molecular patterns (DAMPs) by pattern-recognition receptors (PRRs) triggers downstream signaling cascades to stimulate IFN and inflammatory responses (104). An important PAMP is viral nucleic acid, which is recognized by PRRs including Toll-like receptors (TLRs), RIG-I-like receptors (RLRs), and cytosolic DNA sensors such as cGAS, and acts a major trigger for a type I interferon (IFN)-mediated antiviral immune response (105). Cytosolic dsRNA is primarily sensed by RLR family members RIG-I (106) and MDA5 (107) which share two RNA domains required for RNA sensing (a central DExD/H box RNA helicase domain and a C-terminal domain repressor), and two N-terminal caspase activation and recruitment domains (CARDs) responsible for activation of downstream signaling (108),

Mitochondrial antiviral signaling protein (MAVS), located in the mt outer membrane, is a key CARD-containing adaptor protein essential for RLH-mediated antiviral signaling. Overexpression of MAVS results in the potent induction of type-1 interferons including IFN-b and IFN-a (109). Furthermore, mice lacking MAVS exhibit severely reduced type-1 interferon production in response to several RIG-I and MDA-5 mediated viral infections (110). Seth et al. (2005) discovered that MAVS localizes to the mitochondrial outer membrane via its C-terminal transmembrane domain. Mutation of the transmembrane domain or the targeting of MAVS to other cellular membranes such as the endoplasmic reticulum completely abolished RLH signaling (111). MAVS is thus the critical mediator of downstream IFN responses, activating both type I IFN transcription via the TBK1-IRF3/7 axis, and inflammatory cytokine release via IKK-NFκB (104).

Currently, there are three different pathways through which mitochondria activate innate immunity (**Fig.2.3.1**). The first known pathway is activated as a result of a mitochondrial stress, in which mtDNA nucleotides are sensed by toll-like-receptor 9 (TLR9) that further activate downstream pathway IFN/NFkB (112). A study performed by Marques *at al* showed that chemokines and mtDNA play a significant role in systemic inflammation. They tested mice with liver injury and found that both mtDNA and CXR2 chemokines were elevated, suggesting possible spread of inflammation to other organs. Indeed, in mice lacking TLR9 the inflammation spread to lungs, which was opposite observation from TLR9 wild type mice (113). A second pathway that involves activation of immunity in response to mtDNA is achieved through nod-like receptor protein 3 (NLRP3) inflammasome. NLRP3 is the best known inflammasome that directly targets mtDNA and leads to secretion of IL18 and 1L1b (112). A study conducted by Zhou *et al.* shows that the NLRP3 inflammasome is generated by damaged mt that produce high ROS. This group suggested that NLRP3 inflammasome senses mt dysfunction and starts the inflammation activation by recruiting caspase 1 to secrete IL18 and IL1b from their pro states (114). It is important to emphasize that the NLRP3 pathway is also activated in response to mtDNA leakage from Bcl-2-associated X protein (BAX)/ BCL2 Antagonist/Killer 1 (BAK) macropore. A study conducted by McArthur *at al.* showed that mtDNA appeared on the surface of mt, can be present in the cytosol as a result of BAK/BAX macropore formation, and can possibly activate immune signaling through

NLRP3. They used a combination of different microscopy, such as cell lattice light sheet, 3D structure illumination, and correlative light electron microscopy to confirm the loss of mitochondrial membrane integrity (115). Lastly, the third pathway of mt involvement in immune response best known in the literature is through the STING pathway (112). This pathway, as earlier described, activates IFN and NFkB signaling through detection of dsDNA in the cytosol, and recent evidence shows that mt DNA is essential in activating this pathway (116). In this study, Aarreberg *at al.* showed that cytokine 1L-1b upregulates inflammatory genes by causing mtDNA to leak into the cytoplasm that will activate the STING pathway. They investigated whether MAVS, STING or translation intimin receptor (TIR) domain-containing adaptor protein inducing interferon beta (TRIF) are involved in TBK1/IKKg activation of IRF3 and found that macrophages with STING knockout did not have TBK1 activation. However, *MAVS* or *TRIF* genes knockout responded the same as wild type. In addition, they used cells with *cGAS* and *STING* gene knockouts, treated cells with Il1b and observed a loss of pIRF3 compared to control on both RNA and protein level.

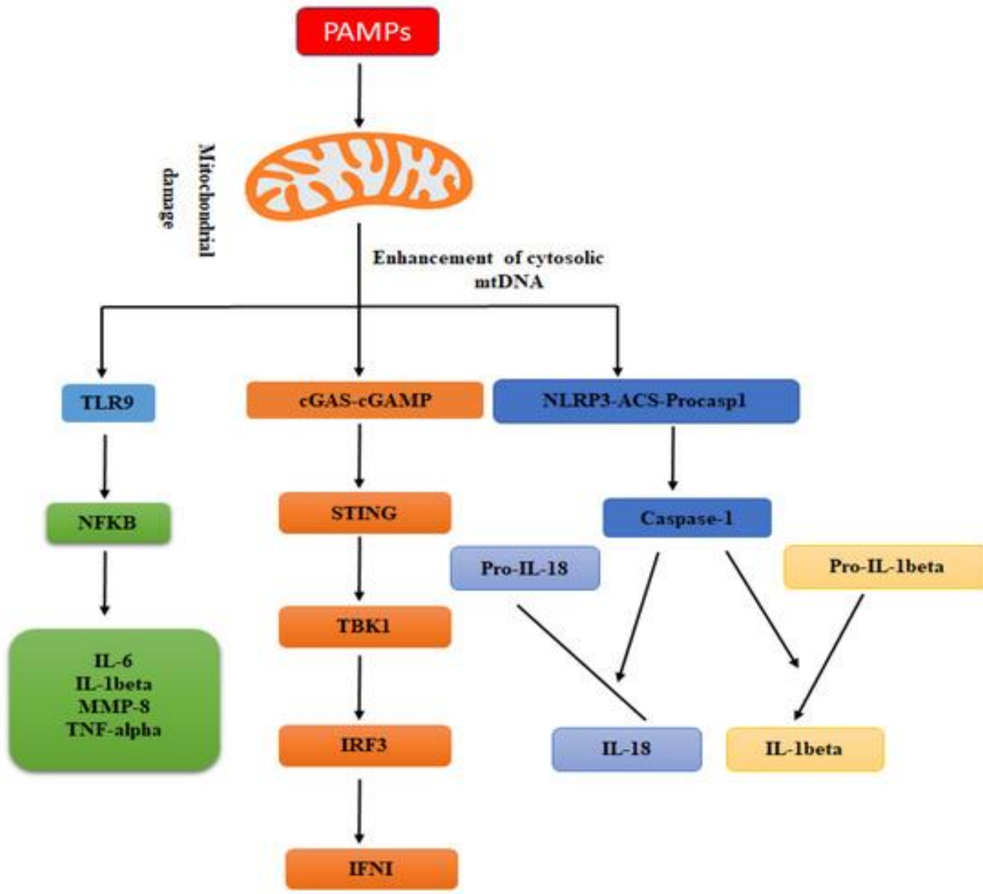

Figure 2.3.1 Schematic diagram showing different pathways of innate immunity activation due to mtDNA stimulation.

(Left) Cytosolic mtDNA stimulates inflammatory cytokines through activation of TLR9. (Middle) Cytosolic mtDNA activates STING pathway through cGAS activation that leads to Type I interferon secretion. (Right) mtDNA stimulates the NLRP3 inflammasome and activates caspase-1, which is involved in the cleavage of pro-IL-18 and pro-IL-1β. Figure from Kausar *et al.*, 2020.

Importantly, mt involvement in immune stimulation became clearer during the pandemic of the coronavirus disease 2019 (COVID-19). One of the first studies on The Severe Acute Respiratory Syndrome Coronavirus 2 (SARS-CoV-2) discovered many important characteristics of the disease and offered to the public valuable information on potential diagnostic and treatment strategies. Butler et al. published in Science 2022, initially performed the study to better understand the impact and characteristics of the disease, and as a result this study interestingly identified a significant mt involvement in response to COVID-19 (117). This group performed a large-scale shotgun metatranscriptomics on 732 COVID-19 clinical samples (from nasopharyngeal swab specimens and oropharyngeal swab lysates) and observed the viral characteristics in infected patients. Based on the results, they evaluated the viral genetic characteristics and linked them to the host's gene expression responses. In addition, they developed a colorimetric assay as a tool to detect the viral load in the patients and compared it to severity of symptoms and gene expression changes. One of the most remarkable discoveries in this study is that in cases with high viral load, the genes essential for mt function were significantly increased compared to the control. Among the genes upregulated are Cytidine/Uridine Monophosphate Kinase 2 *(CMPK2)*, interferon alpha inducible protein 27 *(IFI27)*, and Z-DNA-binding protein 1 (*ZBP1)*, nuclear genes involved in mitochondrial function and pathways, suggesting an important mitochondrial involvement in the response to the disease. Importantly, the most overexpressed gene in the patients related to mitochondrial function was the little-known Zinc Finger NFX1-Type Containing 1 (ZNFX1) gene (**Fig.2.3.2**).

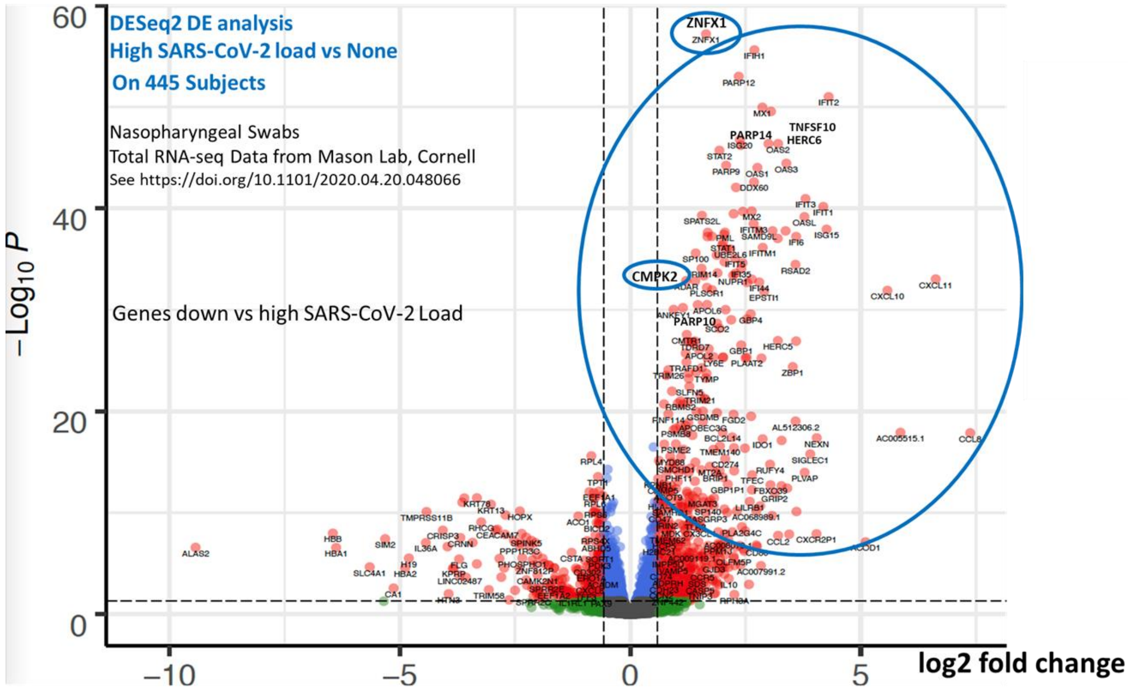

Figure 2.3.2 High SARS-CoV load gene expression.

Volcano plot showing upregulated genes (right of dotted line) and downregulated genes (left of dotted line), compared to genes that do not have change in expression (between dotted lines). ZNFX1 is circled in blue. Figure from Butler *et al*. 2021.

At the time when the Butler *et al.* study was conducted, PubMed listed approximately 40 publications involving ZNFX1, from which the majority was investigating its role in epigenetic inheritance in *C. elegans* (118). Even though the role of this gene in humans was not well known before, in 2020, the trend rapidly changed. A seminal study on the *ZNFX1* gene was performed in 2019 by Wang *et aI.* For the first time, this gene was identified as a dsRNA sensor involved in type I IFN response in the early stage of viral infection (119). A helicase steroidogenic factor 1 (SF1), ZNFX1 binds viral RNA and interacts with the mt localized MAVS protein, promoting the expression of interferon-stimulated genes (ISGs). To show ZNFX1 involvement in activating IFN signaling, Wang *et al.* knocked down *ZNFX1* expression in lung cancer cell lines and infected cells with VSV-eGFP. The flow cytometry results showed that lowering *ZNFX1* expression increased VSV replication and decreased IFN production compared to wild type group. Furthermore, they suggested that ZNFX1 was exclusively activated by dsRNA (**Fig.2.3.3**). This finding, however, was challenged by a study performed by Vavassori *et al.* in 2021 which shows that sensing viruses is not limited by the type of nucleic acid, instead, beside sensing cytosolic RNA viruses ZNFX1 can sense DNA viruses as well (120). Even though Vavassori *et al* observed that ZNFX1 can be activated by both dsRNA and dsDNA, their results agreed with Wang *et al.* that mutation of ZNFX1 does not lead to predisposition to DNA virus infections. Instead, its function can be explained by the observed damage caused by DNA viruses in patients with ZNFX1 mutation is “insufficient resolution of the interferon response to infection and not to excessive viral load”. In addition, Vavassori et al made a remarkable contribution investigating the importance of ZNFX1 mutations in patients.

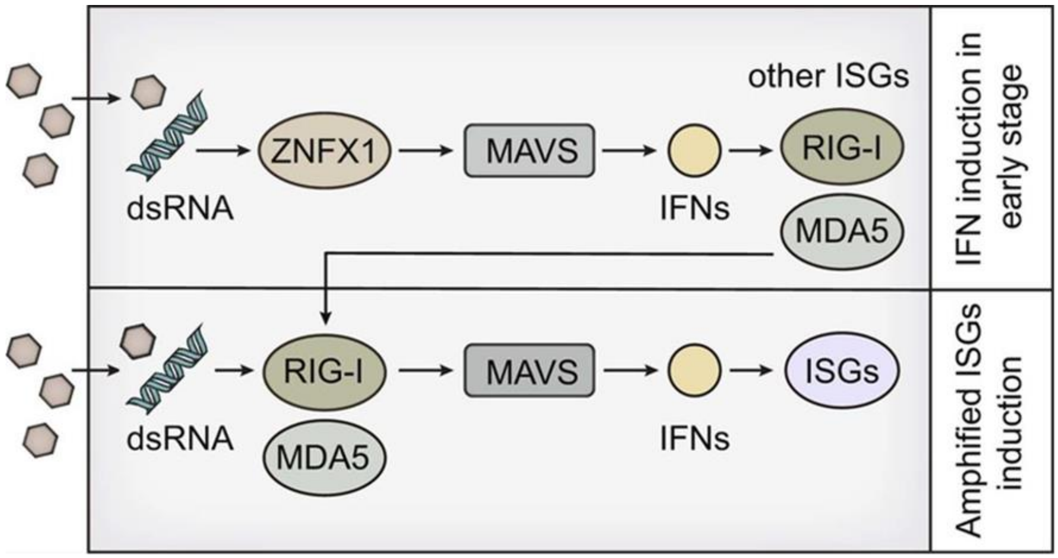

Figure 2.3.3 Schematic representation of cytosolic dsRNA activating immune response.

(Top) Cytosolic dsRNA is sensed by ZNFX1 following MAVS signaling and IFN induction in early stage of viral infection. (Bottom) Cytosolic dsRNA sensed by RIGI and MDA5 activate MAVS and leads to amplified ISGs induction. Figure from Wang *et al*, 2019.

Importantly, it is now known that ZNFX1 deficiency is characterized by susceptibility to viral infection, multiorgan dysfunction and high mortality rate (120). Vavassori *at al.* studied 15 patients with autosomal recessive immunodeficiency and identified deleterious homozygous and compound heterozygous ZNFX1 variants in 13 patients (**Fig.2.3.4**). According to their study, ZNFX1 deficiency is characterized as being between inflammation and immunodeficiency that causes dysfunction of the liver, brain, kidney and lungs. According to another study performed by La Voyer *et al.* deficiency of ZNFX1 gene underlies Mendelian susceptibility to mycobacterial disease (MSMD) or TB with intermittent monocytosis in the four patients from which two suffered recurrent and unexplained episodes of fever, thrombocytopenia, and organomegaly. In addition, the same group show that ZNFX1 is essential for monocyte homeostasis and protective immunity to mycobacteria, and also suggest that ZNFX1 may affect the production of IFN-γ inducing cytokines (121).

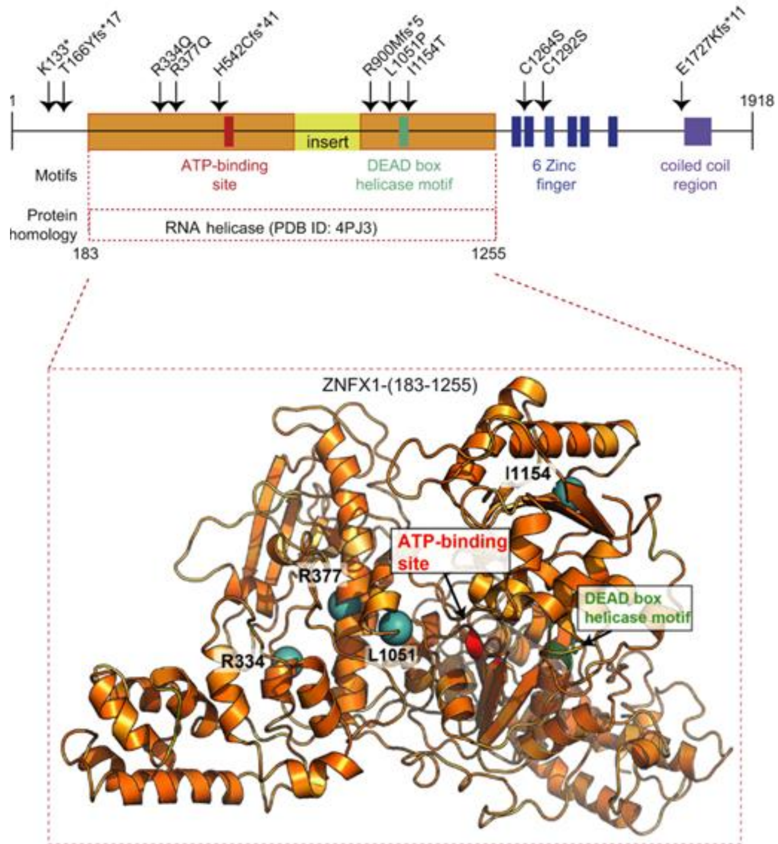

Figure 2.3.4 Model of ZNFX1 showing location of variants.

(Top) Eleven variants in the amino acid sequence of *ZNFX1* six are in the RNA helicase domain (orange) affecting ATP binding site and DEAD box motif. (Bottom) Ribbon diagram showing four missense variants in ATP binding site and DEAD box motif. Figure from Vavassori *et al.,* 2021.

Finally, in 2023, a study that tightly connects mitochondria to COVID offered insight into the importance of studying mitochondrial genes, especially *ZNFX1* and *CMPK2* (122). The study by Guanieri *et al.* confirmed that mitochondrial function is indeed inhibited in COVID patients. They studied 700 nasopharyngeal samples of infected humans and rodents and observed that all five OXPHOS complexes were inhibited in high and medium viral load, while nuclear genes important in mitochondrial function were upregulated. This group was able to follow the progression of the disease by looking at the gene expression in different organs such as liver, lungs, brain, and found that at the beginning of the disease, expression of the nuclear gene *CMPK2* was increasing, suggesting activation of inflammasome with stimulation of mt replication. At the beginning, as well as towards the end of the disease, mitochondrial gene expression in the lungs was not increased, however the high viral load was characterized by significantly downregulated mitochondrial genes expression (122).

Even though in the past 4 years the research conducted in regard to *ZNFX1* discovered important characteristics and function of this gene, much still remains unknown, including its role in cancer cells, including OC. For example, it is not certain whether both dsRNA and dsDNA can activate ZNFX1. In addition, it is not known whether ZNFX1 affects mt function by interacting with mt adaptor protein MAVS that translocate to the mt outer membrane and can lead to alteration of mtROS and mtDNA damage. Hypothetically, ZNFX1 may also act through mt to lead to IFN/inflammasome signaling, because as mentioned before, mt DNA is known to lead to immune signaling activation. Finally, whether a viral mimicry feature of DNMTi can activate ZNFX1 is unclear. Furthermore, if dsRNA, dsDNA can also activate ZNFX1, and PARPi can activate dsRNA, then could a combination of a PARPi with a DNMTi synergistically activate ZNFX1? To investigate these questions in my Ph.D. thesis project, I will test the <u>overall hypothesis</u> that DNMTi and PARPi treatment in EOC triggers mitochondrial dysfunction and mitochondrial DNA (mtDNA) release into the cytoplasm that activates STING-mediated IFN/inflammasome signaling.

This thesis will have the following specific aims:

Aim 1**:** Determine the effects of DNMTi and PARPi combination treatment in inducing mt dysfunction, involving reactive oxygen species (ROS) and DNA damage, leading IFN/inflammasome signaling.

Aim 2: Determine the role of ZNFX1 in the DNMTi and PARPi-induced mt dysfunction leading to IFN/inflammasome signaling.

Chapter 3: Materials and methods

Cell lines

Ovarian cancer (OC) cell lines A2780 and TyKNu were generously gifted from Dr. Stephen Baylin. OVCAR4 OC cell line was a gift from Dr. Kenneth Nephew. A2780 and TyKNu were cultured in RPMI-1640 (Corning), 10% Fetal Bovine Serum (FBS, Sigma), and 1% penicillin-streptomycin (P/S, Sigma). OVCAR4 OC cell line was cultured in DMEM (Gibco), 10% FBS (Sigma), 1% P/S (Sigma), 1% Minimum Essential Medium vitamin solution (MEM, Corning), 1% Non-essential amino acids (Corning). All cell lines were cultured and maintained in 37C incubators with 5% CO2.

Drug Reagents and Treatments in vitro

DNA methyltransferase inhibitor (DNMTi) 5-Azacytidine (AZA, Sigma) was prepared in PBS at 500uM stock solution, stored at -80C and a new aliquot was used for every treatment. A2780 and OVCAR4 were treated with 150nM AZA, and TyKNu was treated with 100nM AZA. Cells were treated with AZA every 24h. PARP inhibitor talazoparib (TAL, Pfizer) was prepared in DMSO at 50mM stock concentration, aliquoted, and stored at -80C. Cells were treated with a new aliquot every 72h. Rotenone, electron transport chain inhibitor in complex I in mitochondria (Invitrogen), was prepared in DMSO at 10uM stock concentration, aliquoted and stored at -80C. Cells were treated with 1uM Rotenone 24h before cell collection for analysis.

RNA Extraction

After 6 days of treatment, total RNA was isolated using NucleoSpin RNA Plus kit (Macherey-Nagel) according to manufacturer protocol.

Quantitative real time PCR (qRT-PCR)

2ug of RNA was converted to cDNA using High Capacity cDNA Reverse Transcription kit (Applied Biosystems). Power Sybr Green PCR Mix (applied Biosystems) was used for qPCR, and process was performed in a CFX384 Touch Real-Time PCR system (BioRad). Genes wer normalized to GAPDH and β-actin. Data presented are the fold change after drug treatment over mock by ΔΔCT method. Primer sequences for qRT-PCR are listed in Appendix: **Table S1**.

Protein extraction and Immunoblotting

After 6 days of treatment, cells were trypsinized (0.25% Trypsyn, Corning), and collected pellets were placed in 1.5ml Eppendorf tubes, and stored in -80C until further handling. Whole cell protein extract: A cocktail made of RIPA buffer (Sigma), 1% phosphatase inhibitor (Thermos Scientific) and 1% protease inhibitor (Thermos Scientific) was used to lyse collected cell pellets. Cells were incubated in RIPA cocktail for 30 min on ice, vertexing every 10 min. Eppendorf tubes were centrifuged at 16,000xg at 4C for 17 min, after which the supernatant was transferred to new prechilled Eppendorf tubes. Mitochondrial protein: Mitochondrial isolation kit (Abcam) was used for extracting mitochondrial protein according to manufacturer protocol. Whole cell extract or mitochondrial protein (20ug) in NuPAGE LDS Sample Buffer with 10% β-mercaptoethanol were boiled for 10 minutes and loaded onto 4-20% SDS-PAGE gel (Bio-

Rad). Polyvinylidene difluoride membranes (GE Life science) used for transfer were blocked at room temperature (RT) with 5% nonfat milk in TBST for 60 min and incubated overnight at 4˚C with antibodies. The following antibodies were used to determine protein abundance: anti-ZNFX1 (1:1000, Abcam, #ab179452), anti-MAVS (1:1000, Abcam, #ab290729), anti-TFAM (1:1000, Cell Signaling, #8076), anti-VDAC (1:1000, Cell Signaling, #4866)., STAT3 (1:1000, Cell Signaling, #4904), NFKB 105/50 (1:1000, Cell Signaling, #12540), NFKB 65 (1:1000, Cell Signaling, #8242) pTBK1 (1:1000, Cell Signaling, #5483), TBK1 (1:5000, Abcam, #ab40676), STING (1:1000, Cell Signaling, #13647), pSTING Ser366 (1:1000, Cell Signaling, #19781), vinculin (1:1000, Cell Signaling, #13907)

Immunofluorescence and proximity ligation assay

After 6 days of treatment, from each treatment group 500,000 cells were plated onto Human Fibronectin Cellware 22mm round coverslips. After 24h, cells were washed three times in PBS supplemented with 1% BSA and 0.1% Triton X-100. Cells were then fixed with 4% paraformaldehyde in PBS for 10 min and permeabilized with PBS supplemented with 50nM NaCl, 3mM MgCl2, 10mM HEPES, 200mM Sucrose and 0.5% Triton X-100 for 5 min at RT and washed twice in PBS supplemented with 1% BSA and 0.1% Triton X-100. Blocking procedure was done at 4C in 10% FBS in PBS overnight. The next day, cells were incubated with Mitotracker green dye for 30 min at 37C and washed three times in PBS. Coverslips were incubated for 1h at 37C with primary antibody: rabbit polyclonal anti human ZNFX1 (1:50 Abcam) and monoclonal mouse anti-MAVS (1:50, Invitrogen), and washed in PBS supplemented with 1% BSA and 0.1% Triton X-100. The secondary antibody (Affinity purified antibody Dylight 488 – green, anti- rabbit, 1:200; and Dylight

594- red, anti-mouse, 1:200) were incubated for 45 min at RT and washed three times in PBS supplemented with 1% BSA and 0.1% Triton X-100. Coverslips were mounted on slides using ProLong Gold Antifade Reagent with DAPI. Images were examined using a Nikon fluorescent microscope Eclipse 80i (100×/1.4 oil, Melville, NY).

For proximity ligation assay, coverslips were blocked in 5% goat serum in PBS, then incubated with primary antibodies against ZNFX1 (rabbit, 1:50, Abcam), MAVS (mouse, 1:50, Invitrogen), or dsRNA (mouse, 1:50, EMD Millipore). Duolink in situ proximity ligation assay was performed per manufacturer protocols (Sigma), and coverslips were mounted on slides using ProLong Gold Antifade Reagent with DAPI. Images were examined using a Nikon fluorescent microscope Eclipse 80i (100×/1.4 oil, Melville, NY).

Reactive oxygen species (ROS) detection

Therapy induced ROS: A2780, TyKNu , and OVCAR4 OC cell lines were plated at a density of 100K/well in 6 well plate, and treated with AZA, TAL and combination of two drugs for 6 days. In addition, the cells were treated with 1uM Rotenone on the fifth day. After 6 days of treatment the media was removed from the wells, cells were washed with 1XPBS, and trypsnized (0.5mL 0.25%, Corning) for 3 min at 37C. Trypsin was neutralized with 1.5mL wormed media. The well content was mixed by pipetting up and down and 0.5mL of each well content was placed to 5 tubes (Falcon) labeled to represent each treatment group, as well as non-treated cells and rotenone as a positive control. The compound mitoSOX (Invitrogen) was added in concentration of 5uM to each of the 5 tubes and incubated for 30 min at room temperature. The same procedure was applied for staining with Dihydroethidium (DHE, Invitrogen). The tubes were then centrifuged at 1400xrpm at

RT after which the media containing mitoSOX or DHE was removed, and cells were resuspended in 1XPBS. The ROS production was measured through flow cytometry using FACS CANTO II.

Polyinosinic:polytidylic acid (poly I:C) / polydeoxyinosinic-deoxycytidylic acid (poly dI:dC) induced ROS*:* A2780, TyKNu, and OVCAR4 cell lines were plated at a density of 200K/well in 24 well plate. After 24h cells were transfected with poly I:C and poly dI:dC in serum free media using Lipofectamine 3000 transfection kit (Invitrogen) according to manufacturer protocol. The serum free media was replaced by cultured media 6h after transfection. After 72h, cultured media was removed, cells were washed with 1XPBS, trypsinized (0.25% Corning) for 3 min at 37C, and transferred to 5mL labeled tubes (Falcon). The cells were stained with MitoSOX and Dihydroethidium (DHE) as described above. The ROS production was measured through flow cytometry using FACS CANTO II.

Fractionization- Obtaining mitochondrial and cytosolic fraction

After 6 days of treatment, mitochondrial and cytosolic fraction were obtained using Mitochondria Isolation Kit for Cultured Cells (Thermo Scientific) according to manufacturer protocol.

DNA extraction

DNA was extracted using QiAamp DNA blood kit (QIAGEN) according to manufacturer protocol.

Detecting mtDNA in the cytosol

A2780, TyKNu, and OVCAR4 lcell lines were plated at a density of 1 million cells/ T175 flask and treated for 6 days. The media was removed, cells were washed with 1XPBS, and trypsinized (0.25%, Corning) for 3min at 37C. The trypsin was neutralized with 10mL warmed media, cells were transferred to 15mL tubes and centrifuged at 1400Xrpm for 5min. Media containing trypsin was then removed and cells were resuspended in 1mL 1XPBS. The cell content of each treatment group was divided to two Eppendorf's tube in such a way that 2/3 of total cells are obtained for cytosolic and mitochondrial fraction, and remaining 1/3 of cells for whole cell RNA extraction. Cytosolic fractions were isolated (Mitochondria Isolation Kit for Cultured Cells, Thermo Scientific) and DNA was extracted (QIAamp DNA Blood Mini Kit) according to manufacturer protocols. Total RNA was extracted and converted to cDNA as specified above. From obtained cytosolic fraction Bicinchoninic acid (BSA, Thermo scientific) protein assay was performed, and 350ug protein of each group was transferred to DNA columns for cytosolic DNA extraction. DNA was extracted as specified above. qPCR was performed using cytosolic DNA with mitochondrial genes primers (mt-ATP 6/8, mt-CO2, mt-ND1, D-loop), as well as cDNA from total cell RNA with Actin and GAPDH primers (normalization purpose). The process was performed in a CFX384 Touch Real-Time PCR system (BioRad).

Mitochondrial DNA damage detection by PCR

Mitochondrial DNA damage detection was adapted for qRT-PCR from previous methods (123) (124). Total cellular DNA was examined by quantitative PCR optimized for detection of ~8-12kb fragments as previously described (123) using GoTaq Long PCR polymerase (Promega), Evagreen (1:20, Biotium), and 1x ROX reference dye (Invitrogen). Primers targeted an 8.9kb long mitochondrial fragment or 221bp short mitochondrial reference sequence (reference to primer table goes here). Cycling conditions for long fragment PCR: hot start 95°C 2min; denaturation 95°C 10s, extension 68°C 4min30s (x40 cycles). Cycling conditions for short fragment PCR: PCR: hot start 95°C 2min; denaturation 95°C 10s, extension 60°C 45s (x40 cycles); final extension 72°C 10min.

Cytokine release ELISA

Cytokine release following combination treatment was detected using Human IFN-γ and TNF-α ELISA kits (Invitrogen) according to manufacturer protocol. Absorbance was read at 450 nm using a VersaMax ELISA Microplate Reader (Molecular Devices).

8-hydroxy-2-deoxyguanosine ELISA

mtDNA was isolated from combination-treated cells and 8-hydroxy-2-deoxyguanosine was detected using Human 8-hydroxy-2-deoxyguano ELISA kit (Abcam) according to manufacturer protocol. Absorbance was read at 450 nm using a VersaMax ELISA Microplate Reader (Molecular Devices).

CRISPR CAS9 knockout of ZNFX1

CRISPR cell lines exhibiting genetic knockout of the ZNFX1 gene were generated using the CRISPR-Cas9 mechanism with synthetic single-guide RNAs (sgRNAs, Synthego) targeting exons 6, 3, 8, and 11 (sequences below). CRISPR-Cas9 KOs were produced by nucleofection on the Lonza Amaxa™ 4D-Nucleofector platform and confirmed by subjecting cells to PCR and Sanger sequencing. Genomic editing was confirmed by INDEL analysis using the Synthego ICE analysis platform. Clonal KO populations were then generated by single-cell plating and screening of clonal sequences using ICE analysis.

sgRNA Sequences, Human:

Exon 6: ACCCTGGAGTGCACCATGCG

Exon 3: GGAGTGTAACTCTCATGTGA

Exon 8: GCCATGAGGCTAGACCATTG

Exon 11: GGTGGTCCCCAATCAAAATG

Mitochondrial DNA Transfection

Total cellular DNA was purified from untreated cells by spin column extraction (Qiagen). Mitochondrial DNA was PCR amplified using a REPLI-g Mitochondrial DNA kit (Qiagen) and fragmented using DNAse I (New England Biolabs). Fragmented DNA was transfected into cells using Lipofectamine 3000 (Invitrogen). At 72h, cellular RNA was collected and assayed by qRT-PCR for expression of interferon-stimulated genes.

Bioinformatics analysis

Raw TCGA counts for ovarian serous cystadenocarcinoma (OC), triple-negative breast invasive carcinoma (TNBC), and colon adenocarcinoma (COAD) were obtained through Broad Institute GDAC Portal. These raw count data were processed using EdgeR and Limma powers differential expression analyses for RNAsequencing and microarray studies. For the comparison between ZNFX1 high vs ZNFX1 low samples were split into respective groups based on median normalized count expression. Volcano plots were generated using pheatmap: Pretty Heatmaps. R package version1.0.12. https://CRAN.R-project.org/package=pheatmap. Pathways analysis was conducted using Clusterprofiler (125), an R package for comparing biological themes among gene clusters (126) , tidyverse

(127) and enrichplot (128). Manually curated dot plots were generated using ggplot2 (129). Microarray expression data were extracted from the GEO using GEOquery (126), including datasets GSE9891 (130), GSE30161 (128), GSE26193 (130). The Z scores of gene expression levels were calculated according to normalization on all genes within samples then across all samples for the same data set. Raw counts of genes from the RNA-seq, GSE211669 (129)and GSE102118 (130), were downloaded from the GEO then converted to FPKMs using edgeR (131) followed by Z scores normalized in the same way as what for microarray expression data. Stage and grade information were retrieved from the GEO and published papers. Wilcoxon test was conducted to determine statistical significance of differences between stage and grade regarding ZNFX1 and CMPK2 expression. The correlations between ZNFX1 and CMPK2 expression were calculated as Pearson corrections with statistical significance. Scatter plots between ZNFX1 and CMPK2 expression were plotted using ggpubr R package.

Statistical Analysis

All data are presented as mean ± SEM with statistical significance derived from two-tailed unpaired Student's t test (or ANOVA).

Chapter 4 Results

DNMTis potentiate innate immune signaling in OC and TNBC by inducing both cytosolic dsRNA and dsDNA; this phenomenon is augmented by combining DNMTis with poly-ADP ribose polymerase inhibitors (PARPi) (45) (69). The induced signaling is mediated by both NFκB and IFNα/β signaling, and is dependent upon STING activation, and we termed this pathogen mimicry response, PMR (45). Pathogen-induced IFN/inflammasome responses have recently been integrally linked to mt signaling (119). ZNFX1 appears to play an important role in sensing viral RNA upon initial virus infection and interacting with mitochondrial protein MAVS to initiate type I IFN response, (119). However, the precise function of ZNFX1 in relation to the dynamics of mt dysfunction and mt-mediated inflammasome signaling has not been clarified.

To elucidate expression of ZNFX1 in OC, we first analyzed ZNFX1 expression in clinical RNA-seq datasets of Cancer Science Institute Singapore (CSIOVDB) and The Cancer Genome Atlas (TCGA) for ovarian serous cystadenocarcinoma (132). We found that ZNFX1 expression was increased with both stage and grade with a most robust median increase in stage III and grade 3 (**Fig.4.1A-D**). In addition, we found a positive correlation between ZNFX1 and cytosine monophosphate kinase 2 (CMPK2) expression in stage III and grade 3 patients in TCGA (**Fig. 4.1E, 1F**). According to recent COVID research (122), similarly to ZNFX1, CMPK2 is a nuclear gene that is involved in mediating antiviral activities through IFN pathways, as well as being required for salvage dNTP synthesis in mitochondria. Next, in TCGA OC samples, we examined ZNFX1 expression with respect to IFN/inflammasome and mitochondrial signaling, finding that it was positively associated with genes and pathways categorized as innate immune, type I IFN, and dsDNA/RNA sensing (**Fig. 4.1G**). In contrast, elevated ZNFX1 expression was associated with downregulation or negative enrichment of genes and pathways mediating mt function including mt nuclear protein translation and import, citric acid cycle, electron transport, and oxidative phosphorylation (OXPHOS) (**Fig. 1H**). Validating the above data, in the MSigDB (90) and MITOCARTA 3.0 (133) databases (the latter including 1136 mitochondrial annotated genes), there was a pronounced negative association between ZNFX1 expression and genes involved in mt metabolism including LYR Motif Containing 4 (LYRM4), acyl-CoA synthetase medium-chain family member 5 (ACSM5), Uncoupling Protein 3 (UCP3) and mt DNA packaging genes such as proline dehydrogenase H and 2 (PRODH, PRODH2) (**Fig. 1I**). Notably, an exception to the above generalized repression of mt-associated genes occurs for the earlier introduced gene, CMPK2 (134) (Fig 4.1I). Thus, collectively, our above data associate high ZNFX1 expression with potential mt dysfunction and OC progression.

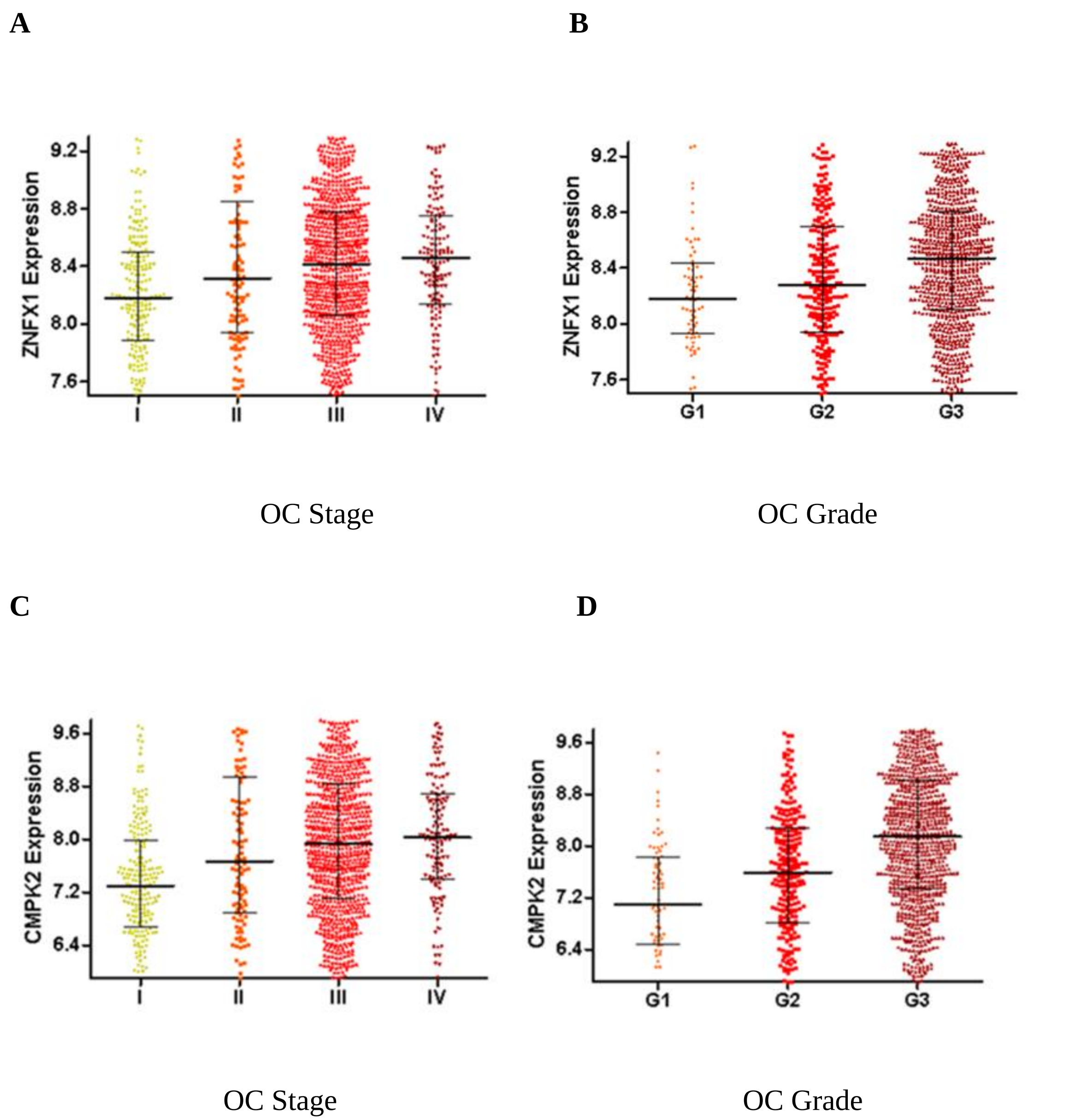

Figure 4.1 ZNFX1 expression is inversely correlated with mt signaling in OC cells.

A. Expression of ZNFX1 (A, B) and CMPK2 (C, D) in ovarian cancer patients at different tumor stages and grades in the Ovarian Cancer Database of Cancer Science Institute Singapore (CSIOVDB).

E

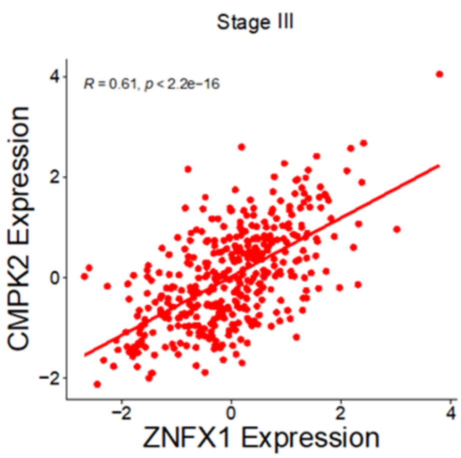

F

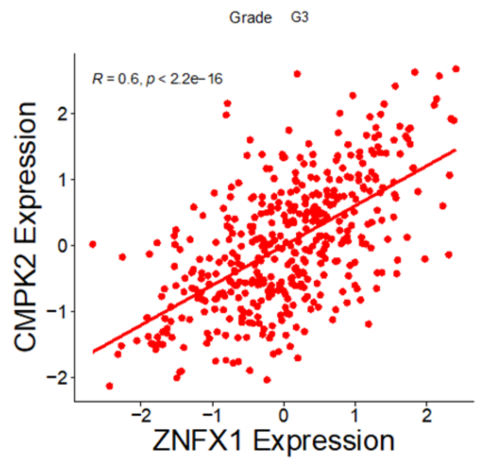

G

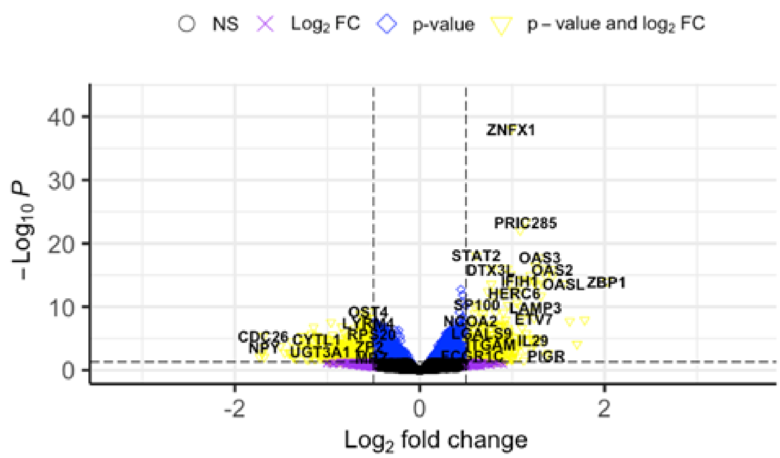

Figure 4.1 Continued: ZNFX1 expression is inversely correlated with mt signaling in OC cells.

E. Correlation of ZNFX1 and CMPK2 in stage III ovarian cancer patients in The Tumor Cancer Genome Atlas (TCGA). F. Correlation of ZNFX1 and CMPK2 in grade 3 ovarian cancer patients in The Tumor Cancer Genome Atlas (TCGA). G. Volcano plot for RNAseq differential expression analysis (TCGA Ovarian serous cystadenocarcinoma), all annotated HGNC symbols, x-axis: log2 fold change in expression: ZNFX1 above median vs. ZNFX1 below median, y-axis: -log10 of FDR controlled adjusted p-value (padj), color mapping: black: padj> 0.10 and log2 fold change < |0.5|, blue: padj< 0.10 and log2 fold change < |0.5|, purple: padj> 0.10 and log2 fold change > |0.5|, and yellow: padj< 0.10 and log2 fold change > |0.5

H

I

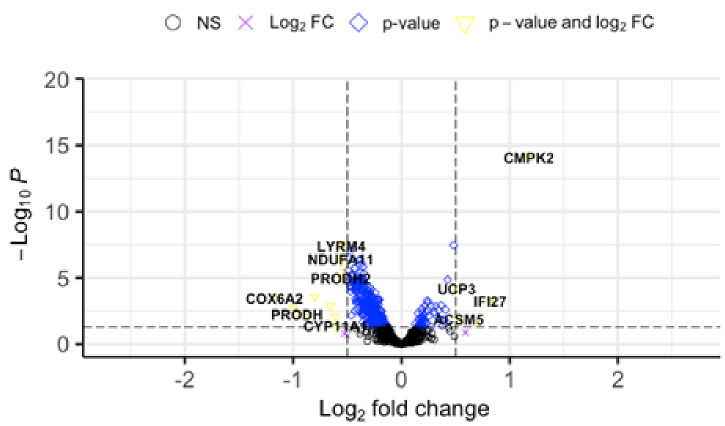

Figure 4.1 Continued: ZNFX1 expression is inversely correlated with mt signaling in OC cells.

H. Pathway dot plot depicting result from gene set enrichment analysis (TCGA Ovarian serous cystadenocarcinoma) on pre-ranked gene list derived from ZNFX1 above median vs. ZNFX1 below median differential expression analysis. Pathways depicted are derived from manual curation of Interferon, Mitochondria, and DNA repair pathways compiled from MSigDB: HALLMARK, KEGG, and REACTOME. x-axis: normalized enrichment score, dot size: enrichment score, color gradation: FDR controlled adjusted p-value. I. Volcano plot for RNAseq differential expression analysis (TCGA Ovarian serous cystadenocarcinoma), MITOCARTA 3.0 symbols, x-axis: log2 fold change in expression: ZNFX1 above median vs. ZNFX1 below median, y-axis: -log10 of FDR controlled adjusted p-value (padj), color mapping: black: padj> 0.10 and log2 fold change < |0.5|, blue: padj< 0.10 and log2 fold change < |0.5|, purple: padj> 0.10 and log2 fold change > |0.5|, and yellow: padj< 0.10 and log2 fold change > |0.5|.

To examine the role of ZNFX1 in the PMR, we first transfected synthetic dsRNA and dsDNA mimics (poly I:C (PIC) and poly(dI:dC) respectively) into high-grade serous OC cell line models (TYK-nu, OVCAR4), finding a significant increase in expression by qPCR and western blot of ZNFX1 (**Fig. 4.2A, 4.2B**). In keeping with these findings, both ZNFX1 mRNA and protein levels in drug-treated whole cell lysates were increased (**Fig.4.2C, 4.2D**). Although MAVS mRNA levels did not increase in OC cell lines (**Fig.4.2C**), this protein, known to be located in the outer membrane of the mt, was increased in isolated mt fractions with all above drug treatment groups, as is ZNFX1 (**Fig.4.2E**). Moreover, immunofluorescence (IF)-based proximity ligation assay (PLA) indicates that ZNFX1 colocalizes with dsRNA and dsDNA (**Fig.4.2F, 4.2G**), and MAVS (**Fig.4.2H, 4.2I**) following AZA or AZA-TAL combination treatments, validating its potential importance in mt signaling.

A

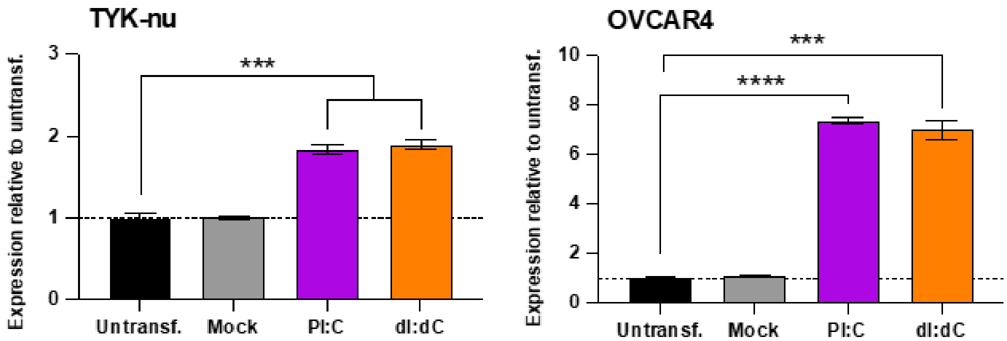

B

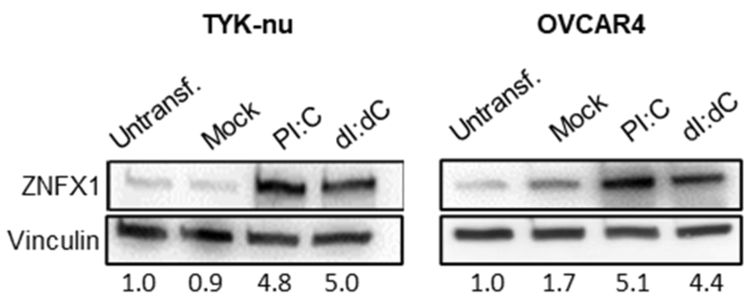

Figure 4.2 DNMTi and PARPi mimic of polyI:C and polydI:dC

A. Relative expression of ZNFX1 transcript by qPCR in TYK-nu or OVCAR4 72 hours after transfection with 1µg poly I:C or poly dI:dC. Complex I inhibitor rotenone (1µM) utilized as positive control. B. Western blot showing ZNFX1 protein expression 72 hours after transfection with 1µg poly I:C or poly dI:dC. In TYK-nu and OVCAR4. All data are presented as mean ± SEM with p values derived from two-tailed unpaired Student's t-test or ANOVA as appropriate.

C

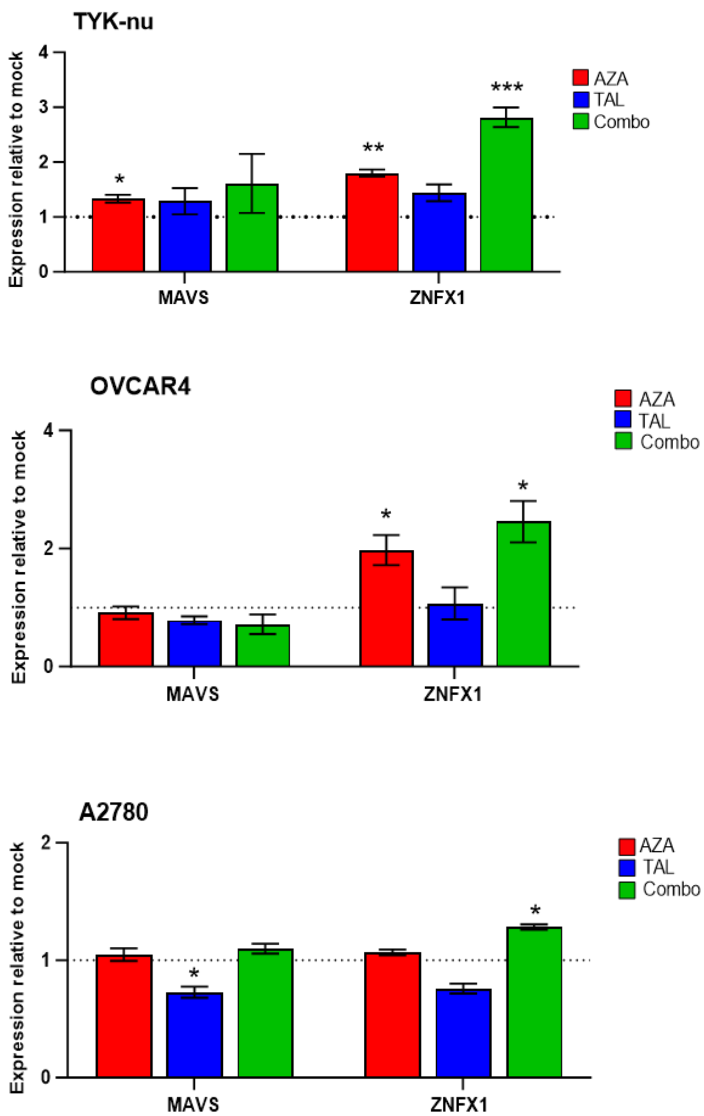

Figure 4.2 Continued: DNMTi and PARPi mimic of polyI:C and polydI:dC

C. Relative expression of gene transcript involved in sensing dsRNA/DNA by qPCR in A2780, TYK-nu and OVCAR4 cells treated with AZA, TAL and combination theraphy. All data are presented as mean ± SEM with p values derived from two-tailed unpaired Student’s t-test or ANOVA as appropriate.

D

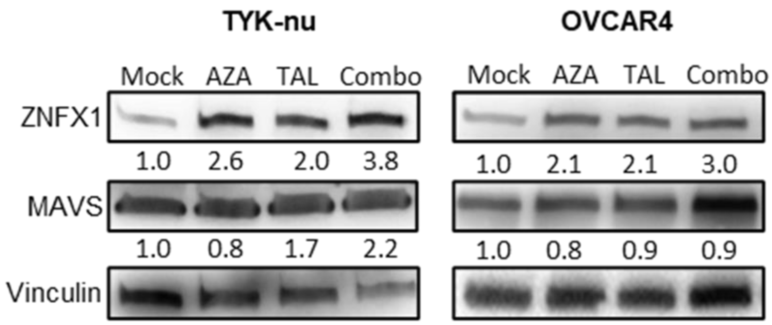

E

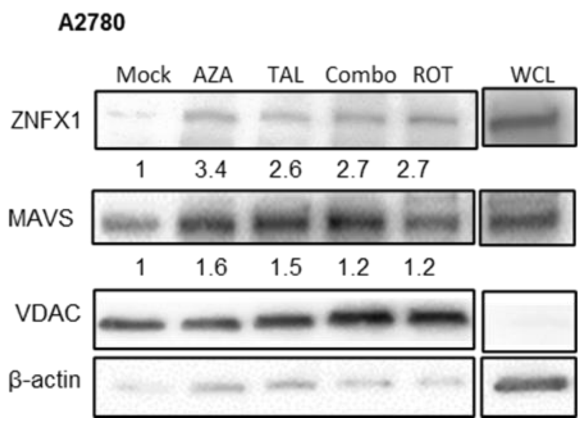

Figure 4.2 Continued: DNMTi and PARPi mimic of polyI:C and polydI:dC

D. Western blot showing ZNFX1 protein expression following 6 days' treatment with AZA, TAL, or combination (TYK-nu: AZA 100nM, TAL 2.5nM, or combination; OVCAR4: AZA 150nM, TAL 10nM, or combination). E. Western blot showing ZNFX1, STAT3 and MAVS protein expression in mitochondrial fraction of A2780 cell line 6 days after AZA, TAL and combination treatment. All data are presented as mean ± SEM with p values derived from two-tailed unpaired Student's t-test or ANOVA as appropriate.

F

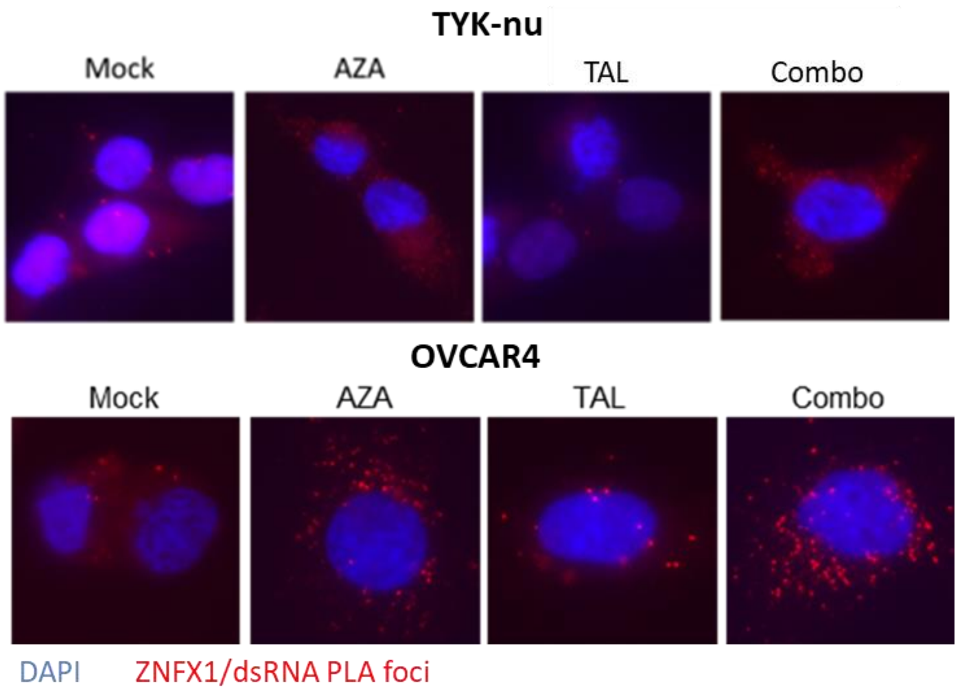

G.

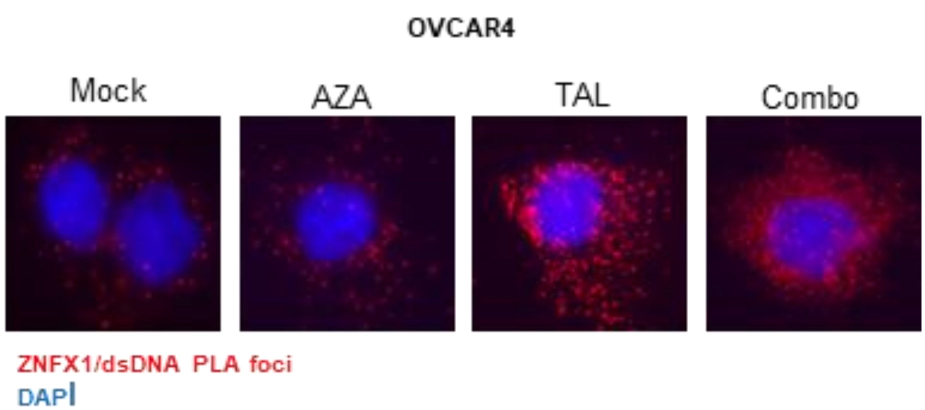

Figure 4.2 Continued: DNMTi and PARPi mimic of polyI:C and polydI:dC

F. Representative immunofluorescence images of ZNFX1 and dsRNA interaction by proximity ligation assay in TYK-nu and OVCAR4 following 6 days' treatment with AZA, TAL, or combination.G.Representative immunofluorescence images of ZNFX1 and dsDNA interaction by proximity ligation assay in OVCAR4 following 6 days' treatment with AZA, TAL, or combination.

H

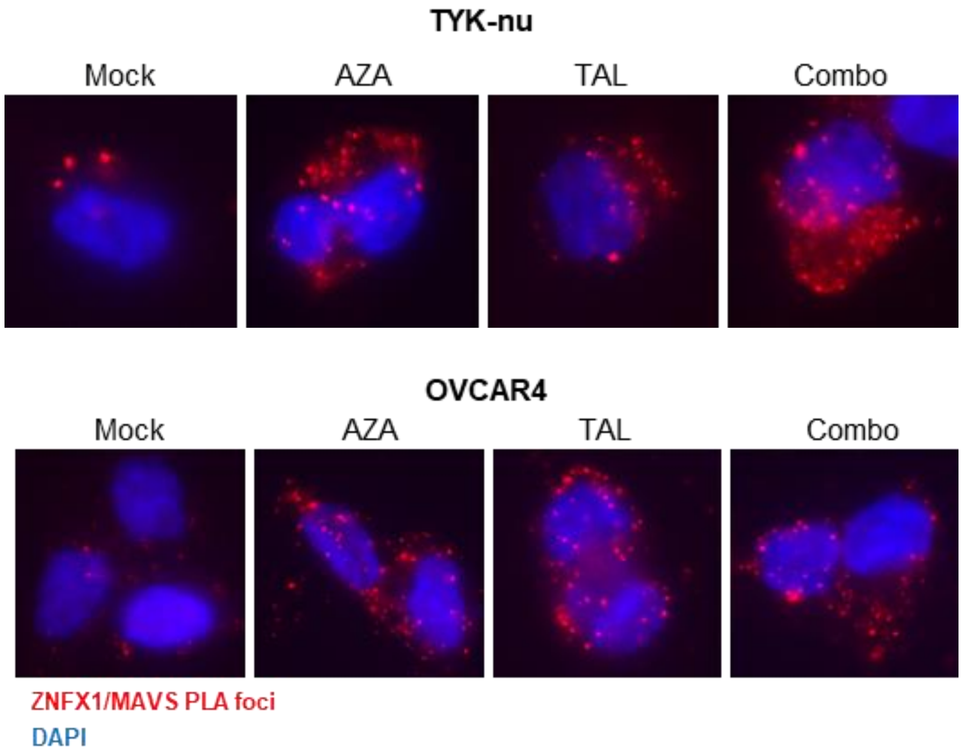

Figure 4.2 Continued: DNMTi and PARPi mimic of polyI:C and polydI:dC

H. Representative immunofluorescence images of ZNFX1 and MAVS interaction by proximity ligation assay in OVCAR4 following 6 days' treatment with AZA, TAL, or combination.

I

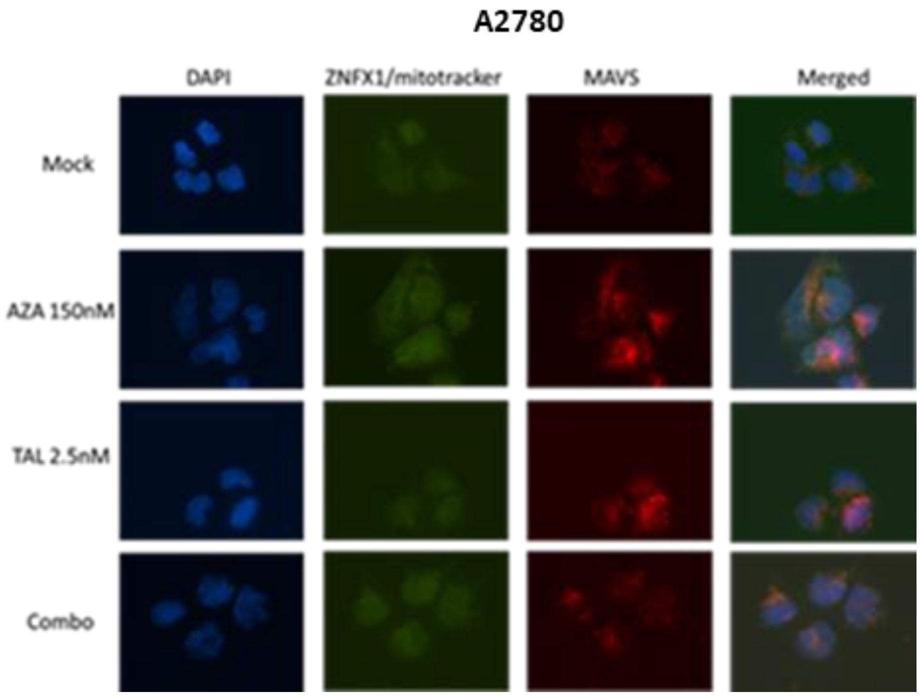

Figure 4.2 Continued: DNMTi and PARPi mimic of polyI:C and polydI:dC

I.Immunofluorescence showing ZNFX1 and MAVS colocalization on mitochondria after 6 days of treatment with AZA, TAL and combination in A2780 cell line. Mitotracker and ZNFX1 are stained green, MAVS is stained red, and DAPI is stained blue.

In keeping with our previous results in other cancer types (45) (135) (136), the anti-cancer PMR drug DNMTi AZA increased endogenous ERV transcription in the above OC cells, as well as in endometrioid OC A2780 cells (**Fig.4.3A-C**).

A

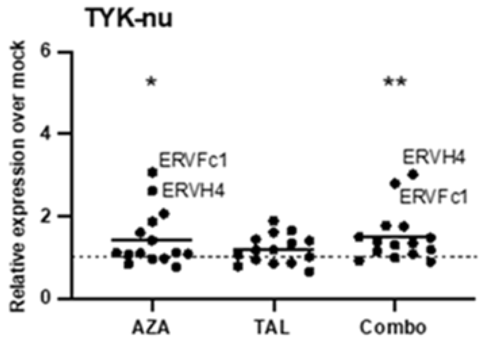

B

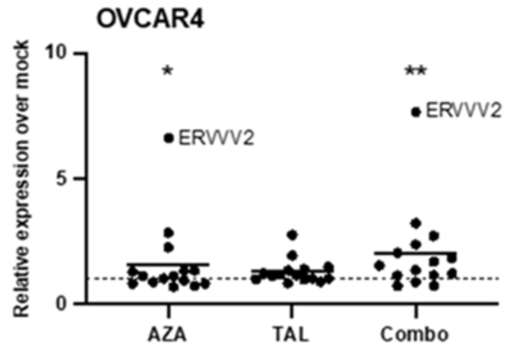

C

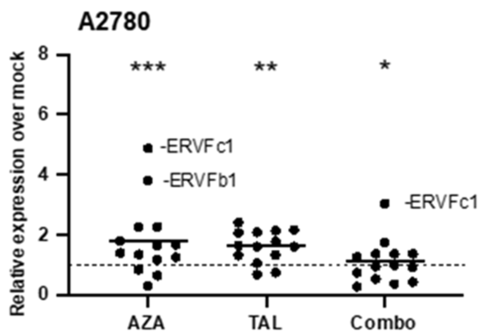

Figure 4.3 DNMTi induce ERV expression in OC.

Relative expression of ERV gene transcripts by qPCR in ovarian cancer cell lines after treatment with AZA, TAL, and combination theraphy for 6 days. (A) TYKN-nu AZA 100nM, TAL 2.5nM, or combination. (B) OVCAR4 AZA 150nM, TAL 10nM, or combination. (C) A2780 AZA 150nM, TAL 2.5nM, or combination. All data are presented as mean ± SEM with p values derived from two-tailed unpaired Student's t-test.

Next, we explored the effects of our drugs on mt signaling and to determine whether the above bioinformatics findings linking ZNFX1 expression to defective mitochondrial bioenergetics could be validated in vitro. We first determined whether our drug treatment altered mtROS which can be generated by defective electron transport chain activity during oxidative phosphorylation, leading to mtDNA damage (137). Accordingly, following transfection of dsDNA/RNA (**Fig.4.4A**), or treatment with AZA, TAL or AZA-TAL combination (**Fig.4.4B**), mtROS levels were increased in OC cell lines TYK-nu, OVCAR4, and A2780, as measured by flow cytometric detection of the mt-specific ROS dye MitoSOX. Complex I inhibitor, rotenone, that leads to increase production of mtROS was utilized as positive control. Furthermore, the above treatments increased generalized cellular ROS, as measured by dihydroethidium flow cytometry (**Fig.4.4C**) (138). Since mt ROS can lead to increased damage of mtDNA (139) we next examined general DNA damage, as measured by long-range PCR (123) (**Fig.4.4D**), and oxidative mtDNA base damage, as measured by 8-oxoguanine (8-oxoG) (**Fig.4.4E**). Our results show that AZA, TAL and combination drug treatment led to increased general DNA damage. However, increased 8-OXOG base damage was only seen with the drug combination. Importantly, treatment with AZA, TAL or the AZA-TAL combination resulted in leakage of mtDNA into the cytosol as measured by qPCR of mt genes mtDloop, mtATP6, and mtCO2 in cytosolic fractions (**Fig.4.4F, 4.4G**).

A

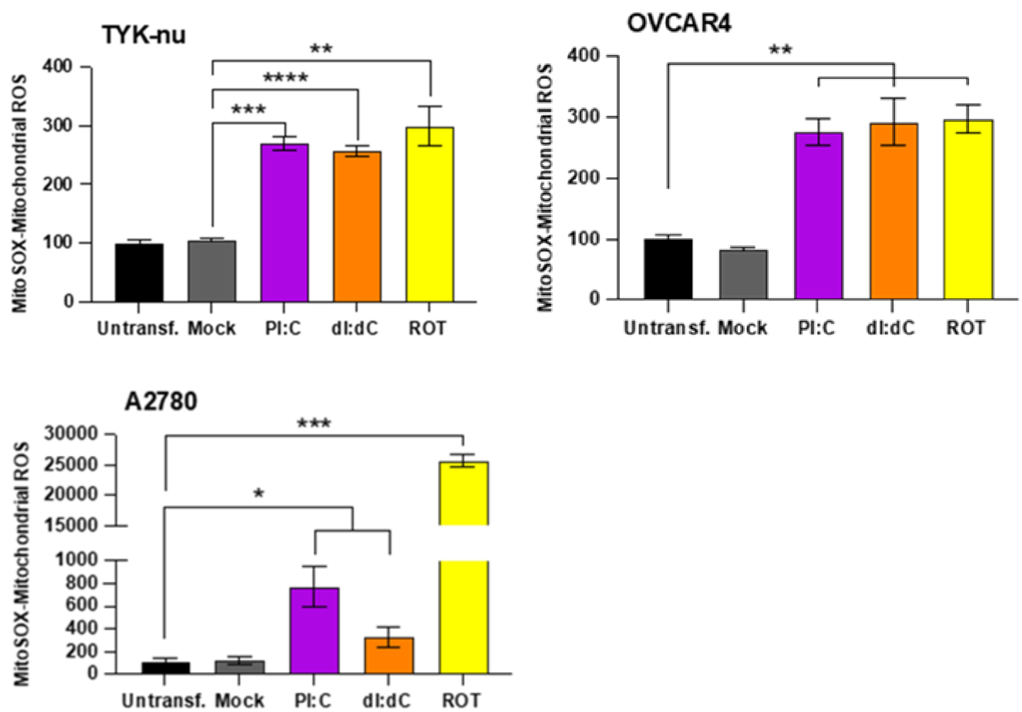

Figure 4.4 Increased ZNFX1 leads to increased mtROS, mtDNA damage and dsDNA leakage into the cytosol.

A. Flow cytometry detection of mitochondrial (mtROS) in TYK-nu or OVCAR4 72 hours after transfection with 1µg poly I:C or poly dI:dC. Complex I inhibitor rotenone (1µM) utilized as positive control. All data are presented as mean ± SEM with p values derived from two-tailed unpaired Student's t-test or ANOVA as appropriate. * $p<0.05$, ** $p<0.01$, *** $p<0.001$, **** $p<0.0001$.

B

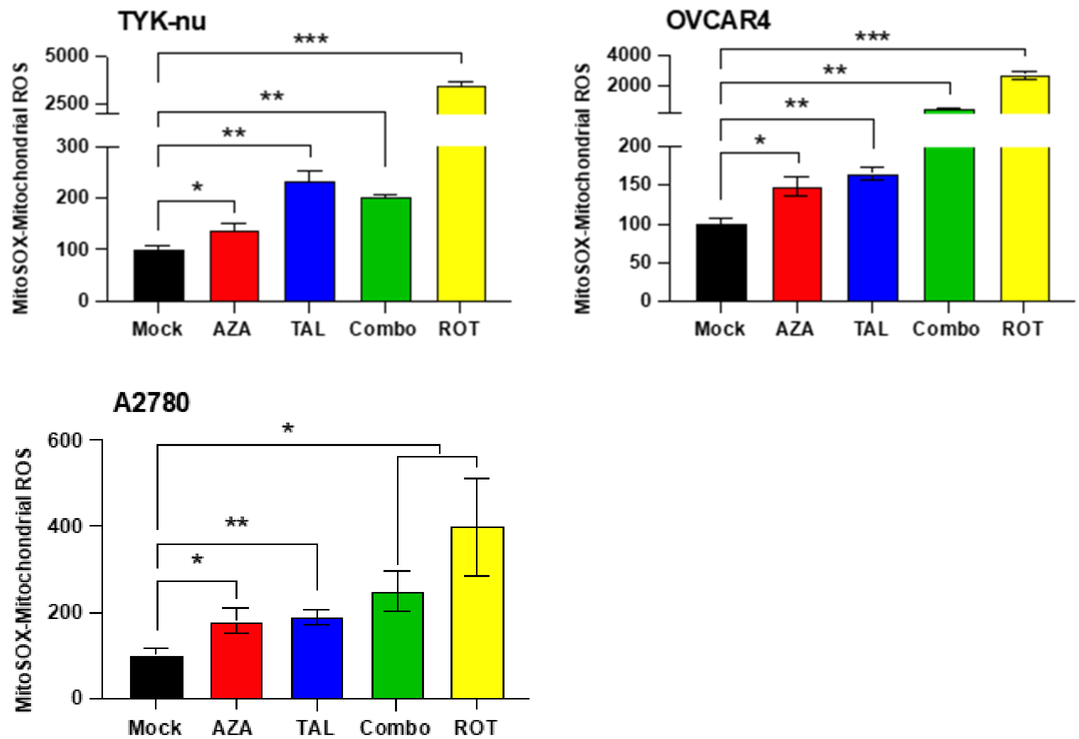

Figure 4.4 Continued: Increased ZNFX1 leads to increased mtROS, mtDNA damage and dsDNA leakage into the cytosol.

B. Flow cytometry detection of mtROS in TYK-nu or OVCAR4 following 6 days' treatment with AZA, TAL, or combination (TYKnu: AZA 100nM, TAL 2.5nM, or combination; OVCAR4: AZA 150nM, TAL 10nM, or combination). All data are presented as mean ± SEM with p values derived from two-tailed unpaired Student's t-test or ANOVA as appropriate. * p<0.05, ** p<0.01, *** p<0.001, **** p<0.0001.

C

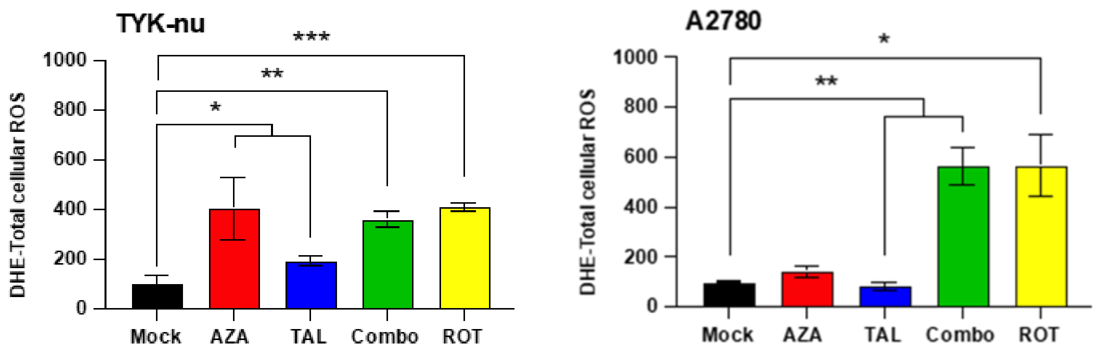

D

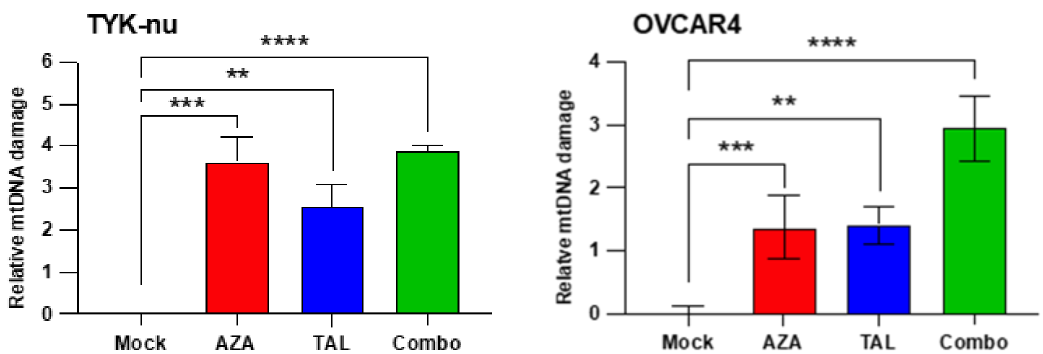

Figure 4.4 Continued: Increased ZNFX1 leads to increased mtROS, mtDNA damage and dsDNA leakage into the cytosol.

C. Flow cytometry detection of total cellular ROS (DHE) in TYK-nu or OVCAR4 following 6 days' treatment with AZA, TAL, or combination (TYKnu: AZA 100nM, TAL 2.5nM, or combination; OVCAR4: AZA 150nM, TAL 10nM, or combination). D. Relative mtDNA damage measured by adapted real-time long-range PCR method in TYK-nu or OVCAR4 following 6 days' treatment with AZA, TAL, or combination. E. Relative 8-oxoG in mtDNA isolated from TYK-nu or OVCAR4 following 6 days' treatment with AZA, TAL, or combination. All data are presented as mean ± SEM with p values derived from two-tailed unpaired Student's t-test or ANOVA as appropriate. * $p<0.05$, ** $p<0.01$, *** $p<0.001$, **** $p<0.0001$.

E

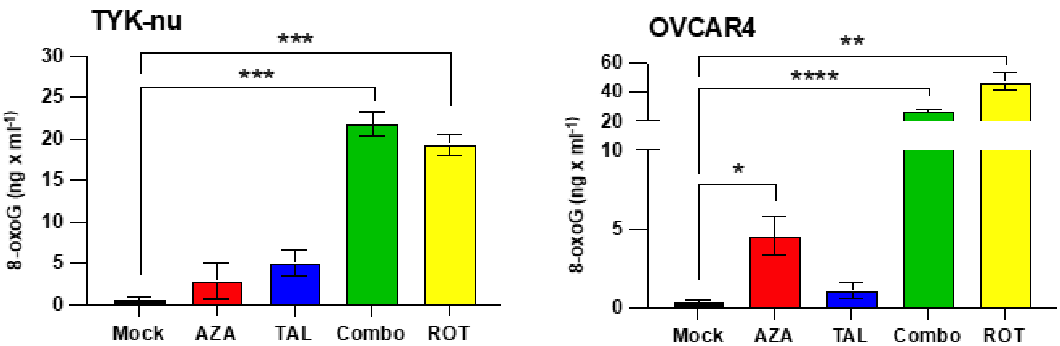

F

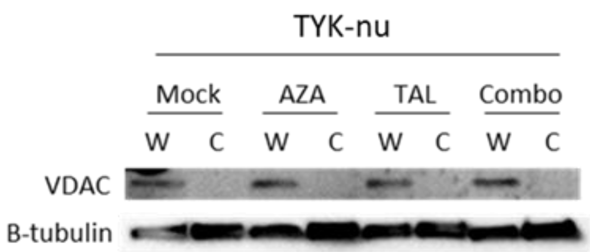

Figure 4.4 Continued: Increased ZNFX1 leads to increased mtROS, mtDNA damage and dsDNA leakage into the cytosol.

E. Relative 8-oxoG in mtDNA isolated from TYK-nu or OVCAR4 following 6 days' treatment with AZA, TAL, or combination. F. Western blot showing VDAC and beta tubulin protein expression in whole lysate and cytoplasmic fraction 6 days after AZA, TAL, and combination treatment in TYK-nu wild type cell line All data are presented as mean ± SEM with p values derived from two-tailed unpaired Student's t-test or ANOVA as appropriate. * $p<0.05$, ** $p<0.01$, *** $p<0.001$, **** $p<0.0001$.

G

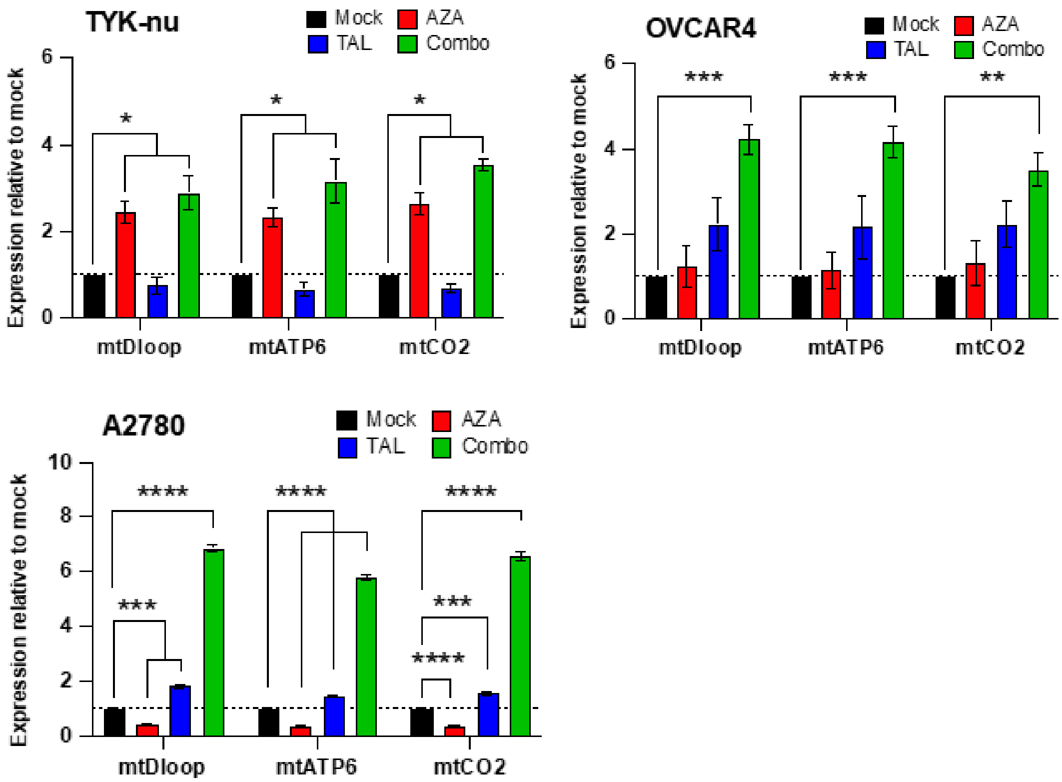

Figure 4.4 Continued: Increased ZNFX1 leads to increased mtROS, mtDNA damage and dsDNA leakage into the cytosol.

G. Relative expression of mt-encoded genes (mtDloop, mtATP6/8, mtCO2) in cytosolic fraction isolated from TYK-nu and OVCAR4 following 6 days' treatment with AZA, TAL, or combination. All data are presented as mean ± SEM with p values derived from two-tailed unpaired Student's t-test or ANOVA as appropriate. * $p<0.05$, ** $p<0.01$, *** $p<0.001$, **** $p<0.0001$.

To examine the connection between mtDNA dynamics and antiviral defense (**Fig. 4.1A-C**), we used the STRING database computational tool (140) to perform network analysis for protein interactions between our targets of interest: ZNFX1, inflammasome signaling, and mt biochemistry. We found that ZNFX1 was linked to nodes of both innate immune and mt networks, including the important immune-responsive mt-localized proteins CMPK2 that as previously mentioned is involved in mediating antiviral activities through IFN pathways, and dNTP synthesis in mitochondria. and mitochondrial transcription factor A (TFAM) that is required for packing newly synthesized mtDNA strands (**Fig.4.5A**). Accordingly, as assessed by qPCR, CMPK2 expression was significantly increased in coordination with ZNFX1 following PIC/dI:dC transfection (**Fig.4.5B**) and AZA/TAL combination treatment (**Fig. 4.5C**), while expression of TFAM was coordinately decreased at the protein level (**Fig. 4.5D**) (137). Thus, increased mtDNA synthesis alone or in concert with decreased DNA packaging may create vulnerability to oxidative damage, leading to the above-demonstrated accumulation of damaged, oxidized mtDNA.

A

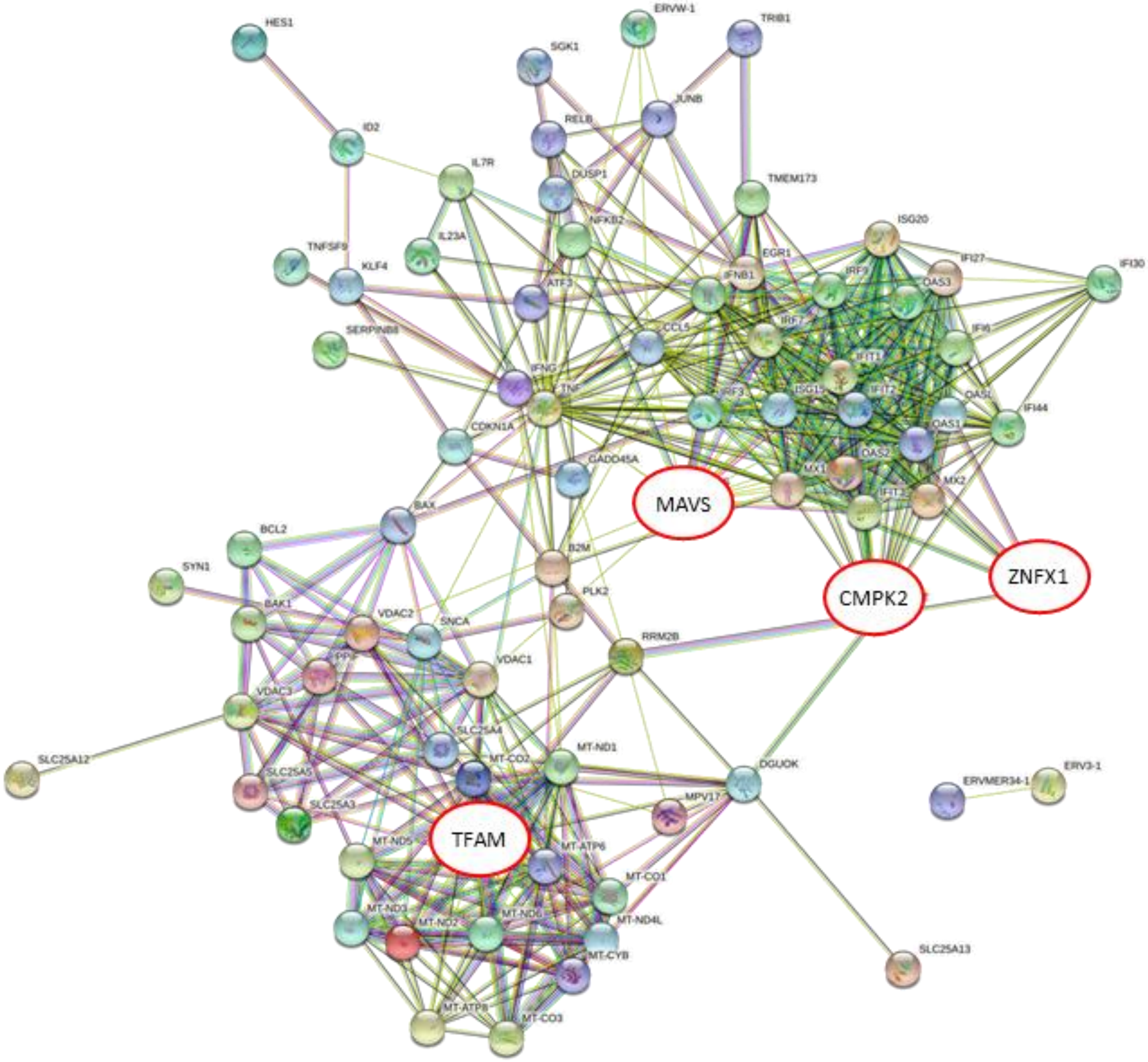

Figure 4.5 ZNFX1 KO is mechanistically linked to CMPK2 and TFAM expression.

A. STRING protein–protein interaction map of ZNFX1 in relation to mt response pathways, including CMPK2, TFAM, and IFN/inflammasome proteins.

B

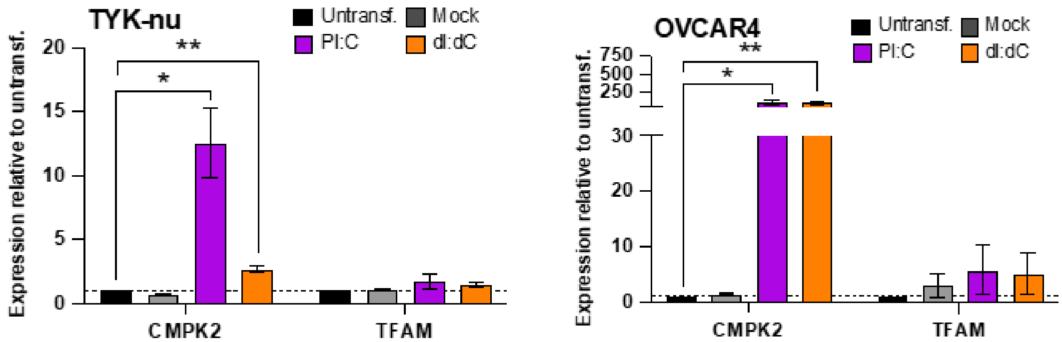

C

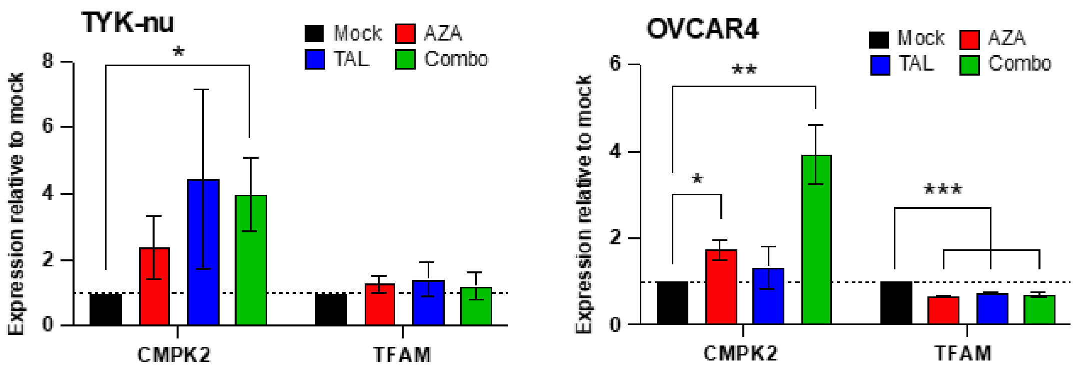

D

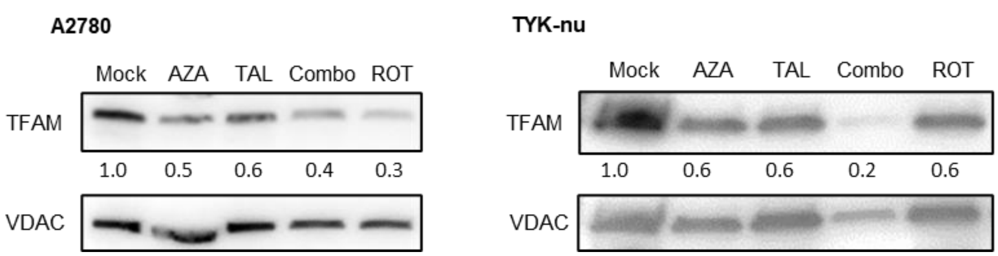

Figure 4.5 Continued: ZNFX1 KO is mechanistically linked to CMPK2 and TFAM expression.

B. Relative expression of CMPK2 and TFAM transcripts by qPCR in TYK-nu or OVCAR4 72 hours after transfection with 1μg poly I:C or poly dI:dC © or following 6 days' treatment with AZA, TAL, or combination (TYK-nu: AZA 100nM, TAL 2.5nM, or combination; OVCAR4: AZA 150nM, TAL 10nM, or combination) D. Western blot showing TFAM protein expression 6 days after AZA, TAL, and combination treatment in mitochondrial fraction of A2780 and TYK-nu cell lines. All data are presented as mean ± SEM with statistical significance p values derived from two-tailed unpaired Student's t test.

To investigate the hierarchy of events linking the above ZNFX1, CMPK2, and TFAM dynamics, ZNFX1 depletion was established by CRISPR knock-out (KO) (Fig.4.6A) in OC (TYK-nu and OVCAR4) cells. Importantly, deletion of ZNFX1 not only abrogated the increase in CMPK2 but blunted the decrease in TFAM seen with our drug treatments (Fig. 4.6B). Concomitantly, ZNFX1 KO also abrogated drug-induced mtROS, without affecting cellular ROS levels (Fig. 4.6C, 4.6D). DNA damage, including mt 8-oxoG, and mtDNA leakage into the cytosol after AZA or AZA-TAL treatment was also blunted with ZNFX1 KO (Fig. 4.6E-H).

A

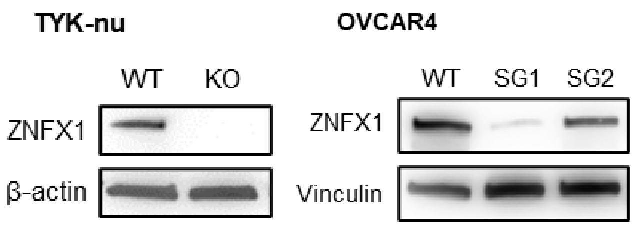

B

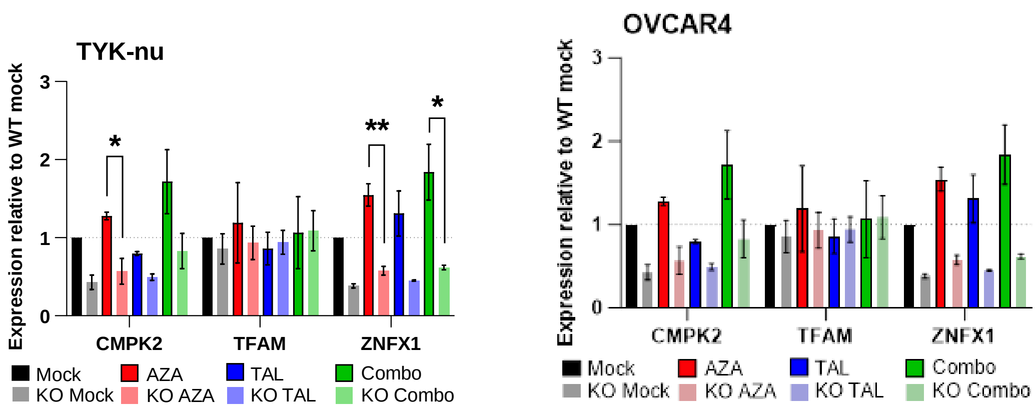

Figure 4.6 ZNFX1 KO abrogates drug-induced mtROS, DNA damage, 8-oxoG, and mtDNA leakage into the cytosol after AZA or AZA-TAL treatment.

A. Western blot for ZNFX1 in TYK-nu, OVCAR4 and A2780 cells with and without CRISPR KO of ZNFX1. B. Relative expression of CMPK2 and TFAM transcripts by qPCR in TYK-nu ZNFX1 WT or KO cells following 6 days' treatment with AZA, TAL, or combination. All data are presented as mean ± SEM with p values derived from two-tailed unpaired Student's ttest or ANOVA as appropriate.

C

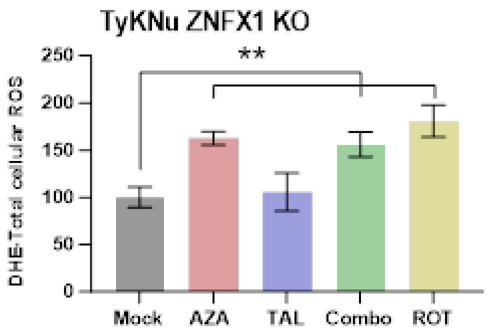

D

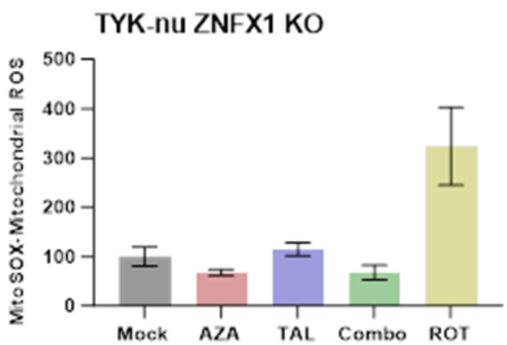

Figure 4.6 Continued: ZNFX1 KO abrogates drug-induced mtROS, DNA damage, 8-oxoG, and mtDNA leakage into the cytosol after AZA or AZA-TAL treatment.

C. Flow cytometry detection of cellular ROS (DHE) in TYK-nu ZNFX1 KO following 6 days' treatment with AZA, TAL, or combination, (D) or mtROS. All data are presented as mean ± SEM with p values derived from two-tailed unpaired Student's ttest or ANOVA as appropriate.

E

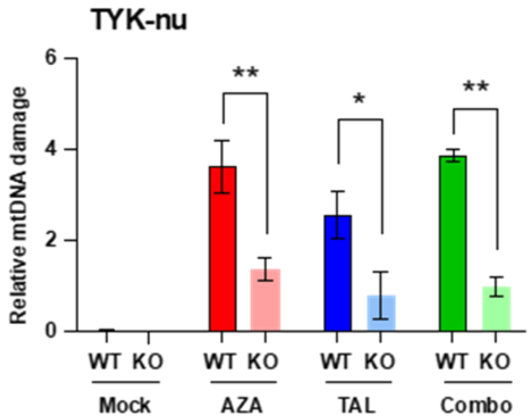

F

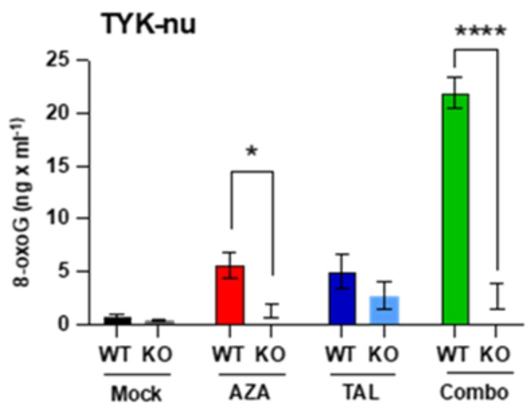

Figure 4.6 Continued: ZNFX1 KO abrogates drug-induced mtROS, DNA damage, 8-oxoG, and mtDNA leakage into the cytosol after AZA or AZA-TAL treatment.

E. Relative mtDNA damage measured by adapted real-time long-range PCR method in TYK-nu ZNFX1 KO following 6 days' treatment with AZA, TAL, or combination. F. Relative 8-oxoG in mtDNA isolated from TYK-nu ZNFX1 following 6 days' treatment with AZA, TAL, or combination. All data are presented as mean ± SEM with p values derived from two-tailed unpaired Student's ttest or ANOVA as appropriate.

G

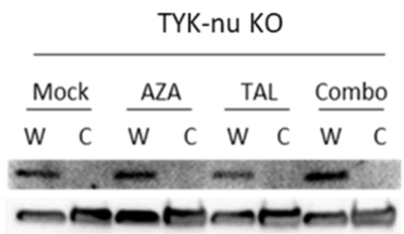

H

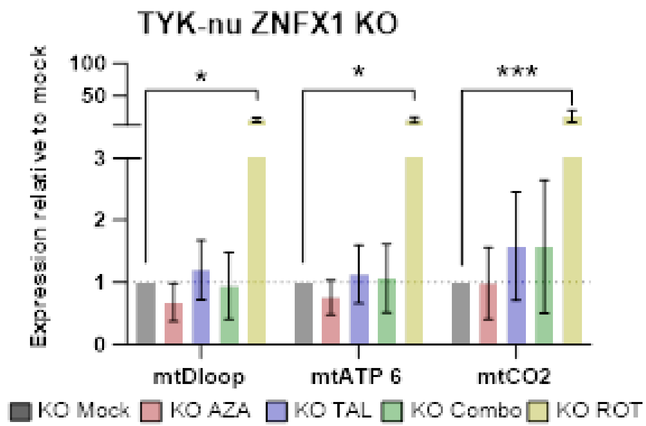

Figure 4.6 Continued: ZNFX1 KO abrogates drug-induced mtROS, DNA damage, 8-oxoG, and mtDNA leakage into the cytosol after AZA or AZA-TAL treatment.

G. Western blot showing VDAC and beta tubulin protein expression in whole lysate and cytoplasmic fraction 6 days after AZA, TAL, and combination treatment in TYK-nu knockout cell line. H. Relative expression of mt-encoded genes (mtDloop, mtATP6/8, mtCO2) in cytosolic fraction isolated from TYK-nu ZNFX1 KO following 6 days' treatment with AZA, TAL, or combination. All data are presented as mean ± SEM with p values derived from two-tailed unpaired Student's ttest or ANOVA as appropriate.

Next to explore the effects of ZNFX1 on inflammasome signaling, we performed qPCR for these genes in mRNA extracts following AZA/Tal treatment. Our data demonstrate that ZNFX1 is required for IFN/inflammasome signaling. ZNFX1 KO abrogated the transcriptional increases of IFN/inflammasome genes which occur with DNMTi and PARPi combination drug treatments, as measured by qPCR (**Fig.4.7A**). Moreover, therapy-induced increases in key inflammasome cytokines TNFα and IFI27 were reduced in both TYK-nu and OVCAR4 ZNFX1 KO cells, as measured by ELISA (**Fig.4.7B, 4.7C**). Consistent with our previous report that AZA/TAL combination therapy induced IFN/inflammasome signaling that is at least partly dependent on STING activation (69), ZNFX1 KO in TYK-nu and OVCAR4 decreased activating Ser366 phosphorylation of STING (pSTING) (**Fig.4.7D**), as well as downstream pSTING targets pTBK1, TBK1, pIRF3, IRF3 (**Fig.4.7E**). Importantly, transfection of mtDNA into ZNFX1 KO TYK-nu and OVCAR4 cells significantly reduced transcripts of TNFα, IFI27, and STING compared to WT cells and untransfected controls (**Fig.4.7F**), thereby validating the effects of ZNFX1 on STING-dependent IFN/inflammasome signaling.

A

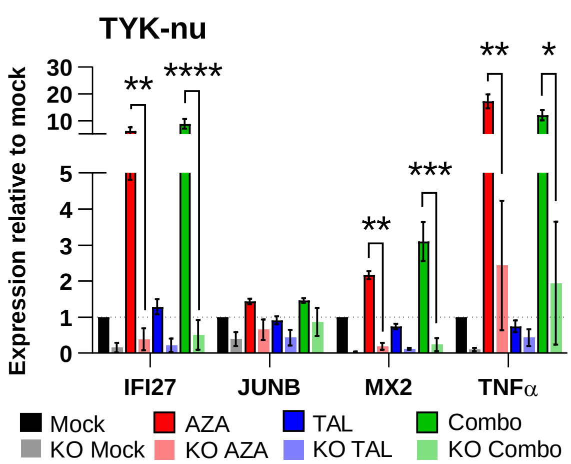

Figure 4.7 ZNFX1 KO abrogates DNMTi/PARPi-induced STING-dependent IFN and inflammasome signaling.

A. Relative expression of IFN (IFI27, MX2) or inflammasome transcript inflammasome (JUNB, TNFα) by qPCR in TYK-nu ZNFX1 WT or KO following 6 days' treatment with 100nM AZA, 2.5nM TAL, or combination. All data are presented as mean ± SEM with p values derived from two-tailed unpaired Student's ttest or ANOVA as appropriate.

B

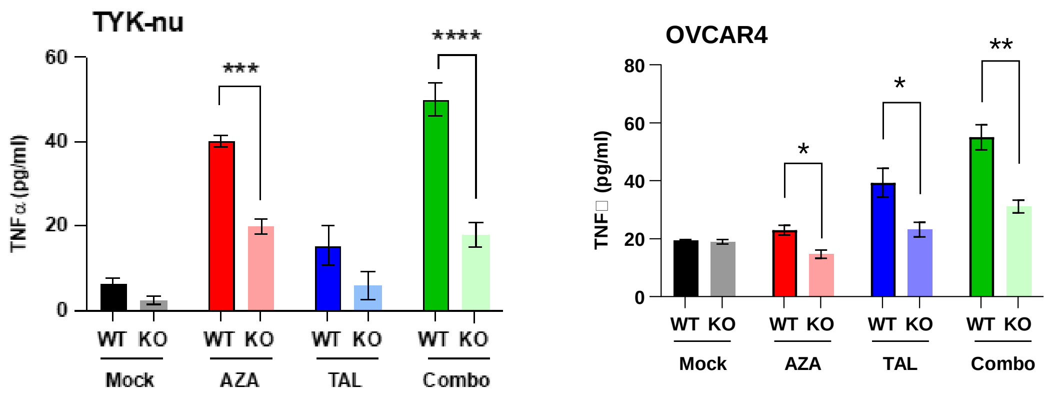

C

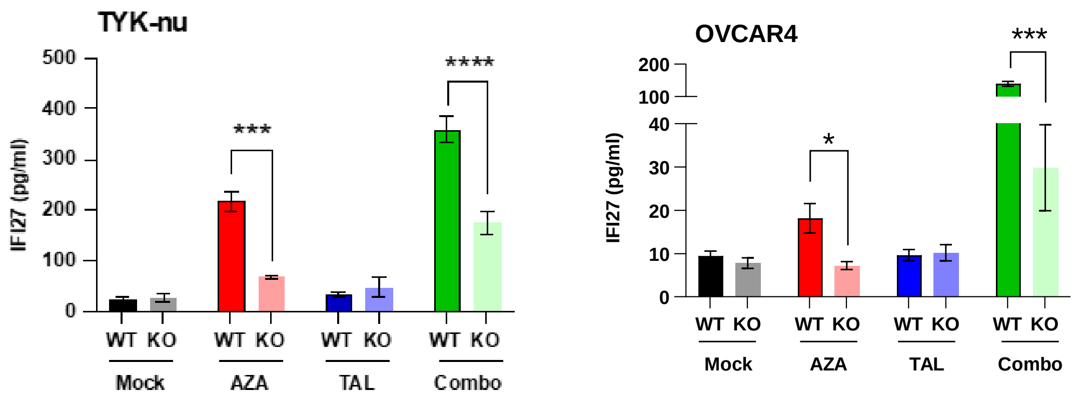

Figure 4.7 Continued: ZNFX1 KO abrogates DNMTi/PARPi-induced STING-dependent IFN and inflammasome signaling.

B, C. TNFα (B) and IFI27 (C) cytokine release by ELISA in TYK-nu ZNFX1 WT or KO following 6 days' treatment with AZA, TAL, or combination (TYK-nu: AZA 100nM, TAL 2.5nM, or combination; OVCAR4: AZA 150nM, TAL 10nM, or combination). All data are presented as mean ± SEM with p values derived from two-tailed unpaired Student's ttest or ANOVA as appropriate.

D

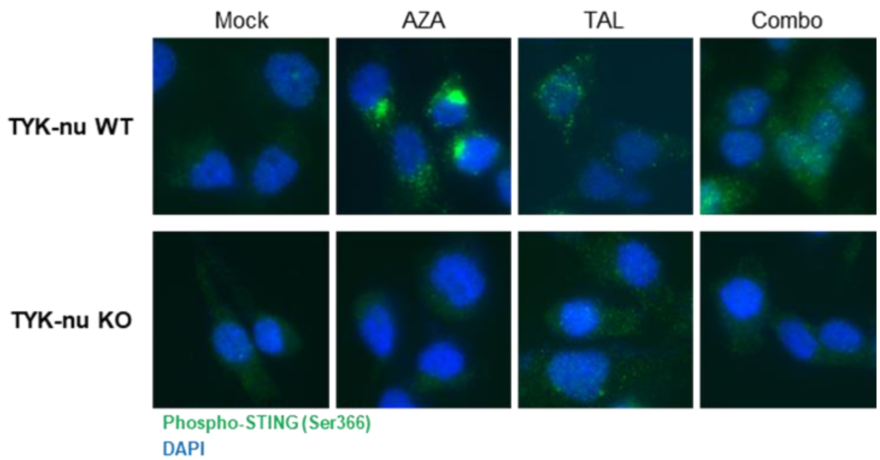

E

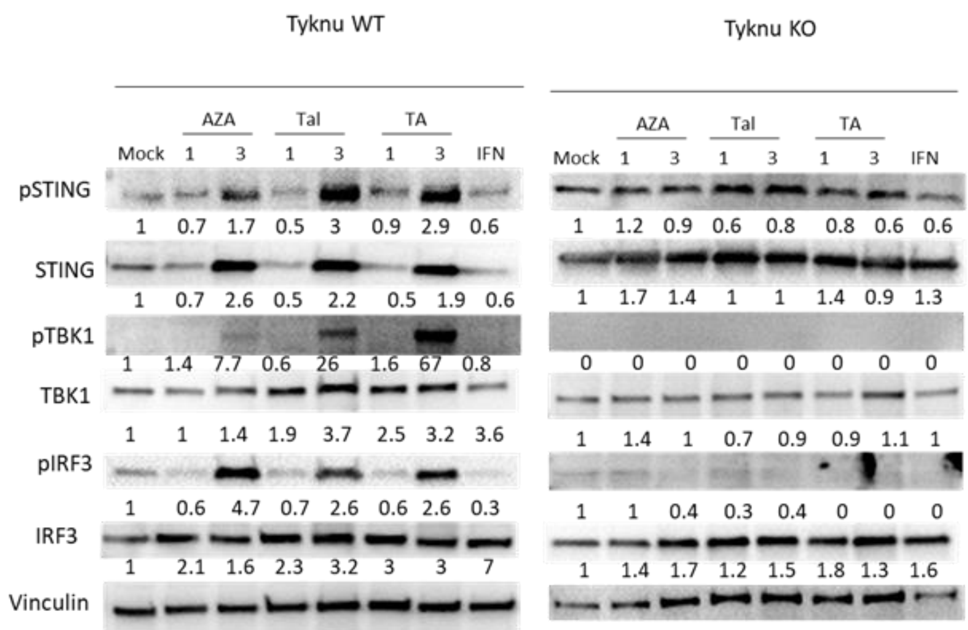

Figure 4.7 Continued: ZNFX1 KO abrogates DNMTi/PARPi-induced STING-dependent IFN and inflammasome signaling.

D. Representative immunofluorescence images of Ser366 phosphorylation of STING in TYKnu ZNFX1 WT or KO following 24h treatment with AZA, TAL, or combination. E. Western blot of proteins for TBK1/pTBK1, STING/pSTING and pIRF3/IRF3 in TYK-nu (parental and ZNFX1 KO) with Vinculin used as loading control. All data are presented as mean ± SEM with p values derived from two-tailed unpaired Student's ttest or ANOVA as appropriate.

F

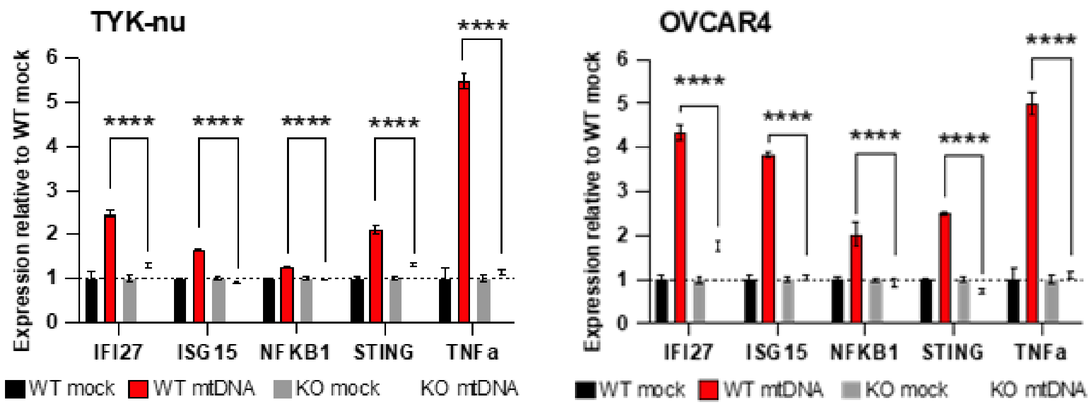

Figure 4.7 Continued: ZNFX1 KO abrogates DNMTi/PARPi-induced STING-dependent IFN and inflammasome signaling.

F. Relative expression of IFN/inflammasome (IFI27, ISG15, NFKB1, STING, TNFα) transcripts by qPCR in TYK-nu or OVCAR ZNFX1 WT or KO 72hrs after transfection of purified mtDNA. All data are presented as mean ± SEM with p values derived from two-tailed unpaired Student's ttest or ANOVA as appropriate.

Lastly, to validate our findings of the role of ZNFX1 in IFN/inflammasome signaling, we performed RNA seq analysis on TYK-nu cells comparing ZNFX1 KO with WT cells. Reactome and Hallmark pathway analysis first showed that IFN and inflammatory as well as cytokine pathways are suppressed in the ZNFX1 KO confirming our in vitro results. Additionally, ZNFX1 KO cells revealed activation of genes and pathways involved in DNA repair, DNA replication, and cell cycle, and negative association with interferon and cytokine signaling. (**Fig. 4.8A, 4.8B**). Together, these data support a master role for ZNFX1 as a specific mediator of mtDNA induction of STING-dependent IFN/inflammasome signaling in OC cells and suggest a potential role of ZNFX1 in DNA replication and repair as well (**Fig.4.8C**).

A

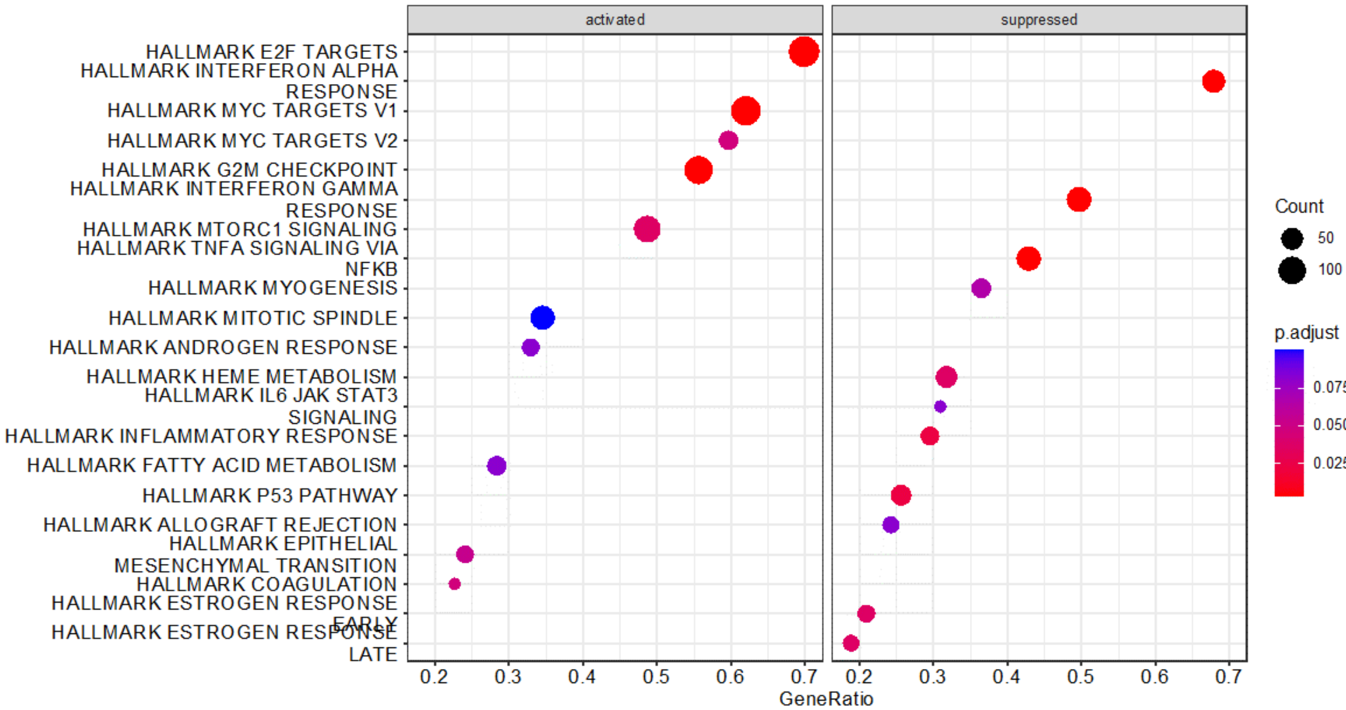

Figure 4.8 ZNFX1 KO correlates with upregulation of DNA repair and downregulation of immune pathways in OC cells.

A. Pathway dot plot depicting result gene set enrichment analysis (ovarian cancer) on pre-ranked gene list derived from ZNFX1 KO above median vs. ZNFX1 below median differential expression analysis. The pathways depicted are derived from manual curation of DNA repair pathways compiled from HALLMARK. x-axis: normalized enrichment score, dot size: enrichment score, color gradation: FDR controlled adjusted p-value.

B

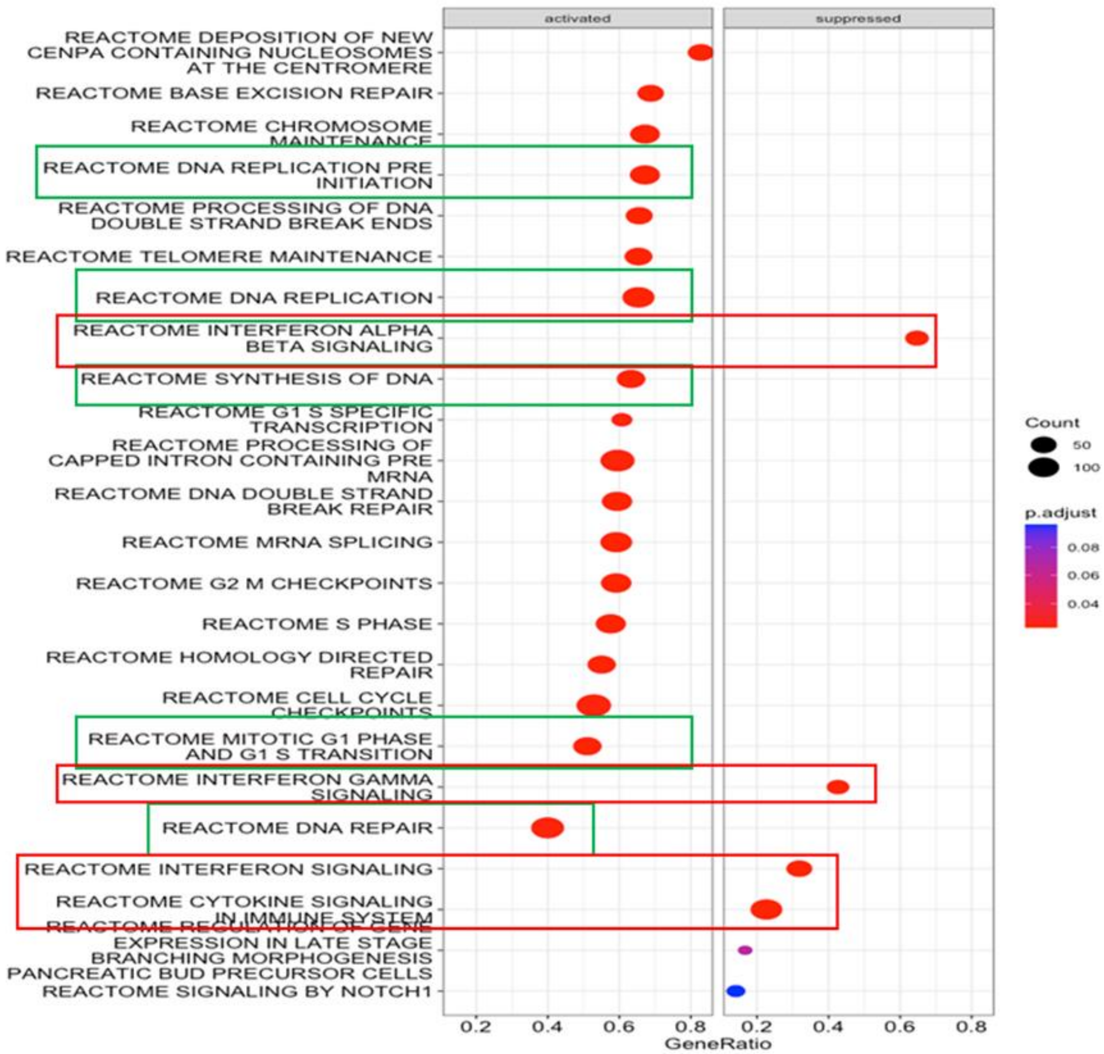

Figure 4.8 Continued: ZNFX1 KO correlates with upregulation of DNA repair and downregulation of immune pathways in OC cells.

B. Pathway dot plot depicting result gene set enrichment analysis (ovarian cancer) on pre-ranked gene list derived from ZNFX1 KO above median vs. ZNFX1 below median differential expression analysis. Green box represents upregulated pathways involved in proliferation, EMT and DNA repair. Red box represents downregulated pathways involved in IFN and cytokine signaling. The pathways depicted are derived from manual curation of DNA repair pathways compiled from REACTOME (B). x-axis: normalized enrichment score, dot size: enrichment score, color gradation: FDR controlled adjusted p-value.

C

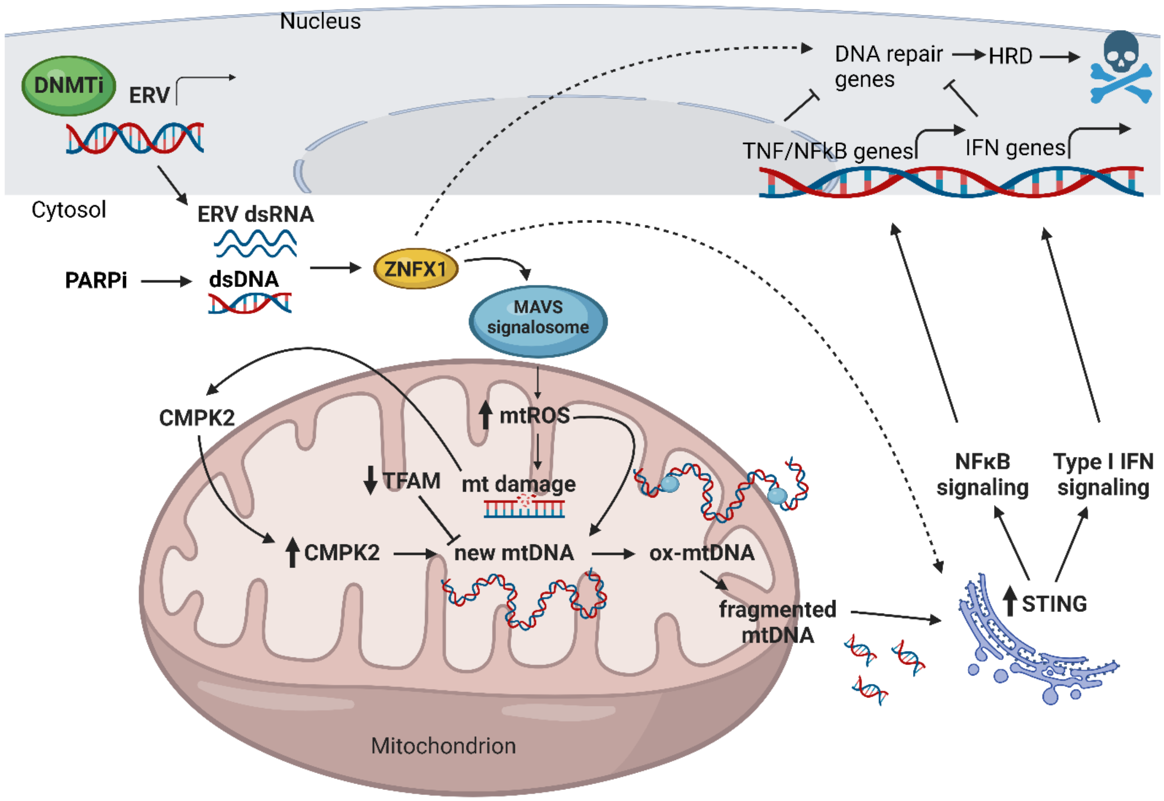

Figure 4.8 Continued: ZNFX1 KO correlates with upregulation of DNA repair and downregulation of immune pathways in OC cells.

G. Model for ZNFX1 induction of mt dysfunction and inflammatory signaling triggered by DNMTi and PARPi therapy in OC. DNMTis increase expression of ERV transcripts which accumulate as cytosolic dsRNA. PARPi treatment produces DNA damage and fragmentation that accumulates as cytosolic dsDNA. ZNFX1 senses dsRNA/DNA, localizes to MAVs on mitochondrial membrane, and produces mt dysfunction that increases mtROS. Increased CMPK2 and decreased TFAM expression impacts de novo mtDNA synthesis and packaging, creating vulnerability to oxidative mtDNA damage, mtDNA fragmentation, and mtDNA leak into the cytosol. Cytosolic mtDNA activates STING-dependent interferon and inflammasome signaling. ZNFX1 may also play a role in detecting mtDNA in the cytosol, leading to STING activation, as indicated by the dashed arrow. Created with Biorender.com. ZNFX1 may also play a role in DNA repair indirectly through induction of HRD or directly by interaction with HR proteins, as indicated by dashed line.

Chapter 5 Discussion

The results presented here uncover a network of hierarchical, cellular, and molecular events in induction of IFN/inflammasome signaling in cancer cells with a central role for mt dysfunction (141). Importantly, these studies highlight ZNFX1 as a master regulator in this signaling leading to mt dysfunction and STING-dependent inflammasome signaling, while providing new key insights for the pathogen mimicry role of anti-cancer drugs, DNMTi and PARPi (45) (69) (134) (135). Our clinical data from CSIOVDB shows that ZNFX1 expression increases with tumor stage and grade and that the association of high ZNFX1 expression with potential mt dysfunction (**Fig.4.1**), which supports both our TCGA and *in vitro* data. Although, we are not certain why ZNFX1 expression drastically increases in stage III and grade 3, we hypothesize that ZNFX1 responds to a stimulus in the cytosol. Potentially, ZNFX1 is responding to increased genomic instability that corelates with progression of the disease. It is known that genomic instability leads to the creation of peptide sequences known as neoantigens that can cause an immune response (142). In addition, genomic instability is linked to increased DNA damage that can potentially leak into cytosol and trigger ZNFX1 activation (143). Further, we demonstrated that upregulated ZNFX1, indeed, leads to increased mtROS, 8-oxoG, and mt damage (**Fig.4.4**). In addition, we show that DNMTi hypomethylate ERVs leading to their transcriptional activation and further interaction with ZNFX1 (**Figs.4.2, 4.3**). The importance of ZNFX1 in mitochondrial function and downstream pathways further involved in IFN/inflammasome signaling is elucidated with our ZNFX1 knockout data (**Figs.4.6, 4.7**).

One of the most important links with inflammation stressed in our present work is between mtROS and oxidative DNA damage, leading to leakage of mtDNA into the cytosol. We hypothesize that increases in de novo mtDNA synthesis factor CMPK2, in concert with decreased TFAM, which is responsible for packaging of newly synthesized mtDNA, creates a vulnerability to oxidative damage in OC cells, leading to the above-demonstrated accumulation of damaged, oxidized mtDNA (**Fig.4.5**). The present work has both basic and translational implications for understanding the role of mitochondria in guiding inflammatory responses in states ranging from pathogen infections, autoimmune diseases, neurodegenerative diseases, immune function, and aging. In these scenarios, the essential role for ZNFX1 would help explain its high genetic conservation across species. ZNFX1 is reported to be required for epigenetic inheritance in *C. elegans*, promoting the 3′ recruitment of machinery that propagates the small RNA epigenetic signal (118). Our findings further support the key role of ZNFX1 in linking epigenetic regulation to immune responses. Germline mutations in IFN-responsive genes cause imbalance in immune responses, leading to devastating “interferonopathies” resulting in death in young children due to pathogenic infections (144). Alongside ZNFX1, as introduced earlier above (120), identified mutations include TLR3, UNC93B, IRF7 and IRF9 (145) (146) (147) (148) (149), which are vital for defense against severe herpes simplex virus type 1 encephalitis, influenza A, and SARS-CoV2 infections. For cancer, it is now recognized and being explored, including in clinical trials, that more nuanced states of viral mimicry in the context of inflammasome signaling and inflammation induction may have potential in anti-cancer therapies (150), and our now defined altered mt bioenergy processes and metabolism can be included in this context.

Activating the pathogenic mimicry response in cancers may have particular importance in increasing the tumor signaling to attract key immune cells and increase efficacy of immune checkpoint therapy (150). Our present introduction of the master role of ZNFX1 in inflammasome signaling could have impact for advancing these therapy approaches. The ZNFX1 KO TCGA data we presented above shows upregulation of various pathways involved in DNA repair (Fig.4.8), base excision repair (BER) being one of them. In this regard, elucidating the DNA repair mechanisms relevant to mtDNA damage and the resulting leakage of DNA is important for fundamental understanding of therapeutic resistance (151). For example, platinum-induced alterations in mitochondrial function in HGSOC cells might contribute to drug response and resistance. Platinum induces an increase in SIRT1 activity that increases TFAM levels (151), which in turn increases expression of OXPHOS genes that leads to an increase in mt activity. In this context, BER, which is responsible for removing non-bulky oxidative DNA lesions and is known to be active in mtDNA repair, requires deeper investigation considering our *in vitro* and TCGA findings (152). Additionally, investigating the role of ZNFX1 in DNA repair may uncover its important function with regard to these pathways. In our previous study (69) we show negative correlation between DNA repair genes and immune genes expression, in which DNA repair genes are downregulated and immune genes are upregulated. Here, we find that this negative correlation persists, however in the opposite direction when ZNFX1 is not present. This suggests that ZNFX1 could potentially control both DNA repair and immune genes expression, and dictate the outcome of cell survival. In addition, this suggests that ZNFX1 can potentially directly regulate DNA repair, leading to HRD and cell death when combined with PARPi. Future studies will provide a deeper insight into the connection between ZNFX1, DNA repair and inflammation. In addition, while PARP1, required for recognizing SSBs, has been reported to localize to the mitochondria (153) (154), the exact role for PARP1 in mammalian mtDNA SSB repair remains insufficiently understood. Inflammasome signaling is tightly linked to processes that can cause damage to mt membranes. Mitochondrial outer membrane permeabilization (MOMP) triggered by ionizing radiation promotes the cytosolic release of mtDNA, activation of the cGAS-STING pathway, and production of type I IFNs, thus collectively facilitating an effective response to radiation therapy (155). In contrast, the BCL2-dependent mitophagy pathway reduces MOMP, limiting the release of mtDNA and associated immune responses (155). Inflammatory processes can also cause various types of regulated cell death, termed PANoptosis (156), an inflammatory cell death pathway that interconnects programmed cell death pathways including apoptosis, pyroptosis, and/or necroptosis. Furthermore, as PANoptosis has now been implicated in viral infections and cancer, it could be important to tumor cell killing induced by our epigenetic drugs in OC and other cancer types (156). Our in vivo studies in immune competent mice will further elucidate the connection between tumor intrinsic pathways and host cell responses in tumor microenvironment.

In conclusion, ZNFX1 could potentially have a translational relevance by becoming a prognostic biomarker in cancer. The high expression of ZNFX1 across stages and grades in OC patients suggests the possible outcome in respect to the treatment.

Appendix

Table S1.

qPCR primer	Supplier	Sequence
Actin F	IDT	CACCATTGGCAATGAGCGGTTC
Actin R	IDT	AGGTCTTTGCGGATGTCCACGT
GAPDH F	IDT	GTCTCCTCTGACTTCAACAGCG
GAPDH R	IDT	ACCACCCTGTTGCTGTAGCCAA
ADAR F	IDT	TGGACTACGACATCCGTTATATG
ADAR R	IDT	GTTGACGCTTGTCTCCTTAGT
AIM2 F	IDT	TCAAGCTGAAATGAGTCCTGC
AIM2 R	IDT	CTTGGGTCTCAAACGTGAAGG
ASC F	IDT	CATGAACTGATCGACAGGATG
ASC R	IDT	GGACCTCCTCCAAATGTTTC
Caspase 1 F	IDT	GCTTTCTGCTCTTCCACACC
Caspase 1 R	IDT	CATCTGGCTGCTCAAATGAA
CCL5	Qiagen	
CMPK2 F	IDT	TGGAGACCAGGCATCTTAATTT
CMPK2 R	IDT	CTCACTGGAACATGATGAGAGG
EIF2AK2 F	IDT	CAAGAGCCTGGGACCTTATTT
EIF2AK2 R	IDT	GGTATGTTTCTAGGGAGGCAATTA
ERV-Fc2 F	IDT	CTGGAAGCTACACACTCCATAC
ERC-Fc2 R	IDT	TGCCAAGAGGTGGGTTATTC

Table S1. continues

qPCR primer	Supplier	Sequence
ERV-Fb1 F	IDT	ATATCCCTCACCACGATCCTAATA
ERV-Fb1 R	IDT	CCCTCTGTAGTGCAAAGACTGATA
ERV-Fc1 F	IDT	TACACCCTTACTCCCGTCTT
ERV-Fc1 R	IDT	GCCTAACATTCCGACCTCATAC
ERV-FRD1 F	IDT	AGCCAGCTCTCAAAGGAAATAG
ERV-FRD1 R	IDT	GAAGGACTACGGCTGCTAAAG
ERV-H1 F	IDT	GCCCATTCTCTCTCTCCATATC
ERV-H1 R	IDT	CCTGACATTCCTGCCTTCTTA
ERV-K1 F	IDT	ATCCTATGGCACCACCTAGTA
ERV-K1 R	IDT	GCCTCAGTATCTCCTTCCTTTC
ERV-K10 F	IDT	GTCCCAAGTGTTTCAGGGAATA
ERV-K10 R	IDT	GAAGCAGAGAGACTGCTTGTATAG
ERV-K8 F	IDT	CCCATCAATCCACCAAGTCTTA
ERV-K8 R	IDT	CCTATTTCTTCGGACCTGTTCTT
ERVFXA34 F	IDT	CAGGAAACTAACTTTCAGCCAGA
ERVFXA34 R	IDT	TAAAGAGGGCATGGAGTAATTGA
ERVFXA34 R	IDT	TAAAGAGGGCATGGAGTAATTGA
ERVMER34-1 F	IDT	CCATGGAAGCTCAAGGTCTATC
ERVMER34-1 R	IDT	GAAGGGTCCACTGCCATTT

Table S1. continues

qPCR primer	Supplier	Sequence
ERVV2 F	IDT	CTTCTTTCTGAGCTCCTGTCTC
ERVV2 R	IDT	GTCCTCTGGTTCTTGGTCTTC
ERVW1 F	IDT	CAAGTCCCTTCCCTCTAATTCC
ERVW1 R	IDT	TCCACTCCAGCCACTTTAAC
ERVW2 F	IDT	CCACTGTCTGTTGGACTTACTT
ERVW2 R	IDT	TGGGAGATTGCTTCCTTTACTT
IFNA F	IDT	GACTCCATCTTGGCTGTGA
IFNA R	IDT	TGATTTCTGCTCTGACAACCT
IFNB1 F	IDT	CTTGGATTCCTACAAAGAAGCAGC
IFNB1 R	IDT	TCCTCCTTCTGGAACTGCTGCA
IL18 F	IDT	ACTGGTTCAGCAGCCATCTT
IL18 R	IDT	GGAATTGTCTCCCAGTGCAT
IL1B F	IDT	GCACAAGGCACAACAGGCTGC
IL1B R	IDT	CAGGTCCTGGAAGGAGCACTTCA
IL6ST	Qiagen	
IL7R	Qiagen	
ISG20	Qiagen	
MAVS F	IDT	GTCACTTCCTGCTGAGA
MAVS R	IDT	TGCTCTGAATTCTCTCCT

Table S1. continues

qPCR primer	Supplier	Sequence
MDA5 F	IDT	GCTGAAGTAGGAGTCAAAGCCC
MDA5 R	IDT	CCACTGTGGTAGCGATAAGCAG
mtATP6/8 F	IDT	TAGCCCACTTCTTACCACAAGGCA
mtATP6/8 R	IDT	TGAGTAGGTGGCCTGCAGTAATGT
mtCO2 F	IDT	AATCGAGTAGTACTCCCGATTG
mtCO2 R	IDT	TTCTAGGACGATGGGCATGAAA
mtDloop F	IDT	CTATCACCCTATTAACCACTCA
mtDloop R	IDT	TTCGCCTGTAATATTGAACGTA
NFKB1 F	IDT	TCTGCTTCCAGGTGACAGTG
NFKB1 R	IDT	ATCTTGAGCTCGGCAGTGTT
NLRP3 F	IDT	TCCTCGGTACTCAGCACTAAT
NLRP3 R	IDT	AAGAGTCCCTCACAGAGTAGTT
NLRX1 F	IDT	GGCCTTGTTGTCTCAGCTCTTTA
NLRX1 R	IDT	CACCAGTCCAGAACCATCTT
OASL F	IDT	TCGTGAAACATCGGCCAACT
OASL R	IDT	ACCTGGCTTTCACATACTGCT
RIG-I F	IDT	CACCTCAGTTGCTGATGAAGGC
RIG-I R	IDT	GTCAGAAGGAAGCACTTGCTACC

Table S1. continues

qPCR primer	Supplier	Sequence
STAT1 F	IDT	TGTATGCCATCCTCGAGAGC
STAT1 R	IDT	AGACATCCTGCCACCTTGTG
STAT2 F	IDT	CCGGGACATTCAGCCCTTTT
STAT2 R	IDT	CTCATGTTGCTGGCTCTCCA
STAT3 F	IDT	CATGTCTCCTTGCGTGTCTAA
STAT3 R	IDT	CATGTCCAACCTGTAACTCTCTC
STAT5A F	IDT	GTTCAGTGTTGGCAGCAATGAGC
STAT5A R	IDT	AGCACAGTAGCCGTGGCATTGT
STAT5B F	IDT	GCCACTGTTCTCTGGGACAATG
STAT5B R	IDT	ACACGAGGTTCTCCTTGGTCAG
TFAM F	IDT	GGGAAGGAGGGTTGTGTATTT
TFAM R	IDT	AGGAGTTAGCCAAACGCAATA
TLR3 F	IDT	TGGTTGGGCCACCTAGAAGTP
TLR3 R	IDT	CCATTCCTGGCCTGTGAGTT
TLR9 F	IDT	GTGACAGATCCAAGGTGAAGT
TLR9 R	IDT	CTTCCTCTACAAATGCATCACT
TMEM173	Qiagen	
TNF	Qiagen	
ZNFX1 F	IDT	GGCAGAGGGAAGAGAGATTTAG
ZNFX1 R	IDT	TTCTCCTGGTCATGTCTTTGG

Reference

1. *Americsn Cancer Society, Cancer facts and figures 2023.* American Cancer Society journal, CA: A Cancer Journal for Clinicians., 2023.

2. Mathieu, K.B., et al., *Screening for ovarian cancer: imaging challenges and opportunities for improvement.* Ultrasound Obstet Gynecol, 2018. **51**(3): p. 293-303.

3. Xie, W., et al., *Ovarian cancer: epigenetics, drug resistance, and progression.* Cancer Cell Int, 2021. **21**(1): p. 434.

4. Doherty, J.A., et al., *Challenges and Opportunities in Studying the Epidemiology of Ovarian Cancer Subtypes.* Curr Epidemiol Rep, 2017. **4**(3): p. 211-220.

5. Jeff Hirst, J.C.a.A.G., *Ovarian Cancer Genetics: Subtypes and Risk Factors.* IntechOpen, , 2018.

6. Ledermann, J.A., et al., *Newly diagnosed and relapsed epithelial ovarian carcinoma: ESMO Clinical Practice Guidelines for diagnosis, treatment and follow-up.* Ann Oncol, 2013. **24 Suppl 6**: p. vi24-32.

7. Khan, M.A., et al., *Platinum-resistant ovarian cancer: From drug resistance mechanisms to liquid biopsy-based biomarkers for disease management.* Semin Cancer Biol, 2021. **77**: p. 99-109.

8. Lee, J.-Y., et al., *Changes in ovarian cancer survival during the 20 years before the era of targeted therapy.* BMC Cancer, 2018. **18**(1): p. 601.

9. Bryant, H.E., et al., *Specific killing of BRCA2-deficient tumours with inhibitors of poly(ADP-ribose) polymerase.* Nature, 2005. **434**(7035): p. 913-7.

10. Jubin, T., et al., *The PARP family: insights into functional aspects of poly (ADP-ribose) polymerase-1 in cell growth and survival.* Cell Prolif, 2016. **49**(4): p. 421-37.

11. Chen, A., *PARP inhibitors: its role in treatment of cancer.* Chin J Cancer, 2011. **30**(7): p. 463-71.

12. Durkacz, B.W., et al., *(ADP-ribose)n participates in DNA excision repair.* Nature, 1980. **283**(5747): p. 593-6.

13. Li, Y., C.F. Liu, and G.W. Rao, *A Review on Poly (ADP-ribose) Polymerase (PARP) Inhibitors and Synthetic Methodologies.* Curr Med Chem, 2021. **28**(8): p. 1565-1584.

14. Wu, Y., et al., *Clinical application of PARP inhibitors in ovarian cancer: from molecular mechanisms to the current status.* J Ovarian Res, 2023. **16**(1): p. 6.

15. Arora, S., et al., *FDA Approval Summary: Olaparib Monotherapy or in Combination with Bevacizumab for the Maintenance Treatment of Patients with Advanced Ovarian Cancer.* Oncologist, 2021. **26**(1): p. e164-e172.

16. Colombo, I., S. Lheureux, and A.M. Oza, *Rucaparib: a novel PARP inhibitor for BRCA advanced ovarian cancer.* Drug Des Devel Ther, 2018. **12**: p. 605-617.

17. Monk, B.J., et al., *Safety and management of niraparib monotherapy in ovarian cancer clinical trials.* Int J Gynecol Cancer, 2023. **33**(6): p. 971-981.

18. Litton, J.K., et al., *Talazoparib in Patients with Advanced Breast Cancer and a Germline BRCA Mutation.* N Engl J Med, 2018. **379**(8): p. 753-763.

19. Boussios, S., et al., *Poly (ADP-Ribose) Polymerase Inhibitors: Talazoparib in Ovarian Cancer and Beyond.* Drugs R D, 2020. **20**(2): p. 55-73.

20. Zheng, J., Z. Li, and W. Min, *Current status and future promise of next-generation poly (ADP-Ribose) polymerase 1-selective inhibitor AZD5305.* Front Pharmacol, 2022. **13**: p. 979873.

21. Jiang, Y.Z., et al., *Genomic and Transcriptomic Landscape of Triple-Negative Breast Cancers: Subtypes and Treatment Strategies.* Cancer Cell, 2019. **35**(3): p. 428-440.e5.

22. Kantarjian, H., et al., *Results of a randomized study of 3 schedules of low-dose decitabine in higher-risk myelodysplastic syndrome and chronic myelomonocytic leukemia.* Blood, 2007. **109**(1): p. 52-7.

23. Issa, J.P., et al., *Phase 1 study of low-dose prolonged exposure schedules of the hypomethylating agent 5-aza-2'-deoxycytidine (decitabine) in hematopoietic malignancies.* Blood, 2004. **103**(5): p. 1635-40.

24. Zampieri, M., et al., *ADP-ribose polymers localized on Ctcf-Parp1-Dnmt1 complex prevent methylation of Ctcf target sites.* Biochem J, 2012. **441**(2): p. 645-52.

25. Diesch, J., et al., *A clinical-molecular update on azanucleoside-based therapy for the treatment of hematologic cancers.* Clin Epigenetics, 2016. **8**: p. 71.

26. Robertson, K.D., *DNA methylation and human disease.* Nat Rev Genet, 2005. **6**(8): p. 597-610.

27. Holliday, R. and J.E. Pugh, *DNA modification mechanisms and gene activity during development.* Science, 1975. **187**(4173): p. 226-32.

28. Weinhold, B., *Epigenetics: the science of change.* Environ Health Perspect, 2006. **114**(3): p. A160-7.

29. Matei, D.E. and K.P. Nephew, *Epigenetic therapies for chemoresensitization of epithelial ovarian cancer.* Gynecol Oncol, 2010. **116**(2): p. 195-201.

30. Mehdipour, P., R. Chen, and D.D. De Carvalho, *The next generation of DNMT inhibitors.* Nat Cancer, 2021. **2**(10): p. 1000-1001.

31. Fang, F., et al., *A phase 1 and pharmacodynamic study of decitabine in combination with carboplatin in patients with recurrent, platinum-resistant, epithelial ovarian cancer.* Cancer, 2010. **116**(17): p. 4043-53.

32. Matei, D., et al., *A Phase I Clinical Trial of Guadecitabine and Carboplatin in Platinum-Resistant, Recurrent Ovarian Cancer: Clinical, Pharmacokinetic, and Pharmacodynamic Analyses.* Clin Cancer Res, 2018. **24**(10): p. 2285-2293.

33. Oza, A.M., et al., *A Randomized Phase II Trial of Epigenetic Priming with Guadecitabine and Carboplatin in Platinum-resistant, Recurrent Ovarian Cancer.* Clin Cancer Res, 2020. **26**(5): p. 1009-1016.

34. Fu, S., et al., *Phase 1b-2a study to reverse platinum resistance through use of a hypomethylating agent, azacitidine, in patients with platinum-resistant or platinum-refractory epithelial ovarian cancer.* Cancer, 2011. **117**(8): p. 1661-9.

35. Glasspool, R.M., et al., *A randomised, phase II trial of the DNA-hypomethylating agent 5-aza-2'-deoxycytidine (decitabine) in combination with carboplatin vs carboplatin alone in patients with recurrent, partially platinum-sensitive ovarian cancer.* British Journal of Cancer, 2014. **110**(8): p. 1923-1929.

36. Ravandi, F., et al., *Phase 2 study of ASTX727 (cedazuridine/decitabine) plus venetoclax (ven) in patients with relapsed/refractory acute myeloid leukemia (AML) or previously untreated, elderly patients (pts) unfit for chemotherapy.* Journal of Clinical Oncology, 2022. **40**(16_suppl): p. 7037-7037.

37. Chen, Q., et al., *GSK-3484862 targets DNMT1 for degradation in cells.* NAR Cancer, 2023. **5**(2): p. zcad022.

38. Tsai, H.C., et al., *Transient low doses of DNA-demethylating agents exert durable antitumor effects on hematological and epithelial tumor cells.* Cancer Cell, 2012. **21**(3): p. 430-46.

39. Hamanishi, J., et al., *Safety and Antitumor Activity of Anti-PD-1 Antibody, Nivolumab, in Patients With Platinum-Resistant Ovarian Cancer.* J Clin Oncol, 2015. **33**(34): p. 4015-22.

40. Maine, C.J., et al., *Programmed death ligand-1 over-expression correlates with malignancy and contributes to immune regulation in ovarian cancer.* Cancer Immunol Immunother, 2014. **63**(3): p. 215-24.

41. Bi-Heng Cheng, H.L., et al., *Characterization of PD-L1 expression and its prognostic value in patients with ovarian cancer.* Transl Cancer Res 2018: p. 1271-81.

42. Goode, E.L., et al., *Dose-Response Association of CD8+ Tumor-Infiltrating Lymphocytes and Survival Time in High-Grade Serous Ovarian Cancer.* JAMA Oncol, 2017. **3**(12): p. e173290.

43. Zhu, J., L. Yan, and Q. Wang, *Efficacy of PD-1/PD-L1 inhibitors in ovarian cancer: a single-arm meta-analysis.* Journal of Ovarian Research, 2021. **14**(1): p. 112.

44. Matulonis, U.A., et al., *Antitumor activity and safety of pembrolizumab in patients with advanced recurrent ovarian cancer: results from the phase II KEYNOTE-100 study.* Ann Oncol, 2019. **30**(7): p. 1080-1087.

45. Chiappinelli, K.B., et al., *Inhibiting DNA Methylation Causes an Interferon Response in Cancer via dsRNA Including Endogenous Retroviruses.* Cell, 2016. **164**(5): p. 1073.

46. Wilkins, A., et al., *Differential and longitudinal immune gene patterns associated with reprogrammed microenvironment and viral mimicry in response to neoadjuvant radiotherapy in rectal cancer.* J Immunother Cancer, 2021. **9**(3).

47. Liu, C., et al., *Nanobooster-encapsulated hybrid RNA as anti-tumor viral mimicry.* Nano Today, 2021. **38**: p. 101211.

48. Wilkinson, D.A., et al., *Autonomous expression of RTVL-H endogenous retroviruslike elements in human cells.* J Virol, 1990. **64**(5): p. 2157-67.

49. Chen, R., C.A. Ishak, and D.D. De Carvalho, *Endogenous Retroelements and the Viral Mimicry Response in Cancer Therapy and Cellular Homeostasis.* Cancer Discov, 2021. **11**(11): p. 2707-2725.

50. Sun, L., et al., *Cyclic GMP-AMP synthase is a cytosolic DNA sensor that activates the type I interferon pathway.* Science, 2013. **339**(6121): p. 786-91.

51. Petrucelli, N., M.B. Daly, and T. Pal, *BRCA1- and BRCA2-Associated Hereditary Breast and Ovarian Cancer*, in *GeneReviews(®)*, M.P. Adam, et al., Editors.

1993, University of Washington, Seattle Copyright © 1993-2023, University of Washington, Seattle. GeneReviews is a registered trademark of the University of Washington, Seattle. All rights reserved.: Seattle (WA).

52. Gayther, S.A., et al., *Germline mutations of the BRCA1 gene in breast and ovarian cancer families provide evidence for a genotype-phenotype correlation.* Nat Genet, 1995. **11**(4): p. 428-33.

53. Sekine, M., K. Nishino, and T. Enomoto, *Differences in Ovarian and Other Cancers Risks by Population and BRCA Mutation Location.* Genes (Basel), 2021. **12**(7).

54. Terdiman, J.P., et al., *Efficient detection of hereditary nonpolyposis colorectal cancer gene carriers by screening for tumor microsatellite instability before germline genetic testing.* Gastroenterology, 2001. **120**(1): p. 21-30.

55. Knudson, A.G., Jr., *Mutation and cancer: statistical study of retinoblastoma.* Proc Natl Acad Sci U S A, 1971. **68**(4): p. 820-3.

56. Mirza, M.R., et al., *Niraparib Maintenance Therapy in Platinum-Sensitive, Recurrent Ovarian Cancer.* N Engl J Med, 2016. **375**(22): p. 2154-2164.

57. Verona Abdelmeseh, P. Britny Rogala, and P. Justin (JC) Liauw, *Overview of PARP Inhibitors in the Treatment of Ovarian Cancer.* Pharmacy Times Oncology Edition, 2021. **3**(5): p. 11.

58. Tian, H., et al., *DNA damage response--a double-edged sword in cancer prevention and cancer therapy.* Cancer Lett, 2015. **358**(1): p. 8-16.

59. Ray Chaudhuri, A. and A. Nussenzweig, *The multifaceted roles of PARP1 in DNA repair and chromatin remodelling.* Nat Rev Mol Cell Biol, 2017. **18**(10): p. 610-621.

60. Muvarak, N.E., et al., *Enhancing the Cytotoxic Effects of PARP Inhibitors with DNA Demethylating Agents - A Potential Therapy for Cancer.* Cancer Cell, 2016. **30**(4): p. 637-650.

61. Murai, J., et al., *Trapping of PARP1 and PARP2 by Clinical PARP Inhibitors.* Cancer Res, 2012. **72**(21): p. 5588-99.

62. Rudolph, J., K. Jung, and K. Luger, *Inhibitors of PARP: Number crunching and structure gazing.* Proceedings of the National Academy of Sciences, 2022. **119**(11): p. e2121979119.

63. Shen, Y., et al., *BMN 673, a novel and highly potent PARP1/2 inhibitor for the treatment of human cancers with DNA repair deficiency.* Clin Cancer Res, 2013. **19**(18): p. 5003-15.

64. Bitler, B.G., et al., *PARP inhibitors: Clinical utility and possibilities of overcoming resistance.* Gynecol Oncol, 2017. **147**(3): p. 695-704.

65. Rigakos, G. and E. Razis, *BRCAness: finding the Achilles heel in ovarian cancer.* Oncologist, 2012. **17**(7): p. 956-62.

66. McCabe, N., et al., *Deficiency in the repair of DNA damage by homologous recombination and sensitivity to poly(ADP-ribose) polymerase inhibition.* Cancer Res, 2006. **66**(16): p. 8109-15.

67. Lord, C.J., et al., *A high-throughput RNA interference screen for DNA repair determinants of PARP inhibitor sensitivity.* DNA Repair (Amst), 2008. **7**(12): p. 2010-9.

68. Abbotts, R., A.J. Dellomo, and F.V. Rassool, *Pharmacologic Induction of BRCAness in BRCA-Proficient Cancers: Expanding PARP Inhibitor Use.* Cancers (Basel), 2022. **14**(11).

69. McLaughlin, L.J., et al., *Pharmacologic induction of innate immune signaling directly drives homologous recombination deficiency.* Proc Natl Acad Sci U S A, 2020. **117**(30): p. 17785-17795.

70. Abbotts, R., et al., *DNA methyltransferase inhibitors induce a BRCAness phenotype that sensitizes NSCLC to PARP inhibitor and ionizing radiation.* Proc Natl Acad Sci U S A, 2019. **116**(45): p. 22609-22618.

71. Chao, O.S. and O.B. Goodman, Jr., *Synergistic loss of prostate cancer cell viability by coinhibition of HDAC and PARP.* Mol Cancer Res, 2014. **12**(12): p. 1755-66.

72. Valdez, B.C., et al., *Combination of a hypomethylating agent and inhibitors of PARP and HDAC traps PARP1 and DNMT1 to chromatin, acetylates DNA repair proteins, down-regulates NuRD and induces apoptosis in human leukemia and lymphoma cells.* Oncotarget, 2018. **9**(3): p. 3908-3921.

73. Pulliam, N., et al., *An Effective Epigenetic-PARP Inhibitor Combination Therapy for Breast and Ovarian Cancers Independent of BRCA Mutations.* Clin Cancer Res, 2018. **24**(13): p. 3163-3175.

74. Violeta, V.A.K.N.S.P.M.F.N.N.R.B.J.W.T.Z.V.A.J.P.N.W.C.H., *Evolution of Neoantigen Landscape during Immune Checkpoint Blockade in Non–Small Cell Lung Cancer.* Cancer discovery, 2017. **7**(3): p. 264-276.

75. Jenkins, R.W., D.A. Barbie, and K.T. Flaherty, *Mechanisms of resistance to immune checkpoint inhibitors.* Br J Cancer, 2018. **118**(1): p. 9-16.

76. Demaria, O., et al., *Harnessing innate immunity in cancer therapy.* Nature, 2019. **574**(7776): p. 45-56.

77. Burnet, F.M., *The concept of immunological surveillance.* Prog Exp Tumor Res, 1970. **13**: p. 1-27.

78. Dhatchinamoorthy, K., J.D. Colbert, and K.L. Rock, *Cancer Immune Evasion Through Loss of MHC Class I Antigen Presentation.* Front Immunol, 2021. **12**: p. 636568.

79. Pardoll, D.M., *The blockade of immune checkpoints in cancer immunotherapy.* Nat Rev Cancer, 2012. **12**(4): p. 252-64.

80. Hudson, K., et al., *The Extrinsic and Intrinsic Roles of PD-L1 and Its Receptor PD-1: Implications for Immunotherapy Treatment.* Front Immunol, 2020. **11**: p. 568931.

81. Latchman, Y.E., et al., *PD-L1-deficient mice show that PD-L1 on T cells, antigen-presenting cells, and host tissues negatively regulates T cells.* Proc Natl Acad Sci U S A, 2004. **101**(29): p. 10691-6.

82. Iranzo, P., et al., *Overview of Checkpoint Inhibitors Mechanism of Action: Role of Immune-Related Adverse Events and Their Treatment on Progression of Underlying Cancer.* Front Med (Lausanne), 2022. **9**: p. 875974.

83. Jiao, S., et al., *PARP Inhibitor Upregulates PD-L1 Expression and Enhances Cancer-Associated Immunosuppression.* Clin Cancer Res, 2017. **23**(14): p. 3711-3720.

84. Peyraud, F. and A. Italiano, *Combined PARP Inhibition and Immune Checkpoint Therapy in Solid Tumors.* Cancers (Basel), 2020. **12**(6).

85. Chen, Q., L. Sun, and Z.J. Chen, *Regulation and function of the cGAS-STING pathway of cytosolic DNA sensing.* Nat Immunol, 2016. **17**(10): p. 1142-9.

86. Pantelidou, C., et al., *PARP Inhibitor Efficacy Depends on CD8(+) T-cell Recruitment via Intratumoral STING Pathway Activation in BRCA-Deficient Models of Triple-Negative Breast Cancer.* Cancer Discov, 2019. **9**(6): p. 722-737.

87. Domchek, S.M., et al., *Olaparib and durvalumab in patients with germline BRCA-mutated metastatic breast cancer (MEDIOLA): an open-label, multicentre, phase 1/2, basket study.* Lancet Oncol, 2020. **21**(9): p. 1155-1164.

88. Staniszewska, A.D., et al., *PARP inhibition is a modulator of anti-tumor immune response in BRCA-deficient tumors.* Oncoimmunology, 2022. **11**(1): p. 2083755.

89. Waddington, C.H., *The epigenotype. 1942.* Int J Epidemiol, 2012. **41**(1): p. 10-3.

90. Deichmann, U., *Epigenetics: The origins and evolution of a fashionable topic.* Dev Biol, 2016. **416**(1): p. 249-254.

91. Barter, M.J., C. Bui, and D.A. Young, *Epigenetic mechanisms in cartilage and osteoarthritis: DNA methylation, histone modifications and microRNAs.* Osteoarthritis Cartilage, 2012. **20**(5): p. 339-349.

92. Portela, A. and M. Esteller, *Epigenetic modifications and human disease.* Nature Biotechnology, 2010. **28**(10): p. 1057-1068.

93. Jones, P.A., J.P. Issa, and S. Baylin, *Targeting the cancer epigenome for therapy.* Nat Rev Genet, 2016. **17**(10): p. 630-41.

94. Derissen, E.J., J.H. Beijnen, and J.H. Schellens, *Concise drug review: azacitidine and decitabine.* Oncologist, 2013. **18**(5): p. 619-24.

95. Hu, C., et al., *DNA methyltransferase inhibitors combination therapy for the treatment of solid tumor: mechanism and clinical application.* Clin Epigenetics, 2021. **13**(1): p. 166.

96. Leone, G., et al., *DNA methylation and demethylating drugs in myelodysplastic syndromes and secondary leukemias.* Haematologica, 2002. **87**(12): p. 1324-41.

97. Anderes, E. and S. Nand, *Chapter 76 - Commonly used drugs in hematologic disorders*, in *Handbook of Clinical Neurology*, J. Biller and J.M. Ferro, Editors. 2014, Elsevier. p. 1125-1139.

98. Sasaki, K., et al., *Low-Dose Decitabine versus Low-Dose Azacitidine in Lower-Risk MDS.* NEJM Evidence, 2022. **1**(10): p. EVIDoa2200034.

99. Li, J., et al., *Epigenetic targeting drugs potentiate chemotherapeutic effects in solid tumor therapy.* Sci Rep, 2017. **7**(1): p. 4035.

100. Hanahan, D. and R.A. Weinberg, *The hallmarks of cancer.* Cell, 2000. **100**(1): p. 57-70.

101. Kim, C., X.D. Wang, and Y. Yu, *PARP1 inhibitors trigger innate immunity via PARP1 trapping-induced DNA damage response.* Elife, 2020. **9**.

102. Chen, S., et al., *Epigenetic priming enhances antitumor immunity in platinum-resistant ovarian cancer.* J Clin Invest, 2022. **132**(14).

103. Luo, N., A. Sugiura, and J.M. Balko, *Therapeutic potential of DNA methyltransferase inhibitors with immune checkpoint inhibitor therapy in breast cancer.* Cell Stress, 2018. **2**(3): p. 69-71.

104. Okude, H., D. Ori, and T. Kawai, *Signaling Through Nucleic Acid Sensors and Their Roles in Inflammatory Diseases.* Front Immunol, 2020. **11**: p. 625833.

105. Goubau, D., S. Deddouche, and C. Reis e Sousa, *Cytosolic sensing of viruses.* Immunity, 2013. **38**(5): p. 855-69.

106. Yoneyama, M., et al., *The RNA helicase RIG-I has an essential function in double-stranded RNA-induced innate antiviral responses.* Nat Immunol, 2004. **5**(7): p. 730-7.

107. Kang, D.C., et al., *Expression analysis and genomic characterization of human melanoma differentiation associated gene-5, mda-5: a novel type I interferon-responsive apoptosis-inducing gene.* Oncogene, 2004. **23**(9): p. 1789-800.

108. Yoneyama, M., et al., *Shared and unique functions of the DExD/H-box helicases RIG-I, MDA5, and LGP2 in antiviral innate immunity.* J Immunol, 2005. **175**(5): p. 2851-8.

109. Moore, C.B., et al., *NLRX1 is a regulator of mitochondrial antiviral immunity.* Nature, 2008. **451**(7178): p. 573-7.

110. Moore, C.B. and J.P. Ting, *Regulation of mitochondrial antiviral signaling pathways.* Immunity, 2008. **28**(6): p. 735-9.

111. Seth, R.B., et al., *Identification and characterization of MAVS, a mitochondrial antiviral signaling protein that activates NF-kappaB and IRF 3.* Cell, 2005. **122**(5): p. 669-82.

112. Kausar, S., et al., *Mitochondrial DNA: A Key Regulator of Anti-Microbial Innate Immunity*. Genes (Basel), 2020. **11**(1).

113. Marques, P.E., et al., *Chemokines and mitochondrial products activate neutrophils to amplify organ injury during mouse acute liver failure.* Hepatology, 2012. **56**(5): p. 1971-82.

114. Zhou, R., et al., *A role for mitochondria in NLRP3 inflammasome activation.* Nature, 2011. **469**(7329): p. 221-5.

115. McArthur, K., et al., *BAK/BAX macropores facilitate mitochondrial herniation and mtDNA efflux during apoptosis.* Science, 2018. **359**(6378).

116. Aarreberg, L.D., et al., *Interleukin-1β Induces mtDNA Release to Activate Innate Immune Signaling via cGAS-STING.* Mol Cell, 2019. **74**(4): p. 801-815.e6.

117. Butler, D., et al., *Shotgun transcriptome, spatial omics, and isothermal profiling of SARS-CoV-2 infection reveals unique host responses, viral diversification, and drug interactions.* Nat Commun, 2021. **12**(1): p. 1660.

118. Ishidate, T., et al., *ZNFX-1 Functions within Perinuclear Nuage to Balance Epigenetic Signals.* Mol Cell, 2018. **70**(4): p. 639-649.e6.

119. Wang, Y., et al., *Mitochondria-localised ZNFX1 functions as a dsRNA sensor to initiate antiviral responses through MAVS.* Nat Cell Biol, 2019. **21**(11): p. 1346-1356.

120. Vavassori, S., et al., *Multisystem inflammation and susceptibility to viral infections in human ZNFX1 deficiency.* J Allergy Clin Immunol, 2021. **148**(2): p. 381-393.

121. Le Voyer, T., et al., *Inherited deficiency of stress granule ZNFX1 in patients with monocytosis and mycobacterial disease.* Proc Natl Acad Sci U S A, 2021. **118**(15).

122. Guarnieri, J.W., et al., *Core mitochondrial genes are down-regulated during SARS-CoV-2 infection of rodent and human hosts.* Sci Transl Med, 2023. **15**(708): p. eabq1533.

123. Furda, A., et al., *Quantitative PCR-based measurement of nuclear and mitochondrial DNA damage and repair in mammalian cells.* Methods Mol Biol, 2014. **1105**: p. 419-37.

124. Edwards, J.G., *Quantification of mitochondrial DNA (mtDNA) damage and error rates by real-time QPCR.* Mitochondrion, 2009. **9**(1): p. 31-5.

125. Yu, G., et al., *clusterProfiler: an R package for comparing biological themes among gene clusters.* Omics, 2012. **16**(5): p. 284-7.

126. Davis, S. and P.S. Meltzer, *GEOquery: a bridge between the Gene Expression Omnibus (GEO) and BioConductor.* Bioinformatics, 2007. **23**(14): p. 1846-7.

127. Tothill, R.W., et al., *Novel molecular subtypes of serous and endometrioid ovarian cancer linked to clinical outcome.* Clin Cancer Res, 2008. **14**(16): p. 5198-208.

128. Ferriss, J.S., et al., *Multi-gene expression predictors of single drug responses to adjuvant chemotherapy in ovarian carcinoma: predicting platinum resistance.* PLoS One, 2012. **7**(2): p. e30550.

129. Garsed, D.W., et al., *The genomic and immune landscape of long-term survivors of high-grade serous ovarian cancer.* Nat Genet, 2022. **54**(12): p. 1853-1864.

130. Fang, F., et al., *Genomic and Epigenomic Signatures in Ovarian Cancer Associated with Resensitization to Platinum Drugs.* Cancer Res, 2018. **78**(3): p. 631-644.

131. McCarthy, D.J., Y. Chen, and G.K. Smyth, *Differential expression analysis of multifactor RNA-Seq experiments with respect to biological variation.* Nucleic Acids Res, 2012. **40**(10): p. 4288-97.

132. Tan, T.Z., et al., *CSIOVDB: a microarray gene expression database of epithelial ovarian cancer subtype.* Oncotarget, 2015. **6**(41): p. 43843-52.

133. Rath, S., et al., *MitoCarta3.0: an updated mitochondrial proteome now with sub-organelle localization and pathway annotations.* Nucleic Acids Res, 2021. **49**(D1): p. D1541-d1547.

134. Roulois, D., et al., *DNA-Demethylating Agents Target Colorectal Cancer Cells by Inducing Viral Mimicry by Endogenous Transcripts.* Cell, 2015. **162**(5): p. 961-73.

135. Topper, M.J., et al., *Epigenetic Therapy Ties MYC Depletion to Reversing Immune Evasion and Treating Lung Cancer.* Cell, 2017. **171**(6): p. 1284-1300.e21.

136. Stone, M.L., et al., *Epigenetic therapy activates type I interferon signaling in murine ovarian cancer to reduce immunosuppression and tumor burden.* Proc Natl Acad Sci U S A, 2017. **114**(51): p. E10981-e10990.

137. Chew, K. and L. Zhao, *Interactions of Mitochondrial Transcription Factor A with DNA Damage: Mechanistic Insights and Functional Implications.* Genes (Basel), 2021. **12**(8).

138. Pulliam, N., et al., *An Effective Epigenetic-PARP Inhibitor Combination Therapy for Breast and Ovarian Cancers Independent of BRCA Mutations.* Clinical Cancer Research, 2018. **24**: p. 3163 - 3175.

139. Guo, C., et al., *Oxidative stress, mitochondrial damage and neurodegenerative diseases.* Neural Regen Res, 2013. **8**(21): p. 2003-14.

140. Szklarczyk, D., et al., *STRING v11: protein-protein association networks with increased coverage, supporting functional discovery in genome-wide experimental datasets.* Nucleic Acids Res, 2019. **47**(D1): p. D607-d613.

141. West, A.P., G.S. Shadel, and S. Ghosh, *Mitochondria in innate immune responses.* Nat Rev Immunol, 2011. **11**(6): p. 389-402.

142. Mardis, E.R., *Neoantigens and genome instability: impact on immunogenomic phenotypes and immunotherapy response.* Genome Medicine, 2019. **11**(1): p. 71.

143. Mammel, A.E. and E.M. Hatch, *Genome instability from nuclear catastrophe and DNA damage.* Seminars in Cell & Developmental Biology, 2022. **123**: p. 131-139.

144. d'Angelo, D.M., et al., *Type I Interferonopathies in Children: An Overview.* Front Pediatr, 2021. **9**: p. 631329.

145. Casrouge, A., et al., *Herpes simplex virus encephalitis in human UNC-93B deficiency.* Science, 2006. **314**(5797): p. 308-12.

146. Ciancanelli, M.J., et al., *Infectious disease. Life-threatening influenza and impaired interferon amplification in human IRF7 deficiency.* Science, 2015. **348**(6233): p. 448-53.

147. Hernandez, N., et al., *Life-threatening influenza pneumonitis in a child with inherited IRF9 deficiency.* J Exp Med, 2018. **215**(10): p. 2567-2585.

148. Lim, H.K., et al., *Severe influenza pneumonitis in children with inherited TLR3 deficiency.* J Exp Med, 2019. **216**(9): p. 2038-2056.

149. Zhang, Q., et al., *Inborn errors of type I IFN immunity in patients with life-threatening COVID-19.* Science, 2020. **370**(6515).

150. Topper, M.J., et al., *The emerging role of epigenetic therapeutics in immuno-oncology.* Nat Rev Clin Oncol, 2020. **17**(2): p. 75-90.

151. Sriramkumar, S., et al., *Platinum-induced mitochondrial OXPHOS contributes to cancer stem cell enrichment in ovarian cancer.* J Transl Med, 2022. **20**(1): p. 246.

152. Krokan, H.E. and M. Bjørås, *Base excision repair.* Cold Spring Harb Perspect Biol, 2013. **5**(4): p. a012583.

153. Rossi, M.N., et al., *Mitochondrial localization of PARP-1 requires interaction with mitofilin and is involved in the maintenance of mitochondrial DNA integrity.* J Biol Chem, 2009. **284**(46): p. 31616-24.

154. Szczesny, B., et al., *Opposing roles of mitochondrial and nuclear PARP1 in the regulation of mitochondrial and nuclear DNA integrity: implications for the regulation of mitochondrial function.* Nucleic Acids Research, 2014. **42**(21): p. 13161-13173.

155. Yamazaki, T. and L. Galluzzi, *Mitochondrial control of innate immune signaling by irradiated cancer cells.* Oncoimmunology, 2020. **9**(1): p. 1797292.

156. Pandian, N. and T.D. Kanneganti, *PANoptosis: A Unique Innate Immune Inflammatory Cell Death Modality*. J Immunol, 2022. **209**(9): p. 1625-1633.